# Oil spill detection and mapping under Arctic sea ice using autonomous underwater vehicles

BSEE Contract E12PC00053

Final Report, August 2014

Ted Maksym, Hanumant Singh, Chris Bassett, Andone Lavery, Lee Freitag, Fritz Sonnichsen

Woods Hole Oceanographic Institution

Jeremy Wilkinson

Polar Ocean Services

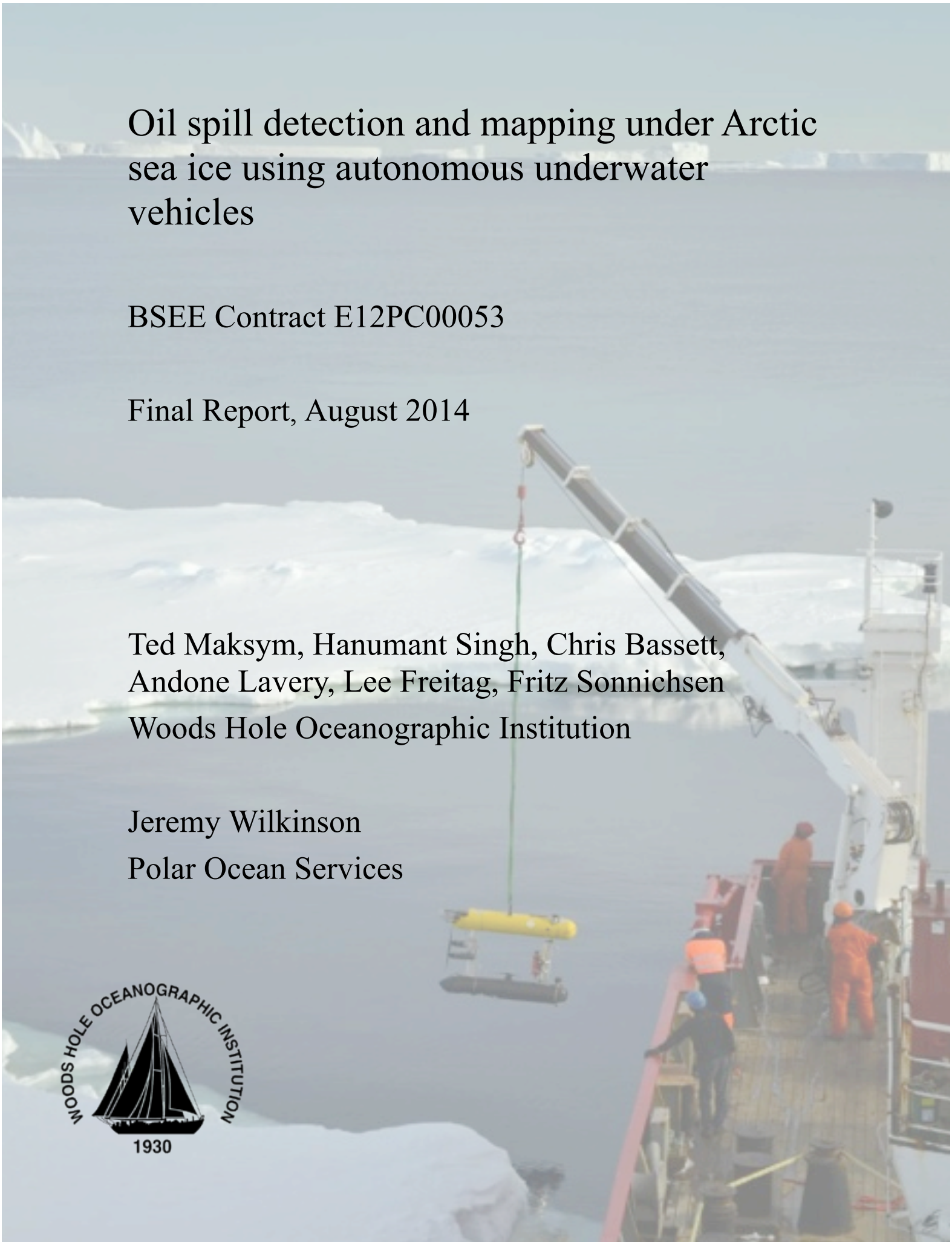

## DISCLAIMER

This final report has been reviewed by the Bureau of Safety and Environmental Enforcement (BSEE) and has been approved for publication. Approval does not signify that the contents necessarily reflect the views and policies of the BSEE, nor does mention of the trade names or commercial products constitute endorsement or recommendation for use.

## ACKNOWLEDGEMENTS

This study was funded by the Bureau of Safety and Environmental Enforcement (BSEE), U.S. Department of the Interior, Washington, D.C. under contract number E12PC00053.

Part of this work was made possible by additional support for laboratory experiments at the Scottish Association for Marine Science (SAMS) and Hamburgische Schiffbau-Versuchsanstalt (HSVA) GmbH. Access to the HSVA facility and support for J. Wilkinson was provided through the EU ACCESS and EU Hydralab programmes. The Prince William Sound Science Center provided support for the SAMS experiments. Alaska Clean Seas kindly provided support for additional equipment for the HSVA experiments and logistical support at Prudhoe Bay. We wish to thank Peter Koski and Sandipa Singh for assistance in the field for the Prudhoe Bay acoustic tests. Bernard Hagen assisted with the SAMS experiments. We thank Rich Hansen and Kurt Hansen from the US Coast Guard Research and Development Center and the officers and crew of the USCGC Healy and USCGC Hollyhock for support during operations in the Great Lakes and Beaufort Sea.

## TABLE OF CONTENTS

# 1. Executive Summary

To advance the capabilities of Autonomous Underwater Vehicle (AUV) operation under Arctic sea ice for the detection and mapping of oil spills, an integrated study of both AUV and sensor suite performance for oil spill response in ice-covered waters was performed. This had two key, complementary foci – (1) a suite of three laboratory experiments were performed to determine the efficacy of three sensor modalities (sonar, digital imagery, and laser fluorescence) for detection of oil beneath, and encapsulated within sea ice, and (2) AUV missions to test the feasibility for extension of the existing under-ice capability of the Seabed Class AUV to oil spill mapping scenarios in variable, drifting ice conditions and under fast ice in shallow water.

Sensor evaluation included testing of a laboratory broadband sonar system, a high-fidelity high-frequency narrowband sonar, digital cameras, and development and testing of a laser fluorosensor prototype system. This suite of instruments was proven to be effective at detecting oil under sheet ice, and encapsulated within the ice to a thickness of up to 15 cm, depending on the sensor. Of particular interest, the acoustic scattering from the basal layer of sea ice was seen to be highly variable and distinct from that of the oil. Both broadband and narrow band sonar techniques proved effective in detecting and quantifying the thickness of oil under sea ice. Experiments demonstrate a clear benefit of acoustic systems is their potential for detecting the thickness of an oil layer, both under the ice, and to some degree encapsulated within the ice, based on detection of multiple acoustic scattering interfaces when oil is present. This thickness, when combined with observations of the spatial extent of the oil (provided by any or all of the sensor systems tested herein), allow quantification of the oil volume. The efficacy of oil detection under differing conditions (e.g. oil thickness, depth of encapsulation) is dependent on a variety of parameters (e.g. pulse width, range resolution). Determination of the most appropriate system configuration, or suite of systems, will require further experiments and analysis of performance under more complex ice conditions typical the variable Arctic ice cover. Broadband sonar techniques have several potential advantages for oil detection; Based on the results presented in this document the development and testing of compact AUV-based broadband systems seems warranted.

Laboratory based experiments provided a unique opportunity to examine the efficacy of undersea oil detection techniques in different young ice types that occur in the Arctic Ocean. Detection of oil with sonar was more complicated in frazil and pancake ice types, although in these cases digital imagery and laser fluorescence proved effective. Results of these experiments suggest that the best solution for oil detection under ice would involve a combination of each of these sensors. Despite the success of these experiments, sensor efficacy under more realistic, highly variable ice conditions is needed, and will require both AUV missions to fully characterize the under ice environment, and further oil spill experiments in more complex ice conditions.

AUV missions in the Great Lakes and the Beaufort Sea demonstrated that rapid, entirely ship-based operation of the AUV under highly varied ice conditions was possible. Long-range acoustic communication capability demonstrated in the shallow water fast ice environment at Prudhoe Bay will permit relatively large scale AUV surveys. AUV navigation techniques that combine inertial, bottom tracking, and acoustic positioning should permit precise large-scale mapping missions in varied sea ice conditions.

These results demonstrate the potential for development of a complete sensor suite and AUV platform for oil spill response in ice-covered waters. In particular, with directed investment, potential exists to advance AUV capabilities for routine large-scale oil spill mapping missions under the full range of ice condition encountered on the Beaufort/Chukchi continental shelf. A path towards this capability should include both further development of under ice AUV capability and evaluation of expected sensor performance under these conditions. For the former, development of long-range and long-endurance capability while maintaining accurate navigation and real-time communication are key to extending current capability to scenarios where rapid response to large spills under variable pack ice is required, or for routine monitoring for leaks from subsea pipelines.

In concert, further testing and analysis of sensor performance in realistic conditions, including at longer ranges and in complex under-ice morphologies is necessary so that the expected characteristics of the signal response and required capabilities of each sensor system in this environment can be better determined. Given that each sensor system will have different performance capabilities in different ice and oil scenarios, it is expected that an operational system will combine several, or all the sensor modalities tested under this project. Techniques for fusion of data from multiple sensors for the most reliable detection of oil should be developed.

## 2. Background and Motivation

### 2.1 Oil detection in ice-covered seas

As the summer Arctic sea ice cover declines over the coming decades, increased shipping traffic and hydrocarbon exploration will require improved capabilities for responding to potential oil spills in ice-covered waters. It is estimated that there are 17 billion barrels of undiscovered economically recoverable oil in the Beaufort and Chukchi Seas outer continental shelves alone (National Research Council, 2014). While oil exploration activities are close to shore (< ~30 km) in the Beaufort Sea, activity in the Chukchi sea is much further offshore (80-120 km). These areas thus span the full range of potential ice conditions, from the landfast ice-cover in shallow water in the Prudhoe Bay region, to drifting ice pack further offshore, and varying seasonally from thinner ice and broken ice conditions in a marginal ice zone, to deformed, continuous, drifting ice pack. While spills from subsea pipelines or well-head blowouts have been deemed to have a low probability of occurrence (but potentially high impact) the potential for minor spills due to shipping accidents is of concern as ship traffic increases, particularly in coastal areas (National Research Council, 2014). The range of ice conditions in which potential spills could occur, from the initial formation of ice crystals through to ice that is many years old, demonstrates the need for comprehensive strategy for oil spill response.

A critical component of any oil spill response in ice-covered seas is the development of a reliable strategy to detect and map the extent (and volume) of the spill. Such information is necessary to guide and inform appropriate response countermeasures (e.g. mechanical recovery, in situ burning, use of dispersants, or simply monitoring of the spill until such countermeasures can be performed). Despite decades of research into oil spill response for ice-infested waters by governmental organizations, academia and industry no operational product or service can yet remotely detect or track oil under or within sea ice. These fundamental deficiencies have been highlighted in numerous reviews, with recent commissioned reports stating that ‘all available technologies have serious drawbacks’ (e.g. USARC, 2004). These methods include electromagnetic induction, impulse radar, acoustics and laser fluorescence. A full description of these and other techniques along with their limitations can be found in the reviews of Dickins et al. (2000) and USARC (2004). The fundamental difficulty with all these techniques is the sensor has to ‘see through’ the sea ice and its snow cover to be able to infer the presence or absence of oil.

Snow and sea ice are highly heterogeneous spatially and temporally. This severely impacts the usefulness of surface-based techniques. Logistical difficulties presented by operating in the marginal ice zone, access and travel over ice in winter, snow-hidden regions of thin ice, and operating in the extreme Arctic environment, suggest that on-ice detection methods can be impractical to impossible for many regions. Airborne methods may be further hampered by availability of light and weather. A search method that can operate independent of ice conditions and can detect oil in a variety of scenarios is highly desirable.

The capability to directly sense oil under ice by sensing from below using an autonomous underwater vehicle (AUV) is an extremely attractive alternative as it avoids most of the difficulties of surface-based techniques and operations can be largely independent of ice

and weather conditions. The complexity of the under ice topography and hence, the spread of oil under ice (Wilkinson et al., 2007), also support the utility of an AUV-based approach. AUVs can cover large areas without the impediments that complex ice terrain, such as thin ice, multiple floes, ridges, or rubble fields would impose on a surface-based approach. The flexibility of current AUV technology and the unimpeded view of the oil permits detailed mapping of both the extent of the oil under complex terrain and potential determination of the oil thickness. To develop this response capability, AUV technology must be proven in ice-covered waters with the capability for reliable, operational rapid deployment and recovery, complex missions under ice in a variety of conditions, and armed with a sensor suite proven to detect oil under sea ice.

This project aims to progress toward these goals by advancing AUV operations in ice-covered waters and to develop and test appropriate sensor technology in laboratory studies to determine their potential for detection of oil under ice when deployed on an AUV.

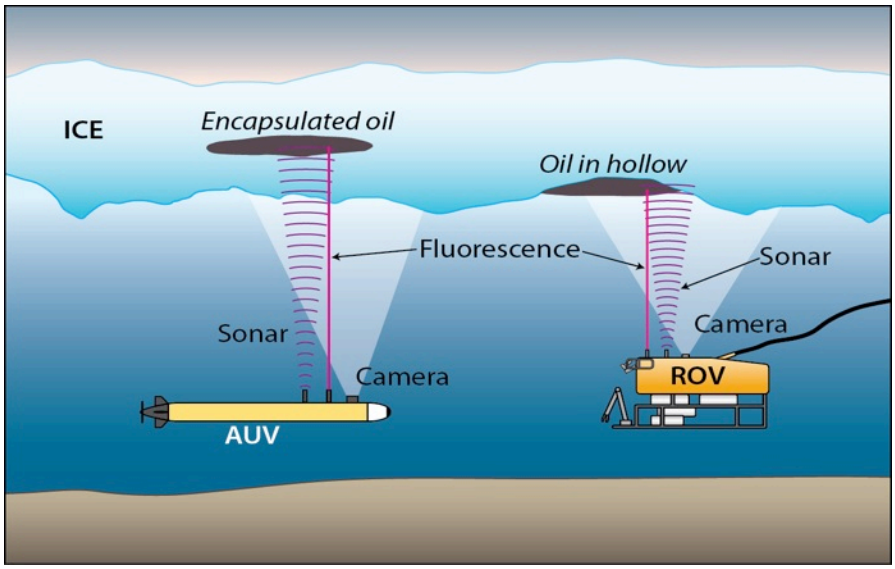


***Figure 2.1.1*** *AUVs and ROVs can be equipped with a variety of sensors to detect oil spills in ice covered waters.*

## 2.2 AUV operations under sea ice – the SeaBed class of vehicles

The last several decades have seen development of an increasing variety of underwater vehicles developed for a wide variety of research, naval, and commercial applications. Both Remotely Operated Vehicles (ROVs) – unmanned vehicles that are controlled from the surface over a tether – and AUVs may both be appropriate platforms for oil spill detection and mapping under sea ice. ROVs are a mature technology that has been widely used in the oil and gas industry, and are relatively straightforward to use under ice. The control afforded by the tether can enable careful maneuvering in tight spaces such as may be found under fast ice in shallow water. However, the tether generally limits the range of an ROV and it can be less flexible logistically than and AUV, particularly in complex ice conditions. ROVs range greatly in size, capability, and payload. In the oil industry, two loosely defined classes are used. Inspection class vehicles are typically ~30-100 kg in

weight with sensor payloads of 10-15 kg and a power budget of up to several kW. The larger work class vehicles may weigh up to several tons, carry payloads of over 200 kg, and have rated power of over 100 kW.

For an AUV, the absence of a tether makes them often easier to deploy and recover and permits missions of much greater range than ROVs. For oil spill response, this enables much broader search missions so that large spill or search area scenarios can be conducted. This affords a greater independence from ice conditions. Long-range AUVs could potentially be launched from an ice edge or in light ice conditions, or even from shore, enabling a more rapid response and much greater flexibility. The lack of tether, however, severely limits real-time data rates to the capabilities of acoustic modem systems, and increases the complexity of vehicle navigation.

AUVs have become ubiquitous in oceanographic applications. In the last decade they have been used in diverse applications including offshore surveys, fisheries, marine geology, marine chemistry, marine biology, marine archaeology, and recently, under ice shelves and sea ice. AUVs can perform missions ranging from several to hundreds of kilometers in length. By 2006 the offshore oil survey industry had logged over 100,000 km and 10,000 hours of operational experience with AUVs (Hagen et al., 2006). However there are far fewer examples of AUVs working under ice.

The Odyssey class AUVs were deployed through the Arctic ice in 1994 (Bellingham et al., 1994). In 1996, the Theseus AUV laid cable for an under-ice acoustic array over a distance of several hundred kilometers (Thorleifson et al., 1997). More recently, the Autosub AUV has performed missions under Antarctic ice shelves (Perkins, 2006, Jenkins et al., 2010), Arctic drifting sea ice (Wadhams et al, 2003), and under fast ice (Plueddemann et al., 2012). As with ROVs, the power availability, payload, and range very greatly. Larger vehicles (e.g. Autosub) can supply power of several kW and payloads of up to ~100 kg, but require greater logistic support than smaller AUVs (e.g. REMUS 100). For an oil spill mission, there will be trade-offs between logistical support, sensor payload, and range.

The WHOI SeaBed class of AUVs has recently performed a number of missions under sea ice in both polar oceans (Sohn et al, 2008, Kunz et al., 2009, Williams et al., 2013, Williams et al., submitted).

The fundamental issues that govern the use of AUVs for oil spill response under-ice include size, shape, and requirements to survey the underside of ice, ice conditions (pack ice or landfast ice), navigation under-ice, and the concepts of mapping in a dynamic environment.

The WHOI SeaBed class of AUVs has worked successfully under ice with efforts centered on smaller, more maneuverable vehicles (Singh et al 2004). The defining differences between other (larger and more expensive) AUV programs and the SeaBed vehicles include a requirement for working close to the seafloor and the underside of ice; a requirement to deploy in an area that is permanently covered with drifting ice; and the ability to accommodate a large and changing suite of scientific sensors based on the mission at hand while maintaining the accuracy of the associated navigation to meter or sub-meter levels.

Originally developed for mapping the sea floor, the original SeaBed vehicles feature a dual-hull design (Fig. 2.2.1). The AUVs are hover-capable, enabling precise movement in complex terrain, and the ability for precise control for deployment and recovery – a

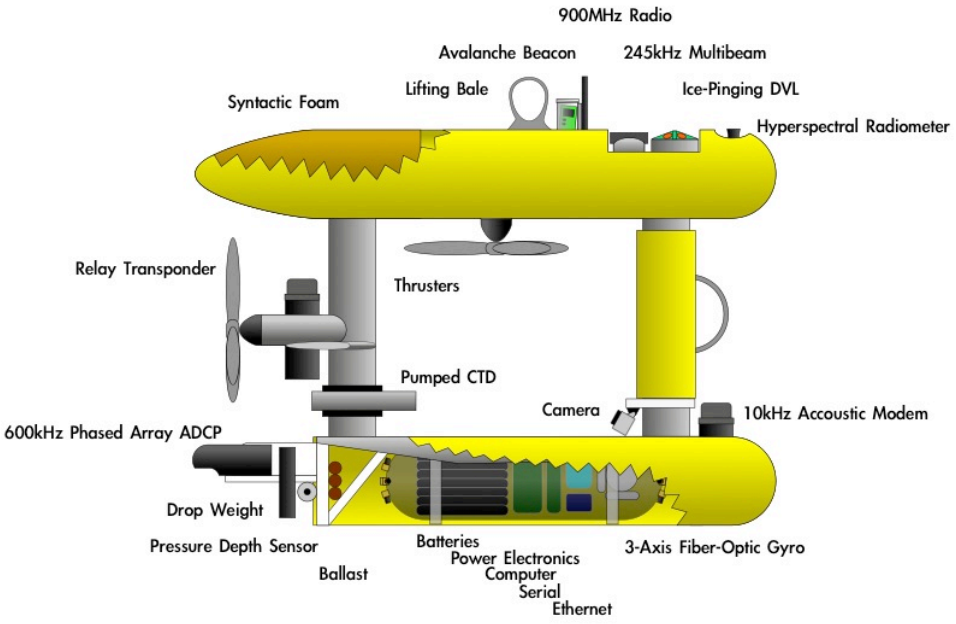


***Figure 2.2.1*** *The Jaguar AUV, one of the SeaBed class of vehicles developed at WHOI, configured for under-ice mapping. This configuration required the multibeam, ADCP and other sensors to face up towards the ice as opposed to looking down on the seafloor (courtesy P. Kimball).*

valuable feature for deployment through a small hole in landfast ice or in close-packed ice. The heart of this AUV system is custom, open sourced software. It is primarily the continued development of this software over the past decade that has driven improved capability for under-ice missions in a variety of scenarios. Recently, a small, inexpensive 100m depth capable torpedo-shaped SeaBed AUV (SeaBed 100) has been developed specifically for long-range transects under sea ice. A torpedo-shaped vehicle is more operationally limited in shallow environments with rugged ice conditions due to more limited maneuverability, but can travel at greater speeds so is more appropriate for large-scale search and surveys and in high currents.

Sea ice mapping missions to date with the SeaBed vehicle (Williams et al., 2013, Williams et al., submitted) have relied on navigation in an ice-centered reference frame. The navigation systems typically involve inertial navigation (which determines position from changes in vehicle velocity provided by the 3-axis Fiber-Optic Gyro) and bottom-tracking Doppler velocity logs (which detect the vehicle velocity relative to the ice) augmented by acoustic transponders placed on the seafloor or moored in the ice. Doppler velocity logs and acoustic transponders generally provide more precise positioning under a single floe or multiple floes that do not move relative to one another. In close-packed ice or under landfast ice, this is the simplest and most appropriate means of navigation.

However, in a dynamic ice environment, with relative floe drift and rotation, particularly in broken ice conditions (such as in the marginal ice zone), the AUV will move in an earth-centered reference frame, while the DVL and transponders both operate in an ice-centered reference frame (Fig. 2.2.2). A solution that has been used in mapping Antarctic ice floes is to place GPS receivers on the floe so that the motion may be compensated in post processing to arrive at a consistent map of the environment. When traversing large areas and multiple floes, this strategy may be impractical.

The above methods have proven reliable for precise scientific surveys of limited area (under ~1 km) under individual floes, where deploying on the ice is possible and time is not a major constraint. To transition this capability to an operational oil spill response requires extending these capabilities so that rapid deployment and recovery from a vessel, potentially moving relative to the ice is possible and extend the survey capability to variable ice conditions, including long-range capabilities under multiple floes. Ideally, this requires the ability to:

1. Maintain constant communication with the vehicle so that its position is always known to the operator
2. Navigate continuously in a constant reference frame, even when passing under multiple, independent floes
3. Telemeter real-time data to provide the operator with situational awareness and real-time location of oil, and the ability to modify the mission on the fly if oil is detected, providing a more efficient mapping of the spill
4. Run missions from a response vessel without the need to place transponders on the ice.

A final, critical aspect of AUV operation under sea ice is the need for long-range acoustic communication, both for determination of vehicle position (Fig. 2.2.2) and vehicle status, but also for real-time telemetry of data. Fortunately, in the Arctic, the upper ocean temperature and salinity profile is such that a sound channel exists in the upper ocean under the ice, with transmission of acoustic data possible over tens of kilometers for low data rates of 5-10 bits per second (Freitag et al., 2012). Under fast ice in shallow water, this range is expected to be much less only as line-of-sight communication is possible, and interaction with the complex ice underside or seafloor may limit sound propagation. For efficient operation of AUVs in the coastal landfast environment, the ability to transmit data over ranges of kilometers is desirable, but this capability is not yet proven.

Within this project, each of these capabilities were successfully tested with the SeaBed class AUV. These trials are described in Chapter 3, below.

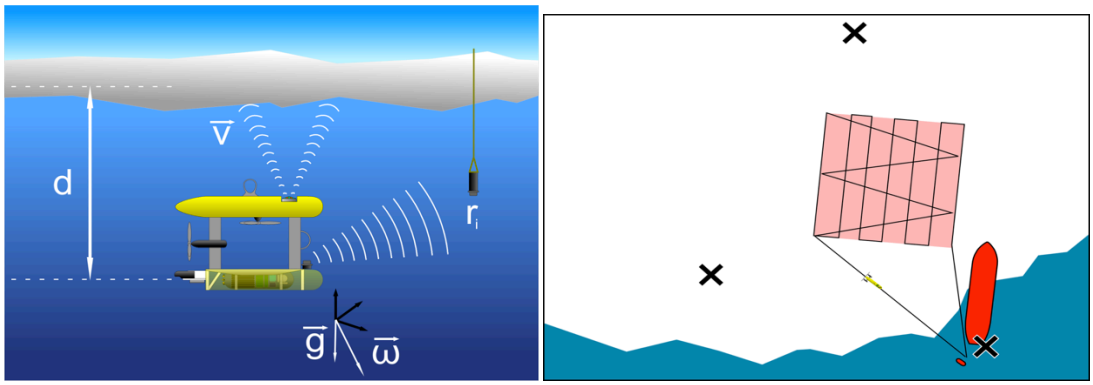


***Figure 2.2.2*** *AUV Navigation under ice has typically relied on inertial navigation systems coupled with bottom-tracking sonar and transponders moored on the ice (left). Ice topography mapping missions have involved gridded surveys under an ice floe, with the position of the vehicle constantly monitored via acoustic transponders deployed through the ice and an acoustic modem from the mother ship (black crosses) (right). (P. Kimball).*

## 2.3 Remote sensing technology for detection of undersea oil spills

In addition to the operational capabilities of AUV navigation under ice, to develop a complete operational system for oil spill mapping and detection requires the integration of an appropriate sensors suite capable of detecting oil in the range of spill and sea ice scenarios likely to be encountered.

In some cases, oil spills under sea ice may be detectable in the water column (such as in a plume from a subsea well-head blowout or pipeline leak). In such cases, water sampling sensors which directly sense hydrocarbons in the water column can be useful. These are reviewed in Wilkinson et al. (2013). Nevertheless, because the buoyant oil will pool and spread underneath the sea ice, potentially become encapsulated within it and/or drift with the ice, the capability to map the extent of the spill beneath the ice is a critical capability for an effective response strategy. This report is focused on those sensors with potential for remote detection of oil under, and potentially encapsulated within, sea ice.

Because of the changing nature of the sea ice cover, ranging from broken and scattered floes in the marginal ice zone, to thick, heavily deformed ice in the drifting pack, to relatively level landfast ice, to ice cover of mixed floes sizes and thickness, and strong seasonal variability (see e.g. Dickens, 2011, Thomas and Dieckmann, 2009), the nature of the oil spill and it's interaction with the ice varies tremendously (Dickens, 2011). Thus, no one sensor is likely to be optimal in all scenarios.

In open water, a typical spill will spread to a fraction of a millimeter thick. Under midwinter ice, it may spread to 4-9 cm thick (SL Ross, 2010), although potentially much thicker in areas of deformed and variable thickness ice that harbor many under ice depressions where oil can become trapped (Wilkinson et al., 2007). Consequently, the extent of the spill may be orders of magnitude less than for an equivalent open water spill (Dickens et al., 2011). For a relatively modest flow rate from a breached subsea pipeline

under drifting ice, however, the oil may disperse within the water column before reaching the ice underside. Depending on the rate of ice drift relative to the flow rate, the oil may form a very thin layer on the ice underside, or the spill may be distributed irregularly (Norcor, 1975). In broken ice conditions such as are found in the marginal ice zone, the spreading of the slick and its thickness will depend on the ice concentration (Dickens, 2011). Oil may also become encapsulated within the ice as it continues to grow in winter, or incorporated during initial ice formation (Dickens and Buist, 1999, Dickens, 2011). Each of these possibilities suggests that different sensors may be useful under different scenarios. Wilkinson et al. (2013) reviewed potential AUV-based sensors for oil detection under sea ice, both in the water column and pooled beneath or within the ice. Here, we are concerned with the latter. This project therefore focuses on a suite of three basic sensor systems with proven capability to detect subsea oil remotely that could be adapted for remote detection of an oil layer pooled beneath sea ice. These are cameras, laser fluorometers, and sonar systems.

### 2.3.1 Cameras

Camera systems are a well-established, widely used technology on ROVs and AUVs. They have the advantage of being easy to interpret (by a human operator). However, they can be limited by available light and turbidity (which will limit range), are unable to detect disperse oil droplets (particularly at low concentration), and interpretation may be difficult under complex ice topography or for encapsulated oil. While camera systems would certainly be part of an AUV-based sensor suite for oil detection, complementary sensors are necessary for detection, and particularly for quantification, of oil in the full range of anticipated spill scenarios.

### 2.3.2 Laser-induced fluorescence

The basic principle behind remotely induced laser fluorescence is straightforward. An ultraviolet (UV) light source (or, to a lesser degree, longer wavelengths) excites broad-spectrum fluorescence in oil (but also other compounds), which is then detected by a sensitive spectrograph or similar light detector. While a range of light sources can be used, we focus here on laser sources because compact, low-power sources that can produce an intense long-range excitation are widely available. Airborne laser fluorosensor systems have been described in a number of reviews (e.g. Brown and Fingas, 2003, Jha et al., 2008, SL Ross et al., 2010), so will not be discussed in detail here. A typical system consists of one or more commercially available UV lasers, in the 300-380 nm range. Some systems will also include a visible laser for optical excitation (e.g. 480 or 532 nm), which will induce fluorescence to a lesser degree than UV light. The fluorescence is generally received through a telescope connected to a photomultiplier and spectrum analyzer, a gated intensified diode-array detector, or with an intensified CCD camera. Existing airborne systems are far too large to be adapted for use on an AUV/ROV platform, and expensive (Jha et al., 2008).

There are several reasons that investigation of a remote laser fluorosensor for an AUV platform is practical. Such a sensor could potentially detect oil in practically any concentration or ice conditions, including oil trapped beneath the ice, suspended in low concentration in the water column, and potentially even encapsulated within the ice (where detection remains a challenge for all other sensors), and under continuous ice,

brash, or loose pack. Although attenuation in the water column is a major issue, an AUV can easily operate within 10-20 m of the ice or subsea plumes – much closer than airborne surveys, and so a smaller, more compact sensor is possible.

Unlike airborne systems relatively little work has been done to develop a compact laser fluorosensor for underwater use, particularly for under ice, although the basic principle is straightforward. The primary challenges with an underwater system are the attenuation of UV light in the water column, potentially high levels of ambient background light, and confounding factors like other fluorescing compounds (dissolved organic matter, or DOM, and chlorophyll), and scatterers (particulate and ice).

Below about 400 nm, attenuation by the water becomes important, so that UV-lasers with significantly lower wavelength (e.g. 308 nm of some Xenon excimer lasers) are not a practical choice. Ambient light also becomes an issue in the daytime, although this is mitigated if operating under thick ice or in deep water. Underwater laser fluorosensors have recently been investigated for biological studies. A ship-based system has been demonstrated for discrimination of live and dead coral at depths of up to 30 m (Sasano et al., 2012).

Limited success with a laser line scan system to detect submerged oil was achieved in ice tank tests at Ohmsett (Hansen et al., 2009). These tests are the most directly comparable to the conditions that might be expected for an AUV-based system under sea ice. They mitigated against UV attenuation by using a 405 nm violet laser. While somewhat above the preferred wavelength to induce fluorescence, the availability of high-powered violet lasers and superior attenuation in water versus true UV lasers makes such a system preferable. The primary difficulty encountered by Hansen et al., (2009) was signal saturation due to solar radiance. This can be mitigated against by using phase-sensitive detection techniques that reject background signals that are not modulated at the same frequency as the laser source (Bello and Toomey, 2012).

### 2.3.3 Sonar Systems

A wide variety of sonar systems have been deployed from ROV and AUV platforms. These include single-beam echosounders capable of profiling the water column or ranging to a target, sidescan sonars for imaging the seafloor, 2D imaging sonars that provide high-resolution acoustic imagery for underwater inspection or obstacle avoidance, and multibeam sonars that can provide swath bathymetry maps of the seafloor, underside of sea ice, or of other features in the ocean. The primary advantages of acoustic detection are the ability to “see” in low visibility waters where cameras cannot, long range sensing capabilities, and for high-frequency sonars, the potential to provide unique quantitative information on sound scatterers (e.g. droplets) from the acoustic backscatter information.

Acoustic techniques are a relatively new method of oil detection that have shown promise in a variety of subsea oil spill scenarios. But there are few experimental data on the technique. Narrowband acoustic backscatter systems have recently been used to monitor the Deep Water Horizon oil spill plume (Weber et al., 2012). Recent laboratory and theoretical work has investigated the acoustic detection of oil droplets in the water column (Panetta et al., 2013). Multibeam sonar has been used to discriminate heavy oil

on the seabed from sand based on its backscatter signature (Hansen et al., 2009). Moreover, there is very limited data for acoustic detection of oil under ice. There have been a small number of measurements and theoretical studies involving the use of high-frequency acoustic scattering techniques to detect and/or quantify sea ice (e.g. Stanton et al., 1986, Williams et al., 1992, Xanaki et al, 2013). However, none of these studies have explored broadband acoustic scattering techniques, investigated the effects of oil under sea ice on acoustic scattering, or examined the potential for detection of encapsulated oil. Recently, experiments with an inexpensive high-frequency, narrowband sonar, Wilkinson et al. (in press) have demonstrated that a thin layer of oil can be detected beneath sea ice through detection of acoustic returns from both the oil/water and oil/ice interfaces (Fig. 2.3.1)

Traditional scientific echosounders, or "sonars", employ short duration gated sine-wave signals with narrowband frequency-content (Bishop, 1989) to detect and image the under-side of sea ice, and many other physical and biological targets and processes in the ocean. Emerging broadband techniques employ broadband signals, typically linearly increasing frequency sweeps or "chirps", allowing the scattering as a function of frequency to be measured. This spectral information results in improved acoustic classification, and consequently improved quantification. Furthermore, the broadband nature of the signals enables time-domain matched-filter processing to be performed, thereby dramatically improving the range resolution of the measurements (Chu and Stanton, 1998). This may improve the ability to detect oil encapsulated within the ice as lower frequency signals can be used (attenuation in ice is greater at higher frequencies) while maintaining range resolution.

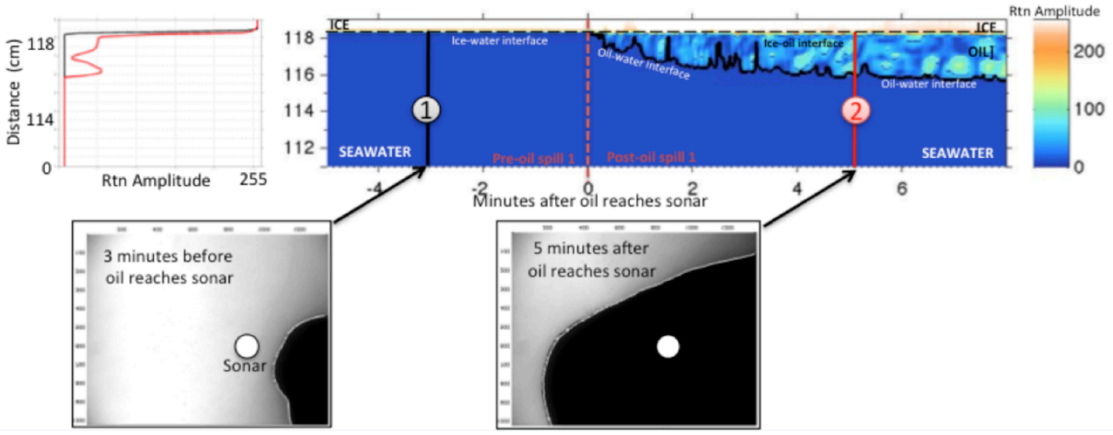


***Figure 2.3.1*** *Acoustic scattering from the oil-water and oil-ice interfaces for a 2 cm thick layer of oil spilled under level sea ice (upper panels). Photography from below prior to and after spread of the oil confirms the detection (from Wilkinson et al., 2014)*

A more complete description of AUV-based sensors for oil spill detection under ice can be found in Wilkinson et al. (2013) (http://www.arcticresponsetechnology.org/)

## 3. AUV Operations

Results from three AUV test mission with the SeaBed-class Jaguar AUV are described here. The overall aim was to demonstrate the ability of the AUV for rapid response to perform an oil spill search and mapping mission under sea ice. As described in section 2, above, an effective AUV-based oil spill search requires flexibility to operate in varied ice conditions and from multiple vessels. To evolve from small, gridded surveys under individual ice floes with a ship moored to the floe (i.e. in the same floe-centric reference frame) to larger-scale adaptable missions under multiple floes from a potentially non-stationary ship, the following objectives were tested:

1. Rapid deployment from a vessel without need to deploy transponders on ice
2. To simulate a search mission where an operator monitors for oil in real time, perform a mission with real-time acoustic transmission of sensor data providing a proxy for oil detection
3. Perform a standard mapping mission solely from a vessel (i.e. without deploying transponders on the ice) in marginal ice zone conditions
4. Perform a relatively long-range mission under variable sea ice, including multiple floes, in a drifting pack
5. Perform an adaptive mission to demonstrate the ability for an operator to remotely change a mission to respond to an oil detection event to map a spill. This mission has application to large-scale search strategies and adaptive mapping, and detection of undersea pipeline leaks where an extended search
6. Test acoustic communication in shallow water under ice to determine the potential range of operation

These AUV objectives were achieved in two primary deployments: 1) under ice testing of in relatively shallow water in the Great Lakes and 2) testing from the USCGC Healy in the marginal ice zone of the Chukchi/Beaufort Seas. In addition, a test of adaptive mission was performed in open water in Woods Hole, MA, and tests of acoustic communication under landfast ice in shallow water were performed at Prudhoe Bay.

### 3.1 AUV Missions under lake ice in the Great Lakes

The Jaguar AUV (a SeaBed class vehicle) was deployed from the USCGC Hollyhock during a Coast Guard spill mitigation demonstration exercise to test mission strategies, deployment and recovery, and real time data telemetry. Conducted Feb 19-21, 2013 in Mackinac Strait, Lake Huron, this exercise provided an example of the potential for rapid operational deployment of the vehicle in response to an oil spill.

#### 3.1.1 Mission Preparation

The Jaguar AUV has a dual-hulled design, so normally it is shipped broken down, and requires a couple days on site to put together, test, and ballast before missions can be run. To demonstrate the ability for relatively rapid deployment the AUV was pre-ballasted at WHOI before shipment and shipped intact in a 20’ container, together with all required support equipment. This container was loaded onto the foredeck of the vessel on the morning of February 19 and served as both a staging and storage container and as a command center during missions (Fig. 3.1.1 and 3.1.2). While this is a sensible approach when deploying from a new vessel, it was clear that the operation would be most

effective with a dedicated containerized command station with built in heat, power, and lighting.

The first day of operations was spent ballasting the vehicle – i.e. altering the buoyancy so that when completely immersed it was only slightly positively buoyant. This is critical so that thrusters can dive and surface the vehicle effectively, and in the event of a problem, the AUV can rise to the surface rather than sink. Although the plan was to minimize the need for ballasting on site, further ballasting was required on site as this was the first time the vehicle was deployed in fresh water. For operational use in the Beaufort/Chukchi Sea, this could be mostly done prior to deployment, so missions could be run more rapidly.

The first mission was run on the afternoon of the Feb 19th – the first day of the exercises. First, two Benthos Teledyne LBL acoustic transponders and a WHOI micromodem were suspended from the starboard side of the vessel. The LBL transponders provide acoustic ranging to position the vessel, while the micromodem allows acoustic communication with the AUV and telemetry of data during the mission. Because of the limitations of the vessel, both transponders were placed forward of the bridge, providing a baseline of only about 15 m in length, which limits the accuracy of positioning. This was adequate for the short-range missions that were conducted, but for missions of several hundred meters or more from the vessel, a longer baseline is desired. This may be impractical for missions from relatively small vessels, so a means for establishing a longer baseline, possibly by deployment of transponders from a dedicated buoy lowered from the ship, is desirable.

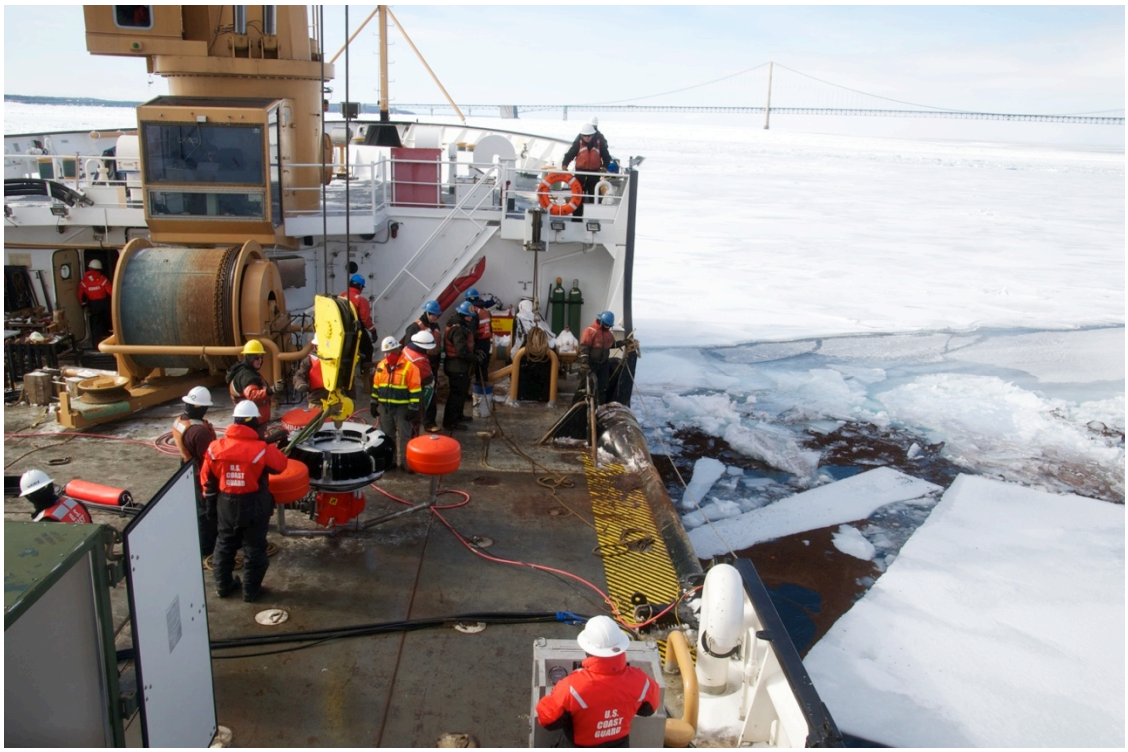

***Figure 3.1.1*** *The foredeck of the USCGC Hollyhock from where operations were staged. The AUV container is just left of the picture. The base of the crane used for deployment and recovery is visible at the center. The ice under which the AUV performed its mission is visible ahead, with the Mackinac bridge in the background.*

A problem with initial free-floating testing of the vehicle occurred with the vehicle descending to the bottom. This necessitated recovery using an Ocean Engineering Phantom HD2+2 ROV from Lake Erie Diving. Because of the extremely limited visibility, a micromodem was mounted on the ROV so that distance to the AUV could be determined and the AUV was located by moving the ROV to minimize this range. Recovery effort took about three hours. It was determined that the primary cause of the failure was due to icing of the Paroscientific depth sensor. In this case, the vehicle fails to obtain an accurate depth reading, and continues to descend. This problem appears to be associated with freshwater dives in sub-freezing temperatures only. Two factors would mitigate this behavior in deep salt water. First, saltwater forms a brine film between the ice and vehicle surfaces when it freezes, so that the ice does not adhere as readily to the vehicle or its sensors. Second, if the vehicle continues to descend into deeper ocean water, it will encounter a layer of warmer water which will melt ice covering the sensor, and the vehicle would then respond and the mission instructions would then tell it to rise back to the surface.

***Figure 3.1.2.*** *The Jaguar AUV in the storage container on the deck of the Hollyhock. The vehicle was pushed out of the container on the wooden A-frame trolley, where it was hooked to the ship's crane for deployment.*

### 3.1.2 Under-ice real-time sensor data telemetry

An important capability for oil spill response operations is the ability to transmit sensor data in real time. This was tested in the under ice mission in Lake Huron performed on the third day of exercises once the vehicle software was improved to ensure that in the event of a similar failure, the vehicle could be called back via commands over the acoustic modem.

The mission was conducted in the late afternoon as other projects by other exercise participants were conducted during the morning and early afternoon. While this delayed the mission, it also demonstrated the rapidity with which a mission could be conducted. Checking ballast, testing communication, a test dive and resurface, and the actual mission, including recovery, were all conducted within two hours.

***Figure 3.1.3.*** *Ice conditions during the mission. Level ice was about 6 inches thick, with several small ridges in the vicinity.*

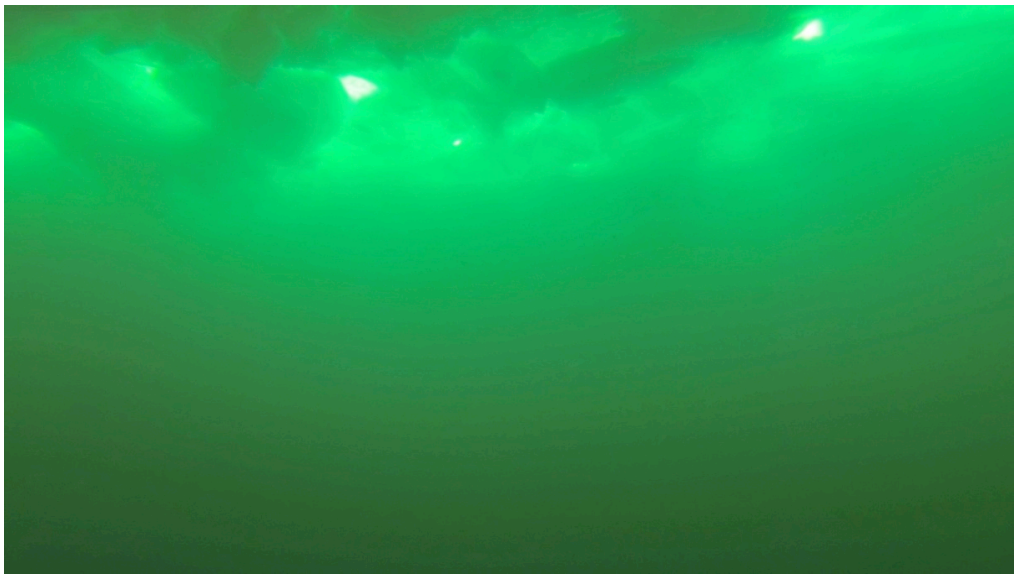

***Figure 3.1.4.*** *The underside of the ice as seen from a camera mounted on the Jaguar AUV.*

This mission was limited to a simple 100 m out-and-back run under thin ice with modest ridging (Fig. 3.1.3, 3.1.4), although there is little substantive difference between this short mission and a longer mission, except for less accurate real-time positioning at longer ranges due to the lower relative length of the long-base line acoustic array. The vehicle returned to the open water area in which it was deployed, and returned to the vessel using RF remote control once it had surfaced.

Onboard the AUV were an Imagenex Delta-T multibeam sonar, Paroscientific depth sensor, 600 and 1200 kHz Acoustic Doppler Current Profilers (ADCP), a Satlantic HyperOCR hyperspectral sensor, and a GoPro camera.

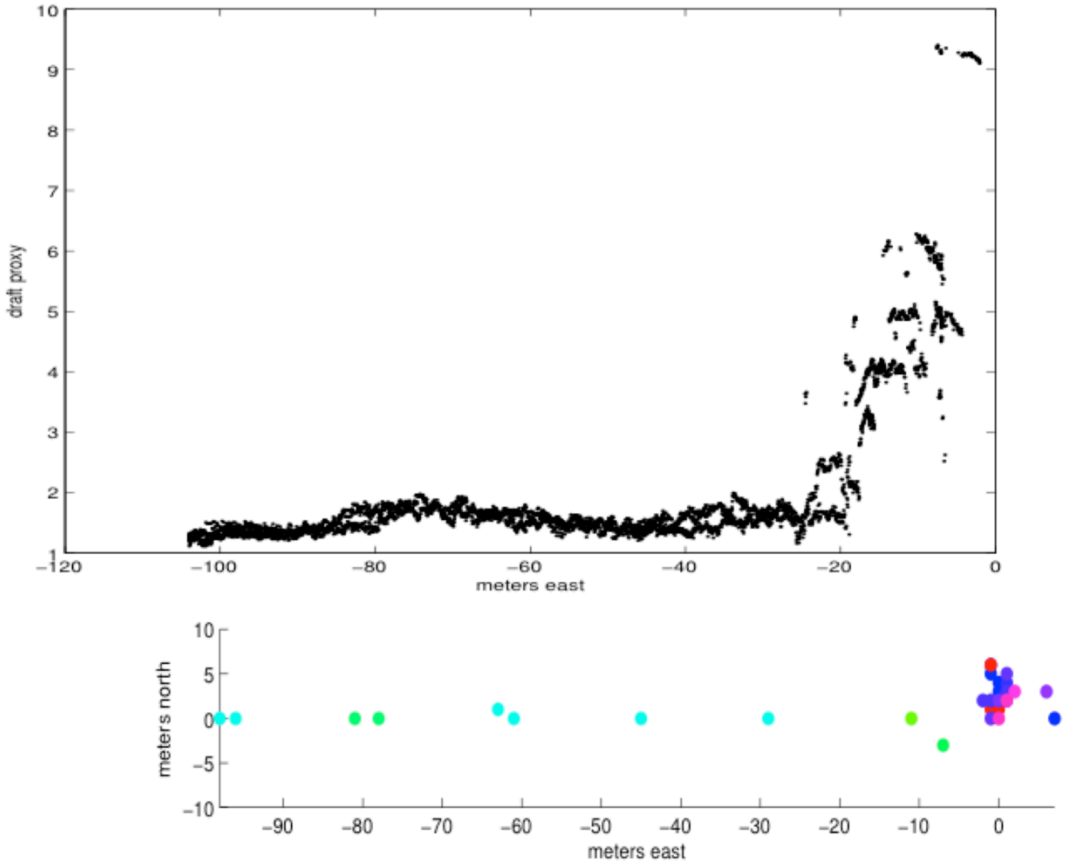


***Figure 3.1.5.*** *Ice draft proxy determined by subtracting the ADCP range to the ice bottom from the AUV depth (determined by a Paroscientific pressure sensor) (top). There is an offset to this due to positioning of sensors, so these are relative positions. The deep drafts between 0-20 m are from the ship keel. A slight increase in thickness is observable between 70-80 m. A hyperspectral radiance channel provided another thickness proxy (bottom) by observing the attenuation of sunlight through different ice thickness (blue is thinnest – i.e. highest solar radiance, purple is the least radiance). This shows the lowest light under the ship and the slightly thicker ice at ~80 m. This is a potential proxy detector for oil, where the oil should attenuate light strongly.*

Navigation and depth data were transmitted to the operator as in normal operation. This also included the ADCP range to the bottom of the ice. In addition, a single channel from the hyperspectral unit was transmitted to provide an estimate of the light penetrating

beneath the ice, which provides both a proxy for whether the vehicle is under ice (low light levels) or in open water (where light levels will be higher), but can also serve as an indicator for the presence of oil. This is because oil will strongly attenuate light, so that where the range to the ice (i.e. thickness) has not changed significantly, but a significant drop in one or more spectral channels is detected, this can provide an indication of the presence of oil. Given the large bandwidth required to send digital imagery, a few hyperspectral channels may provide a low data rate alternative. Ice draft would normally be provided by an upward looking sonar (in this case, the ADCP)

During the mission, changes in ice thickness were determined by subtracting the range to the ice (provided by the ADCP) from the vehicle depth (provided by the pressure sensor) (Fig. 3.1.5, top panel). At the same time, a single channel from the hyperOCR showed attenuation of light consistent with the estimated ice thickness (Fig. 3.1.5., bottom panel). Change in the detected solar radiance indicates greater attenuation of the light through thicker ice (and possibly snow). This suggests that it may be possible to provide a preliminary oil detection metric that requires transmission of only a small amount of data by detecting changes in the strength and spectral variation of transmitted light. While a camera has the advantage providing image textural information to aid in oil detection, it only provides three spectral channels. Greater spectral information may aid in discriminating changes in light level due to changes in snow cover, which has different spectral attenuation characteristics than oil (changes in ice thickness are most readily detected by sonar). Testing of a hyperspectral sensor with realistic oil spill tests coincident with a camera system is warranted to determine if oil under ice can be reliably detected with this sensor.

Based on this exercise, we have identified the following recommendations for under ice AUV missions in response to an oil spill:

1. For rapid response, a dedicated container or mobile lab that can be placed on a response vessel with a pre-prepared and ballasted AUV is the most efficient means of operating.
2. Until routine operational use has been established, an ROV for vehicle recovery is advisable.
3. Care should be taken to prevent icing of the vehicle in cold weather. This might involve rapid deployment from a well-heated container via a dedicated gantry.
4. For rapid deployments directly from the ice (for example, from fast ice at Prudhoe Bay, when a vessel is not available), similar infrastructure is required. In such cases, a smaller AUV, such as the SeaBed 100, may be more appropriate as it is designed to be deployed by hand by two people. In this case, all equipment could be transported on sleds pulled by snowmobile or tracked vehicles.

### 3.2 USCGC Healy AUV oil spill search and detection tests

Four AUV missions were run off the USCGC Healy during the Coast Guard Research and Development Center (RDC) Arctic Shield oil spill response exercises in September, 2013. These exercise were intended to test the deployment of various oil spill response technologies. The RDC goals were to evaluate the various technologies on board primarily to identify the logistics necessary for operation from the Healy, and to identify

possible limitations and possible improvements in the deployment, operation, and recovery of these technologies in a real oil spill response scenario. These included factors such as the length of time required for deployment and recovery, expertise required for operation, and constraints placed on other operations (e.g. ship movement) by the AUV operation. The exercise was not intended to test the actual efficacy of any technology for detecting or recovering oil. The USCG Research and Development Center (RDC) chose to run the exercise in a simulated oil spill response mode such that, when possible, all oil spill response technologies on board would be deployed together.

These considerations were somewhat peripheral to our objectives. The goals of the AUV deployment were to test the feasibility of particular oil spill search missions and AUV navigation under varied ice conditions. While many aspects of the logistics of operating from the Healy (e.g. deployment of transponders from the ship) are of relevance, to some degree, the logistics of deployment and recovery for the Jaguar AUV are not particularly germane to the broader goals of the AUV tests. For instance, it is expected that a single-hulled torpedo-shaped version of the SeaBed AUV would be most appropriate for long-range or large-area surveys.

The exercise was carried out near the September minimum ice edge – a region with variable ice conditions, significant quantities of thin ice and open water, and rapidly changing ice conditions in response to weather. This permitted testing in conditions more challenging than standard gridded surveys under individual floes that we have previously conducted in the Antarctic (Williams et al., submitted). This was a marginal ice zone (MIZ) scenario where broken ice conditions and multiple, small floes would be present – representative of an oil spill scenario in an offshore accident at the end of summer, or where a spill in open water is complicated by an advancing ice edge in the autumn.

In the MIZ, the ice cover is discontinuous, with multiple floes moving relative to one another. The thin ice cover may preclude deployment of personnel onto the ice, so that all operations must be from the ship. During the Arctic Shield exercise, this meant deployment from a ship that was not stationary relative to the ice, nor moored to the ice, so that the acoustic communication network necessary for vehicle navigation was deployed only from the ship (and not the ice).

These factors provided the additional challenge of separate reference frames for the ice, AUV, and ship to complicate navigation, a limited acoustic baseline for tracking the AUV position during missions, and the challenge of the vehicle moving from under moving ice to under open water several times during the mission, affecting navigational accuracy. It is these challenges that we aimed to test to determine the capability of the AUV for oil detection in MIZ conditions and to identify avenues for improvement in the AUV system so that its efficacy for oil spill search and detection could be improved.

### 3.2.1 Mission Objectives

With the considerations described above in mind, we identified the following objectives for the exercise.

1. Run a standard AUV grid mission under sea ice from the CGC Healy with an imposed constraint of not being able to deploy personnel on the ice. This would test the feasibility of rapid deployment and recovery. (section 3.2.2.3)

2. Run a mission under sea ice in marginal ice conditions or ice edge environment with variable ice conditions. This would test the feasibility of mapping under variable ice conditions (section 3.2.2.2)
3. Run a mission traversing under multiple sea ice floes to test the ability to accurately map oil spilled in this scenario. Similar to (2), above, this would test the ability of the AUV to navigate, in addition to providing a map in a consistent reference frame under multiple floes moving relative to one another and the vessel. (section 3.2.2.4)
4. Run an adaptive mission to simulate a large-area oil search phase, followed by a mapping phase when oil was detected. First, a coarse survey would be conducted to search for oil. Once oil is first 'detected' (in principle, this would be determined by a positive sensor response) a finer grid survey would be initiated by the operator to simulate the mapping of the detected spill. (section 3.3.2.5)

### 3.2.2 Ice Conditions

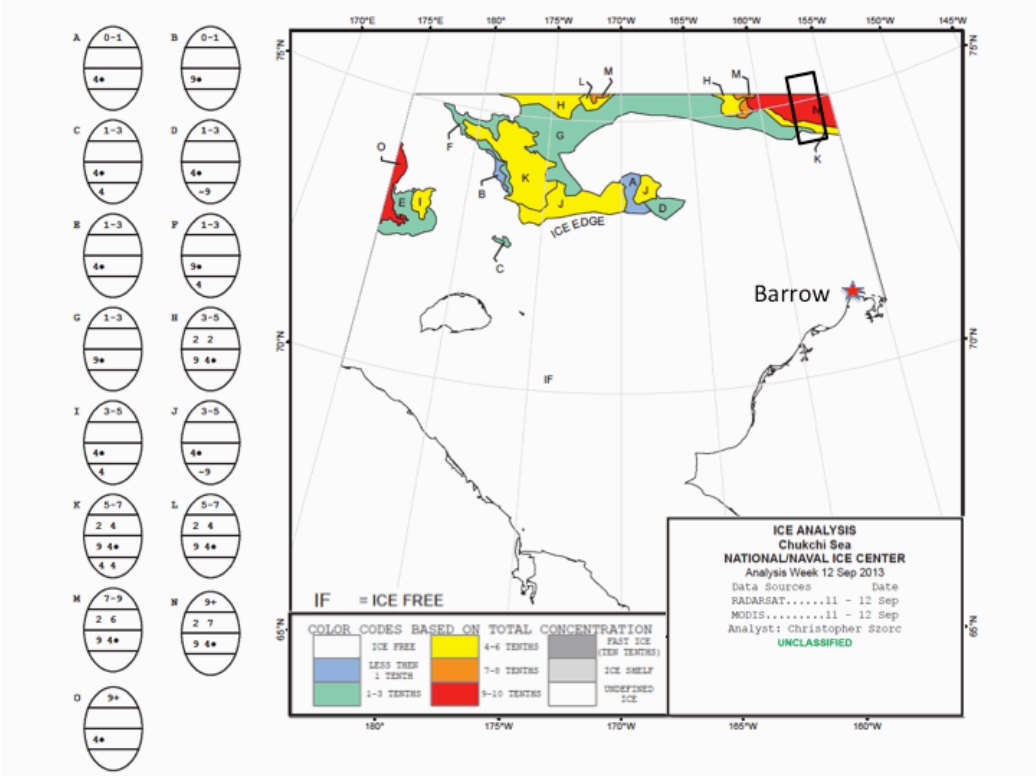


***Figure 3.6*** *National Ice Center ice chart for the week of September 12. The box indicates the approximate area of operation of the Healy during July 9-14. The ice edge in the area was fairly compact. Most of the operation was conducted in > 90% ice concentration (indicated by the red area). The ice chart suggested that ice conditions where a mixture of first year thin (30-70 cm) and thick first year ice (> 120 cm).*

The Healy travelled roughly due North from Barrow on September 8, 2013, reaching the ice edge on September 9. After traversing a narrow band of broken first year ice, the Healy entered a zone of ~95% concentration ice on September 9. The ice, as observed from the bridge, was a mixture of mostly level first year thin (30-70 cm thick) and thin ice and nilas (thin ice less than 10 cm thick). Broken floes were encountered in a thin band near the ice edge; north of the edge floes were typically 100-500m in size, with some big floes (500-2000m).

### 3.2.2 AUV missions from the Healy

#### 3.2.2.1 System setup and deployment from the Healy

As before, the AUV was shipped fully constructed for rapid deployment. The AUV command station was set up in the Aft control room, permitting a good view of the deployment and allowing direct feed of the ships navigational data into the AUV control station. The AUV was deployed via the aft A-frame (Fig. 3.2.1) as the port crane was not operating properly and the starboard crane was allocated to skimmer and small boat operations. This often required deploying and recovery of the AUV in thin or broken ice, as the ice tended to accumulate behind the stern of the vessel. A more desirable mode of deployment would be via the starboard crane, as the positioning of the ship relative to the wind during missions tended to keep the aft starboard of the vessel free of ice, and the reach afforded by the crane would allow greater flexibility in the deployment and recovery location to help avoid ice. Alternatively, deployment via the CTD winch is also a good option, as it would be very easy to bring the AUV in and out of the Baltic room for storage and keep it warm.

***Figure 3.2.1*** *A-frame on stern of the Healy viewed from adjacent to the vehicle conning station. This was used to deploy the AUV as the port crane reportedly was not working properly and the starboard crane was used for other operations during the exercise. Nilas (thin grey ice < 10 cm thick) and broken ice were frequently present off the stern so that the AUV was often deployed and recovered amongst ice.*

Although the vehicle was ballasted at WHOI prior to shipment, the extensive ice melt in the area freshened the surface water significantly; the salinity was ~25 ppt, or 5 or 6 ppt less than at the WHOI dock. A fresh-water layer above the saltier water below can complicate the AUV's failsafe behavior of floating passively to the surface in the event of on-board failure, so careful ballasting to achieve appropriate buoyancy was necessary.

The Jaguar AUV was outfitted with the following sensors:

1. Two RDI Acoustic Doppler Current Profilers (ADCP) – one providing current velocities and the second providing a Doppler Velocity Log for navigation beneath the ice, and underway ranging to the ice underside.
2. SeaBird SBE-49 CTD Fastcat to provide upper ocean properties
3. Imaganex Delta-T100 multibeam sonar to map the ice underside.
4. GoPro 3 camera for imagery of the dive.

#### 3.2.2.2 UAV MIZ mission

The marginal ice zone (MIZ) is typically characterized by thin ice, small or broken ice floes, and high temporal and spatial variability in ice conditions, often in the presence of waves or swell. There was little swell at the ice edge and the Healy was some distance from the edge, so there was no significant waves or swell to deal with for this mission. Such conditions would complicate deployment and recovery on a future mission.

***Figure 3.2.2*** *Ice conditions for Sept 9-10, 2013. Ice consisted of a mixture of broken ice, small to medium floes, and thin nilas (grey), and small patches of open water – typical of the MIZ.*

Ice conditions on Sept 9-10, 2013 consisted of a mixture of small and medium floes, broken ice, narrow expanses of open water, and thin nilas (Fig. 3.2.2), typical of the high Arctic MIZ. In such conditions, it is usually impractical to deploy personnel or equipment

on the ice, so for this mission (and all others on this cruise), we tested operation of the AUV with acoustic transponders deployed from the ship, rather than on the ice as we have done on prior under ice missions. Two acoustic transponders to assist in vehicle navigation were deployed - one near the bow on the starboard side, the second at the port stern – as well as a WHOI micromodem for communication with the AUV near the stern on lines to a depth of approximately 15m.

The mission was a simple out-and-back mission under the broken ice cover. This mission, although short, demonstrated the capability to traverse under multiple ice floes and maintain DVL navigation. With the transponder array fixed in the ship's reference frame, AUV navigation would be impacted if there were drift or rotation of the ice relative to the ship. Provided there is limited relative motion of ice floes relative to one another, the AUV reference frame could be transformed into an earth-centered reference frame using the AUV range data from the transponders and the ship's GPS and compass data, so that any spill identified by the AUV could be located. If significant relative ice motion occurred, then location of the spill would be determined solely by the transponder ranges and ships navigation data.

***Figure 3.2.3****. Recovery of the AUV by small boat in 100% ice cover.*

Recovery was accomplished with the small boat due to ice accumulation at the stern (Fig. 3.2.3). Under normal circumstance, recovery would be simpler to use the AUV remote control to guide it to open water on the starboard side if the crane was available, avoiding the need for small boat operations.

This provided a successful proof-of-concept of mission objective 2 – marginal ice zone conditions.

### 3.2.2.3 Rapid deployment gridded mission

In an area of larger floes in the vicinity of 74° 45' N, 157° W, about 200 miles from the ice edge, the Healy stopped adjacent to a small pool of open water (~300 m across) in near continuous ice, but with several broken floes and areas of nilas at the edge of the pool. Two missions were run in succession, a grid mission and a long out and back.

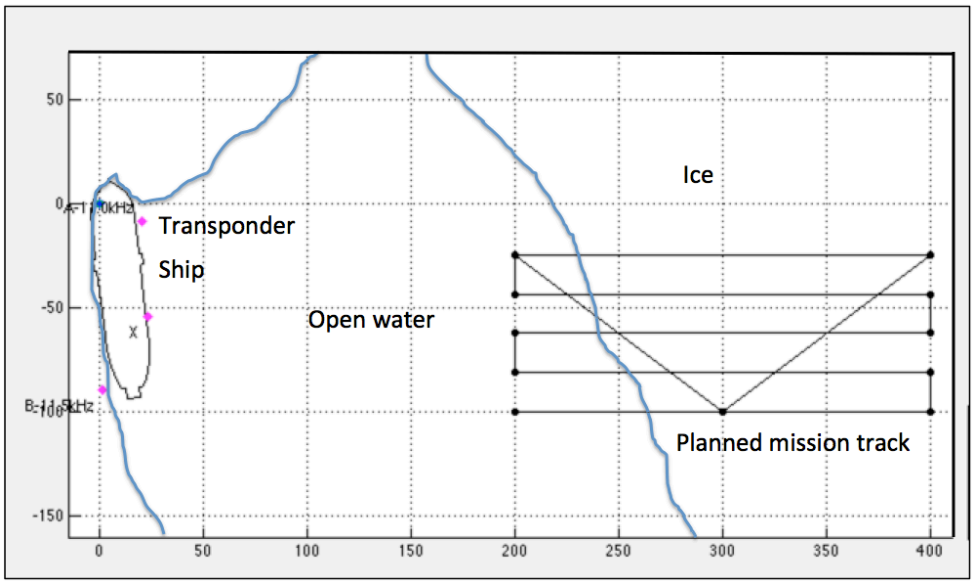


***Figure 3.2.4*** *Mission plan of the grid mission. The ship and approximate locations of the acoustic transponders for navigation and communications with the vehicle are shown on the left. The programmed mission track is on the right, with nominal position of the ice edge shown by the blue line.*

The grid mission comprised five track lines 200 meters long, spaced 15 meters apart. The AUV operated at a constant depth of 15 meters, and the total imaged area under the ice was about 20,000 square meters (Fig. 3.2.4). This mission is a standard ice mapping mission that has been performed on prior cruises, but with the transponder network deployed completely from the vessel. Unlike these prior cruises, the vessel was not moored to the ice, so that movement of the vessel within the AUV or ice reference frame was possible. These variations add some complexity in that the acoustic baseline provided by the transponder locations may not be ideal relative to the AUV position during the mission. The AUV location is determined while underway by triangulating the acoustic ranges to the AUV. Thus, more accurate positions can be obtained with a greater spacing between the transponders.

A further complication occurs if the ship moves relative to the ice or AUV. While underway, the AUV follows a programmed mission with best navigation provided relative to the ice using DVL. If the ship (and transponders) and/or ice move relative to the programmed mission, then the absolute AUV position will change relative to the vehicle reference frame. In this case, the AUV is programmed to return to open water near where the ship was when the dive initiated. If the ship and ice move relative to this location, the AUV will return to a different location, which may not be in open water. Securing or mooring the ship within the ice, or placing transponders on ice may not be

feasible in a rapid oils spill response, or in thin or marginal ice conditions, so this arrangement allowed us to test the logistics of running in this scenario.

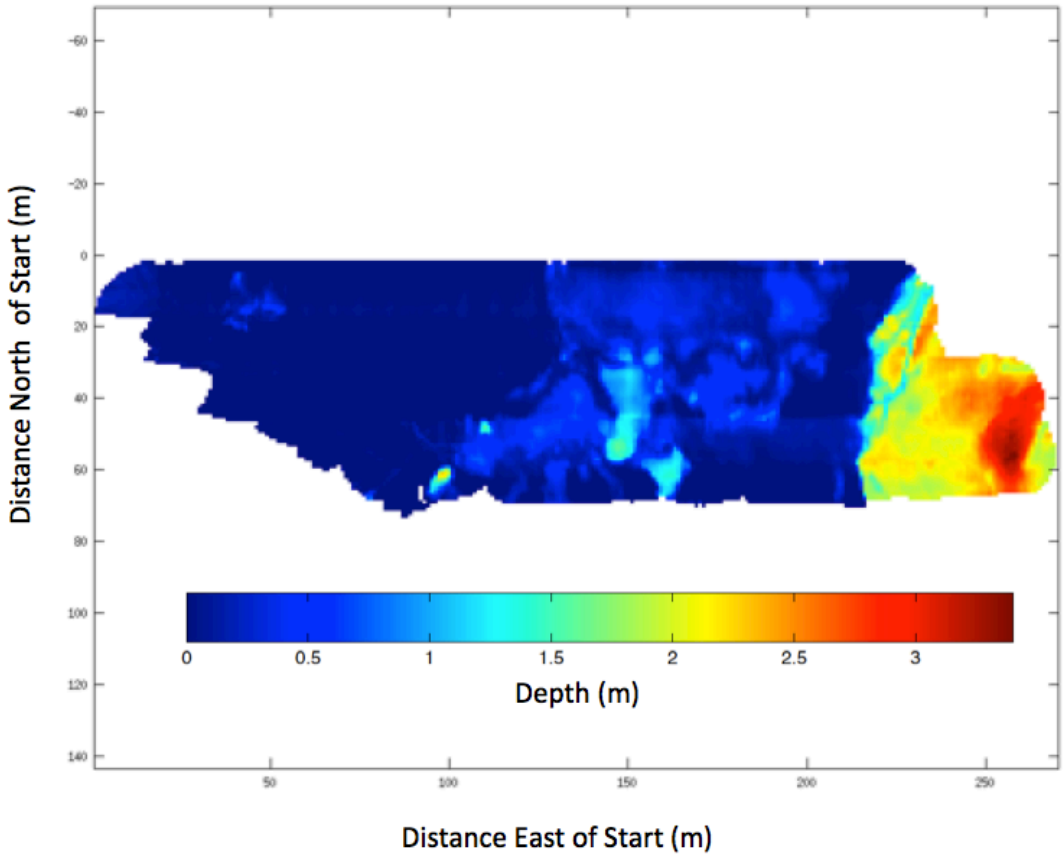


***Figure 3.2.5*** *Sea ice draft map from gridded mission. Open water (or nilas) appears dark blue, with thicker is lighter blue to red. Each leg of the grid was displaced relative to the programmed mission in Fig. 3.2.4) due to a relative current (drift of the surface relative to 15 m depth) affecting navigation from thruster speed. The AUV traversed back and forth from open water (at left) to broken ice cover (center) and then under thicker ice (right).*

Most of the surveyed area was either under open water or under ice with essentially zero thickness (Fig. 3.2.4 and 3.2.5). During the grid portion of the deployment, the AUV was localizing by integrating velocities either measured by the Doppler velocity log (DVL) or estimated from thruster speed, depending on the strength of the signal return from the DVL (this occurred in open water). At the beginning and end of the dive, the AUV used the transponder network deployed from the ship to navigate relative to open water.

This mission provided a useful test of mission objectives 1 (a standard grid mission with transponders deployed on a ship not moored into the ice) and 3 (traversing under multiple floes and open water). A positive outcome was that DVL performed reasonably well even in open water (or very thin ice) conditions, so that navigation under multiple floes is possible while maintaining accurate positioning. Because of relative drift of the ice to the AUV (at 15m depth with lighter currents) where navigation based on dead reckoning from the thruster speed was required because of loss of DVL in open water each track

line of the grid was offset from one another by several meters (Fig. 3.2.5). The final ice bathymetry map was reconstructed by post-correction for this drift. As mentioned, an important consequence of this drift is the AUV ends its mission in a different location than from which it was deployed, particularly for a long mission. If there is limited open water for recovery, then the AUV will end its mission under the ice. In these cases, an appropriate strategy would be to have the AUV return home via the transponder array position estimates before resurfacing.

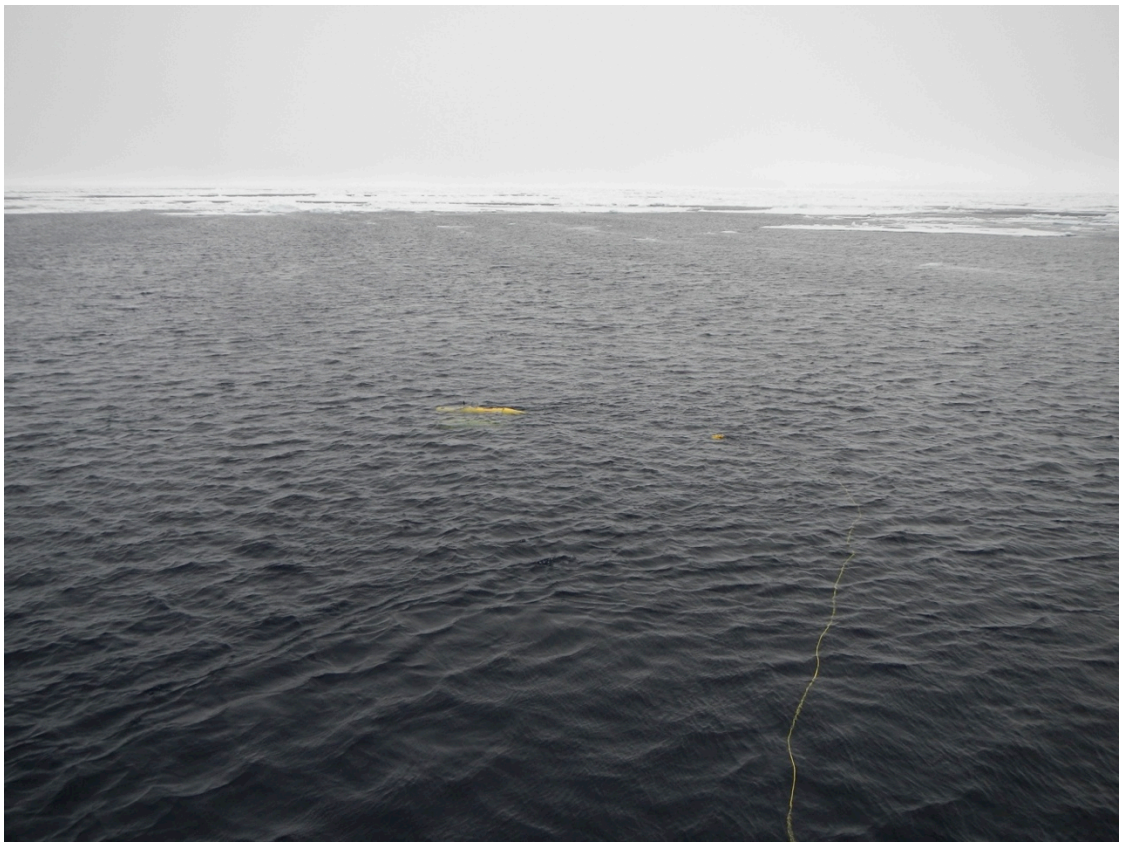

***Figure 3.2.6*** *AUV in the water prior to deployment on grid mission (being followed by ROV). Ice conditions (visible at the edge of the open water) consist of broken ice and some thicker, medium sized floes).*

**3.2.2.4 Longer mission under multiple floes**

A 650 meter out-and-back mission was executed to traverse under multiple larger floes in a drifting reference frame (Fig. 3.2.6). During the mission, the ship and surrounding ice began rotating at about 25 degrees per hour, which could significantly affect the AUV localization estimate since the AUV uses a north-seeking gyro to estimate its velocity direction. The AUV was commanded to return once it had reached 650 m. Even in the presence of this rotation, however, the AUV was able to return to within 20 meters of the start point after more than 1300 meters of total transit distance (Fig. 3.2.7). The dip to the south in the AUV's track on the return leg is due to an apparent water current caused by the relative drift and rotation of the ice above the AUV. As the AUV was commanded to

return directly to the ship on its return, this drift and rotation shows up in the DVL navigation.

During the return mission, the ship was moved without the transponders being pulled from the water. Communications with the AUV were lost after the acoustic transducer hanging from the side of the ship was fouled in the ship's propeller, but once a replacement transducer was deployed, communications were restored and the AUV was commanded to move roughly 20 meters from under a small ice floe back into open water, where it surfaced.

Despite the complexity of significant ice drift and rotation during the latter mission, the acoustic LBL network successfully guided the AUV to open water adjacent to the ship on its return. This mission successfully demonstrated objective 3.

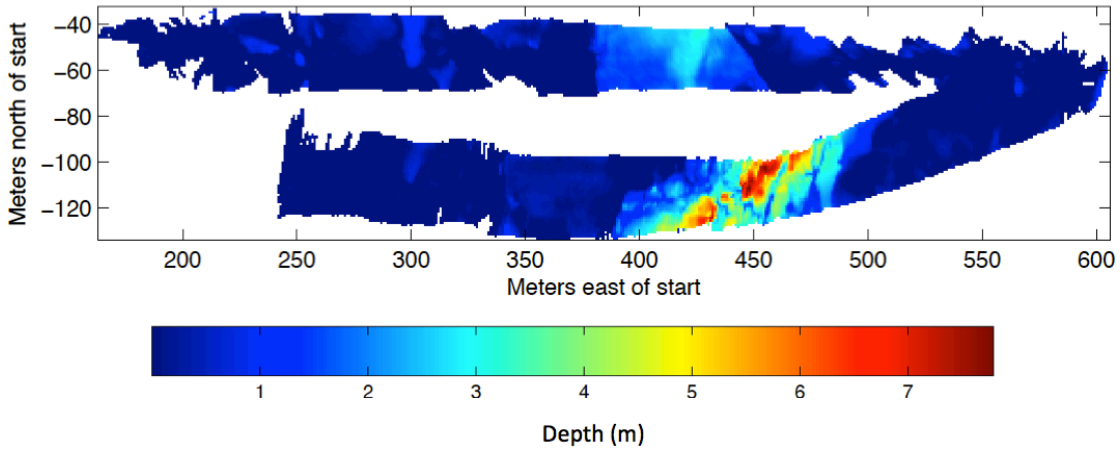


***Figure 3.2.7*** *Multibeam ice draft during long out and back mission. Many small floes are apparent, with open water or new ice in between. Thick, deformed ice can be seen on the lower, return leg.*

### 3.2.2.5 Adaptive oil spill search mission

On the last day of the experiment dynamic re-programming of the AUV to carry out a fine-scale survey of an area of interest was tested. The principle is the AUV would carry out a wide-area search for evidence of oil under ice, telemetering data back to operators on board the ship via the acoustic modem. Once evidence of oil has been found, operators send a command for the AUV to perform a fine-scale survey to map the extent of the discovered oil spill. This scenario was tested with the AUV remaining on the surface, due to the lack of a spare transducer and the limited amount of contingency time available after the loss of the primary transducer the previous day. Since the primary purpose of the test was to test this capability, and all other conditions remained the same, running the mission under ice would provide no additional information over an open water trial.

The mission consisted of a simple out and back mission to simulate a broad search for oil, then when oil was detected (in this case, based on the vehicle entering a slick of grease ice, which has characteristics comparable to a thin oil slick on the ocean surface) a fine 50m grid survey was initiated. Once this was successfully executed, the AUV was commanded back to its start position, and RF remote control was used to pilot the AUV to the stern of the ship where it was recovered with the A-frame.

High winds during the deployment led to a strong drift of the Healy relative to the AUV. Although the Healy ASB was used to reposition the AUV in open water, it was determined that RF remote control could position the vehicle despite winds greater than 20 kts, and this would be a safer, and more rapid method than deploying a small boat for recovery.

This mission successfully demonstrated objective 4. This adaptive mission was successfully repeated at Woods Hole in open water (see Section 3.3).

### 3.2.4 Summary of Healy AUV Deployment

1. Prior experience has shown that the AUV operates well under continuous sea ice with transponders deployed on the ice. These tests demonstrated the AUV is also capable of operation under mixed sea ice conditions with the added complications of drifting and rotating ice.
2. Navigation with Doppler velocity log (tracking the underside of the ice) appeared to be reasonable even when traversing under open water patches. This may allow an effective means of navigation in marginal ice conditions.
3. Vehicle navigation was effective with acoustic transponders deployed over the side of the ship, simplifying deployments in the marginal ice zone.
4. Adaptive missions under ice are possible, where the mission plan can be modified on the fly based on sensor data. This ensures next deployments under ice will be capable of detecting oil in a broad survey and then undertaking fine scale mapping during the same mission.
5. The most expedient means of AUV recovery is via radio control of the AUV when it is at the surface. Small boat recovery is an option, but in most conditions, radio control is quicker than deployment and recovery of the small boat.
6. The Jaguar AUV (or the SeaBed family of vehicles built at WHOI) is an effective platform for under ice mapping missions and well suited for detection of oil trapped beneath sea ice.
7. All mission objections were accomplished – (1) normal grid mission under an ice floe with transponders deployed from the ship (2) mission in marginal ice zone conditions, (3) mission traversing under multiple ice floes, and (4) and adaptive mission where the mission was changed on-the-fly.

With capability for under ice missions in spatially and temporally varied ice conditions now established, future work should focus on the following issues.

(1) More realistic scenarios with oil simulant under the ice (or effects on sensor signals inferred from the spatial variability in ice conditions) so that an appropriate sensor suite can be tested under operational conditions .
(2) Navigation in shallow water with potential obstacles due to grounded ridges, such as is found at Prudhoe Bay and other near-shore coastal regions on the Northern Alaska coast.

(3) For large-scale mapping missions in a temporally and spatially varying ice cover, an outstanding issue is how the information gathered by the AUV can be translated into useful operational information. For this, translation of the observed ice and oil conditions into a consistent reference frame in which a surface response can be initiated is needed. This requires a framework where navigational information from several sources (DVL, inertial navigation, and acoustic LBL navigation) can be combined with appropriate sensor data and potentially ice drift information to reconstruct the most accurate map of oil and ice distribution possible.
(4) Perhaps most important for mitigating oil spills as the areas subject to oil exploration rapidly expand on the Alaskan outer continental shelf, the development of extended range capabilities with precise navigation is needed. For example, subsea pipeline monitoring for future exploration activities in the Chukchi continental shelf region, where missions of > 100 km are required, capabilities for precise navigation and data telemetry over extended distances must be developed.

### 3.3 Adaptive AUV missions

A useful capability for efficient oil spill search, detection and mapping by AUVs is to be able to run a large-scale search mission and, upon detecting oil (based on any particular sensor response), to trigger a more detailed mapping mission.

AUV missions similar to that performed from the USCGC Healy were run. The vehicle was deployed off the dock in Woods Hole, MA on missions while we monitored its progress over the acoustic modem. These missions consisted of a linear search mission along which the oil was presumed to be detected at an arbitrary point (no oil could actually deployed). At this point a gridded survey was initiated when triggered by the operator. For simplicity, this grid consisted of a simple two leg return mission. The capability developed for the Healy missions was enhanced by encoding the ability to use any sensor to trigger an adaptive survey and this was tested with multiple sensors. In this case, both the CTD and a single beam from the ADCP were tested. As from the Healy, an adaptive mission could be triggered based on sensor input received over the acoustic communications link.

A significant issue with a sparse oil spill search mission is the potential patchiness of the signal due to either dispersed oil under the ice or that the sparse mission may only catch the edges of a spill initially. This creates a problem similar to prior work for detection of sparse events in a scalar data time series over an acoustic communication link (Murphy and Singh, 2010). The latency and bandwidth constraints in communications - only about 50 bytes every 30 seconds can be sent due to constraints associated with working underwater - could mean that the signal could be aliased and thus miss relevant events. This is critical, for example, when transmitting sonar vertical profile data (with its relatively high data volume per profile) over the acoustic modem to confirm oil detection.

Therefore we implemented a technique from earlier work associated with in-situ data compression (Murphy and Singh, 2010). Fig. 3.3.1 shows an example of this technique using uncompressed data from an eH sensor that measures redox potential. The upper

plot shows the raw data and how sampling every 30 seconds might alias and cause us to miss a significant event for a typical patchy sensor. A scalar sensor (e.g. laser fluorescence) that might produce patchy data when traversing under small patches of oil might produce similar data (see, for example, Fig. 6.2.2). A SPIHT (Set Partitioning In Hierarchical Trees) encoding based compression mechanism which faithfully reproduces the shape of the curve and gives us a far better understanding of sensor values in real-time while respecting the constraints of underwater communications (Fig. 3.3.1, lower panel). This method was tested successfully with the CTD data during the WHOI test, though as no oil could be used, the data was uninteresting, and so we show a prior data example in Fig. 3.3.1 to illustrate the utility of this technique.

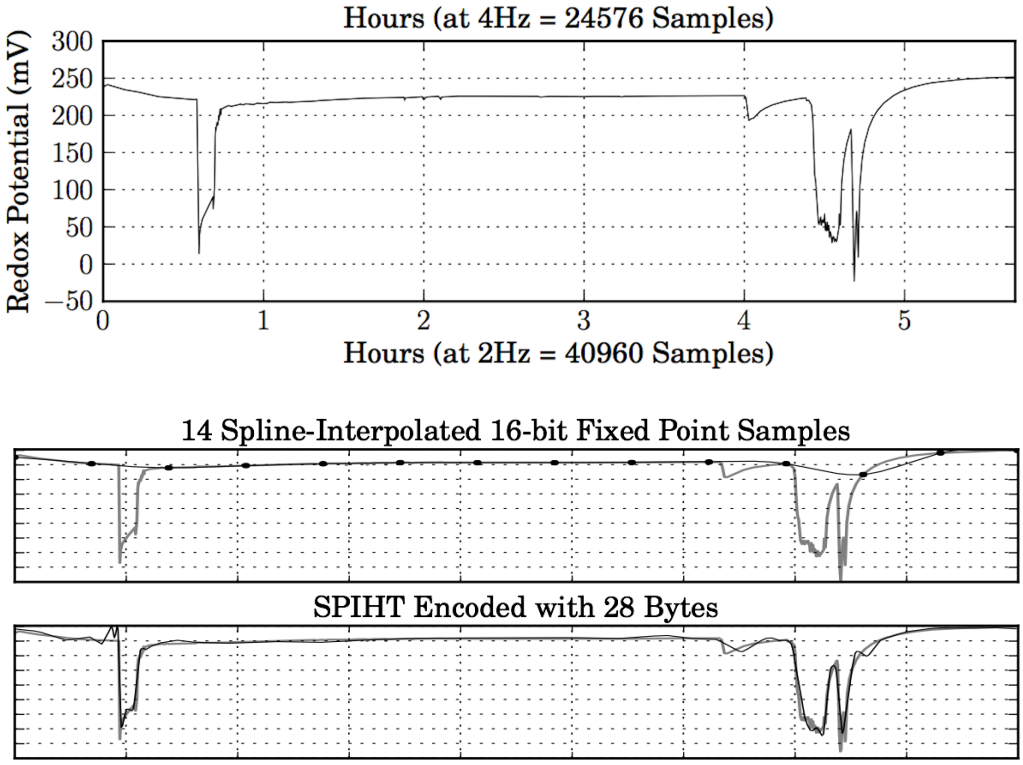


***Figure 3.3.1***. *An example of patchy data (top) that data leads to aliasing due to subsampling when sent through a naive sampling protocol over acoustic communications (middle). Use of a SPIHT (wavelet) based compression algorithm allows the capture of the dynamics of the data while respecting the constraints of underwater communications (bottom) (After Murphy and Singh, 2010).*

These results demonstrate the ability for adaptive surveying with an AUV, and in particular, the capability to perform efficient surveys in areas where the location of a potential spill is not known a priori and may require an initial search over a wide area, or the spill may be sparsely distributed.

### 3.4 Prudhoe Bay Acoustic Communications Tests

The purpose of the work was to determine over what range underwater acoustic communications (acomms) were viable under fast ice in shallow water. The Arctic Ocean is a unique environment for underwater acoustic propagation because the sound-speed profile refracts sound to the surface where they scatter off of the ice. Previous work in deep water (2500 m) has shown that under ice that communication can take place over tens of kilometers or more (this depends on frequency). This implies that for acoustic navigation and communication with autonomous vehicles, a sparse network of transponders can supports communication over large areas, making the logistics easier. What was not known was how effective communications would be in a very shallow water environment, such as at Prudhoe Bay. Because the propagation channel is very narrow relative to distance, only direct path propagation is likely to exist, which means that any intrusion due to ice keels may block propagation completely.

There is very little data on acoustic propagation in shallow water under ice in the context of AUV operations. One previous exercise off Barrow showed that range could be quite limited, sometimes just a few hundred meters. The results are reported in (Plueddemann, 2012).

The purpose of this experiment was to demonstrate the feasibility of 10 kHz band acoustic communications for use under shore fast ice in water depths from 5 to 10m. Because the communications signals are similar to those used for navigation, it will simultaneously reveal whether acoustic navigation is feasible at these depths and in these conditions. In summary, the goals are:

1. Characterize acoustic communications performance (data rate and success rate) with respect to water depth and range.
2. Develop an empirical estimate of maximum reliable range for acoustic communications by measuring the link parameters including signal to noise ratio (SNR) at the input of the modem receiver.
3. Measure performance and propagation conditions across and along underwater bottom topology features if available (e.g. ridges, mounds).

#### 3.4.1 Acoustic communications equipment

The experiment utilized the WHOI Micro-Modem, a research modem that is also used in production AUVs and commercialized via Hydroid and other underwater vehicle manufacturers. The core of the modem is a small set of electronics that can be used with a variety of acoustic transducers and thus many different operating frequencies. Typical frequencies are 10 and 25 kHz, with typical ranges at 25 kHz 2-3 km, and up to 10 km at 10 kHz, with data rates that vary considerably in different conditions.

For this experiment a pair of 10 kHz modems was used in order to maximize range. This is standard equipment on many underwater vehicles, e.g. Seabed and the REMUS 100. This frequency was also used during the only other similar test, done off Barrow in very broken near-shore ice (Plueddemann, 2012). The modem is packaged in a portable weather-tight case, and uses a laptop to initiate transmissions and to record receptions (Fig. 3.4.1).

In addition to the acoustic modem, which provides immediate output for evaluation, broadband acoustic recorders were deployed several times to gather raw data for later analysis. The data is also useful for looking at noise in other bands.

***Figure 3.4.1*** *Laptop (left) and acoustic modem (right) with ice hole for transducer in background.*

The source level for the equipment is approximately 183-185 dB, depending on the exact frequency and accounting for variability from unit to unit. The source level dropped below 160 dB within approximately 15 meters ensuring that there was no risk of disturbance to seals that might be in the area (none were during the tests). The carrier was exactly 10 kHz, and the bandwidth 5 kHz. The duty cycle for the transmissions varied, but was typically 10% or less over the course of the day.

A conductivity-temperature-depth (CTD) sensor was brought and used to profile the water column through the ice holes. The unit worked well for several profiles, but was affected by cold eventually and stopped reporting correctly. However, the profiles that were taken are instructive and described below.

### 3.4.2 Ice conditions and environment at Prudhoe Bay

The experiment logistics was supported by Alaska Clean Seas, which has a continuous presence in Prudhoe Bay to support oil spill response activities. The equipment available for operations on the ice includes pickup trucks with trailers, Kubota tracked vehicles and snowmobiles with trailers (Fig. 3.4.2).


***Figure 3.4.2*** *Kubota tracked vehicle (left) and snowmobile (right) on typical ice conditions. The BP Northstar platform can be seen in the background on the right*

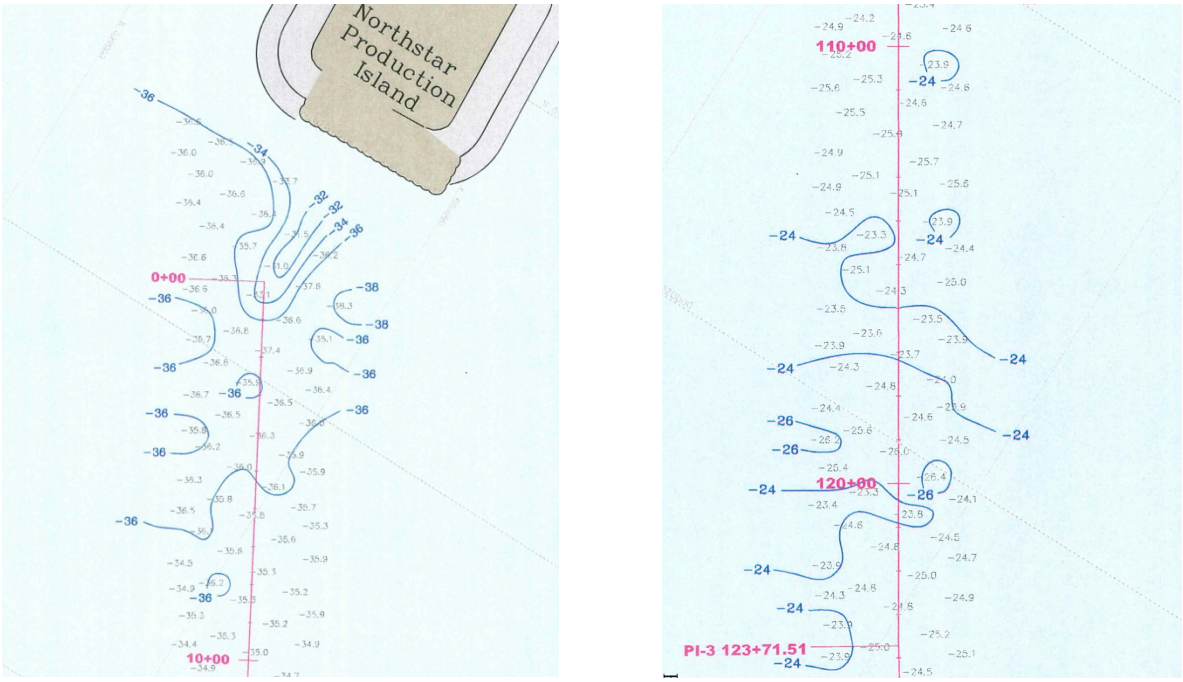


***Figure 3.4.3*** *The bathymetry along the ice road near the start of the long range, level ice test at 6 miles from shore (left) and at about 4 miles where tests under a ridge were carried out (right). The longer range test traversed parallel to shore (roughly perpendicular to the ice road) to the east in about 30-35 feet of water. The short range test under the ridge was performed in ~25 feet of water parallel to the ice road at right.*

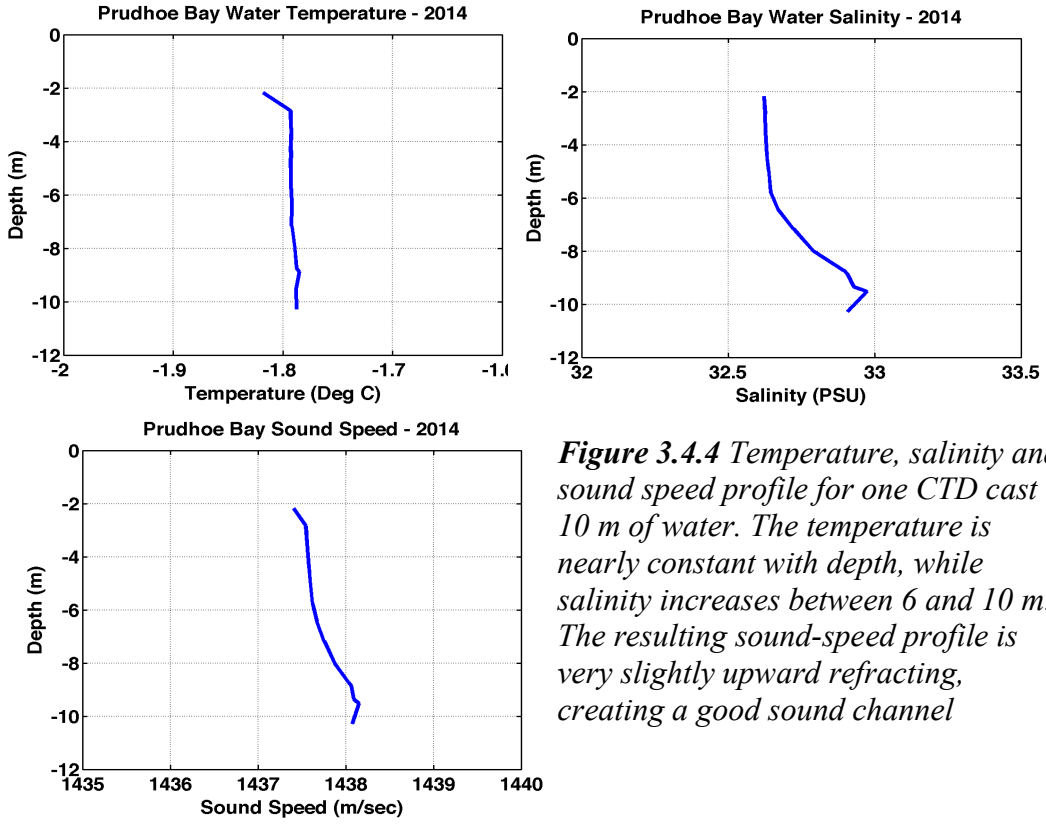


***Figure 3.4.4*** *Temperature, salinity and sound speed profile for one CTD cast in 10 m of water. The temperature is nearly constant with depth, while salinity increases between 6 and 10 m. The resulting sound-speed profile is very slightly upward refracting, creating a good sound channel*

The ice that forms around Prudhoe Bay is typically uniform in depth. The depth of the ice along the haul road to the Northstar site is monitored regularly, and while it varies from year to year, is typically 60-80 inches thick. Although most of the ice is level, there are many small ridges and rubble fields created during initial ice formation in autumn. Typically, a shear margin occurs a couple miles to the east of the ice road in shallower water. In 2014, the ice near the BP Northstar platform was quite level (Fig. 3.4.2). Within a few miles of shore in shallower (20-25 ft) water, there was an irregular low ridge that descended up to 10-15 feet in places (as measured by a Geonics EM-31 electromagnetic induction instrument) and possibly was grounded in some places.

The water depth along the haul road is indicative of the depths adjacent to the road where the experiments were performed. Near the end of the ice road at the man-made Northstar Production Island facility the depth is approximately 36-38 feet. The longer range acomms tests (see below) under level ice were carried out here. Tests under a ridge were performed at station 123+00, 3.8 km closer to shore, where the depth is 24 feet (Fig. 3.4.3).

The temperature and salinity that were measured using the CTD, and the sound speed computed based on those measurements, are shown in Fig. 3.4.4. The temperature is very uniform at -1.8 degrees C, though there is a very slight increase in the bottom few meters. There is more depth-dependence to the salinity, with slightly fresher water just under the ice, increasing below 6 m to almost 33 PSU (Practical Salinity Units, similar to parts per thousand). The result is that the sound-speed profile is nearly constant with depth, except for the slight increase near the bottom due in part to the salinity (and to a very small degree the slight temperature increase). Note that the apparent decrease in salinity and sound speed in the bottom ~50 cm is likely not real, but an artifact due to the CTD hitting the bottom.

The implication of the sound-speed profile is that direct-path propagation will be supported at ranges that depend on spreading and absorption loss. At 10 kHz carrier frequency those maximum ranges are approximately 5-8 km, depending on signal level and background noise. If the profile is much warmer at the bottom the sound will bend away from it, refracting back toward the surface where it will reflect from the ice and undergo some loss due to scatter. However, the underside of this first-year ice is relatively smooth in most places, and that loss is less than what would occur in highly-ridged ice or multi-year ice.

As will be discussed in the results section, the biggest impact on range is the presence of ice keels that simply block the signal. While under certain conditions sound rays may pass under and then refract upwards, the situations where this may occur will depend on the source-receiver range and their depths.

### 3.4.3 Results of acoustic range testing

The tests were performed over several days and at different depths and ranges. Three data rates that utilize two modulation methods were used and the results are tabulated below. The 80 bps rate uses a frequency-hopping, frequency-shift keying (FH-FSK) modulation method, while the higher rates use phase-shift keying (PSK). While the FSK uses 4 kHz

of bandwidth, PSK utilizes 5 kHz. Error-correction coding of varying strengths and redundancy levels provide different throughput and reliability. While rates to 5000 bps (burst) are feasible at close ranges, to achieve longer ranges the lower bit rates are necessary.

The metrics for the link tests are the input and output signal-to-noise ratios (SNR). The input SNR is measured at the receiver after band-pass filtering to the signal band, while the output SNR is measured after the adaptive equalizer attempts to remove multipath and Doppler shifts which may be present. High input SNR with low output SNR typically means that there is some multipath that is not completely compensated with the receiver. The FSK modulation method, as processed by the real-time acoustic modem, does not report input and output SNR.

The first tests were performed in shallow water a few km from shore in an area of fairly level ice. The transect was conducted roughly parallel to the shore so that there was little bathymetric variability along the test; the water depth decreased by about 1 m along the full range. The tests were performed at ranges of 2 and 3 km in 5-6 m depth. The range was limited by the shear margin at the eastern end of the transect. The transmitter was deployed approximately 3 m below the ice (mid-water), while the receiver was deployed similarly at two stations, at 2 and 3 km away from the transmitter. Table 3.4.1 shows modem performance for FSK and PSK packets at three data rates. The input signal-to-noise ratio (SNR) drops 16 dB between the ranges 2 and 3 km, a decrease that is much higher than that of just spreading losses. At 2 km, all data rates perform well, though the 1300 bps rate is 94% rather than 100% like the other two. At 3 km, 500 bps is clearly the best performer with an 83% success rate, while the 1300 bps data is reduced to 50%.

**Table 3.4.1: Performance in 6 m depth, with respect to range and data rate.**

| Rate # (bits/sec) | Range, km | Input SNR, dB | Output SNR, dB | Total packets sent | Percent received | Percent good |
|---|---|---|---|---|---|---|
| 80 bps | 2.0 | - | - | 36 | 100% | 94% |
| | 3.0 | - | - | 38 | 74% | 60% |
| 500 bps | 2.0 | 32.7 | 15.5 | 18 | 100% | 100% |
| | 3.0 | 7.1 | 3.0 | 18 | 89% | 83% |
| 1300 bps | 2.0 | 33.4 | 15.6 | 17 | 100% | 94% |
| | 3.0 | 7.3 | 3.0 | 18 | 78% | 50% |

For the second set of tests, performed in water 10 m deep starting at a distance about 6 miles along the ice road towards the Northstar platform, (table 3.4.2) the transmitter was deployed at approximately 5 m below the ice, and the receiver was deployed at three stations, 2, 4 and 5.6 km away from the transmitter. The distances shown in table 3.4.2 are derived from measuring acoustic round-trip travel time using the ranging capability that is built into the acoustic modem. Table 3.4.2 shows modem performance for FSK and PSK packets at four data rates (the higher data rate was added because the performance showed improvement and the potential to support it).

All rates perform equally well at 2 km and achieve 100% packet success rate. At 4 km the success rates drop to the 90% region. At 5.6 km 1300 and 5300 bps have success rates of

87% and 89% respectively, while 500 bps is at 90%. However, these can be considered essentially the same for this sample size. The uniformity in the success rate may be peculiar to this particular channel and so bears further testing, but these results are encouraging, as they indicate relatively high rate communication over many kilometers may be possible.

The input SNR drops 7 dB between ranges 2 and 4 km, which is consistent with spreading losses. Further out, at 5.6 km, we expect to see additional loss, however that is not reflected in the data and the signal levels are approximately equal. Some signal reinforcement from paths reflecting or refracting near the bottom may be the cause.

**Table 3.4.1: Performance at 10 m depth, with respect to range and data rate.**

| Rate | Range, km | Input SNR, dB | Output SNR, dB | Total packets sent | Percent received | Percent good |
|---|---|---|---|---|---|---|
| 80 bps | 2.0 | - | - | 42 | 100% | 100% |
| | 4.0 | - | - | 58 | 100% | 100% |
| | 5.6 | - | - | 74 | 99% | 94% |
| 500 bps | 2.0 | 24 | 13 | 22 | 100% | 100% |
| | 4.0 | 17 | 10 | 31 | 100% | 97% |
| | 5.6 | 17 | 11 | 40 | 90% | 90% |
| 1300 bps | 2.0 | 24 | 14 | 20 | 100% | 100% |
| | 4.0 | 17 | 11 | 29 | 97% | 93% |
| | 5.6 | 18 | 11 | 37 | 92% | 87% |
| 5300 bps | 2.0 | 25 | 14 | 20 | 100% | 100% |
| | 4.0 | 17 | 11 | 29 | 97% | 93% |
| | 5.6 | 18 | 11 | 37 | 92% | 89% |

The last tests were performed across a blocky ridge that ran perpendicular to the direction of the ice road, at about 6 km from shore in 25 feet water. The ridge was an irregular rubble field that was as much as 10-15 feet thick in places (level ice was about 5 feet thick). These "ridges" appear fairly common in the area, and form during onshore ice movement as the fast ice develops. It is unclear if any of these are thick enough to descend to the seafloor, but they are a potential hazard to vehicle operations in shallow water. With the source and receiver on opposite sides of the ridge, the range was limited to less than 1.5 km.

Recordings of the raw acoustic signal were made at several sites to allow for post-processing and to characterize channel multipath (arrival of the signal at the receiver along different paths, which can make decoding messages difficult) by matched-filtering the frequency-modulated sweep that starts every acoustic packet. Fig. 3.4.5 shows the channel impulse response in water depths of 10 m and 6 m respectively. There is a strong first arrival on all channels. In the 10 m data, a secondary arrival can be seen a millisecond later, though it is low amplitude relative to the first arrival. In the 6 m data, the secondary arrival is not so clearly resolved from the main peak, but broadens the peak.

### 3.4.5 Summary and application to AUVs in shallow water under ice

High rate PSK communications are feasible under shore fast ice at depths of 6 to 10 m and ranges to approximately 5 km, and potentially higher. Success rates to 100% were achieved, with overall performance dependent upon data rate, but could be as low as 50% at 3 km in shallower water.

Based on these results it is clear that deeper water supports longer ranges, and other tests showed that range is limited when ice keels are located between the source and receiver. Differences in input SNR could be due to changing bathymetry; however they did not affect the final packet success rate for the low rate.

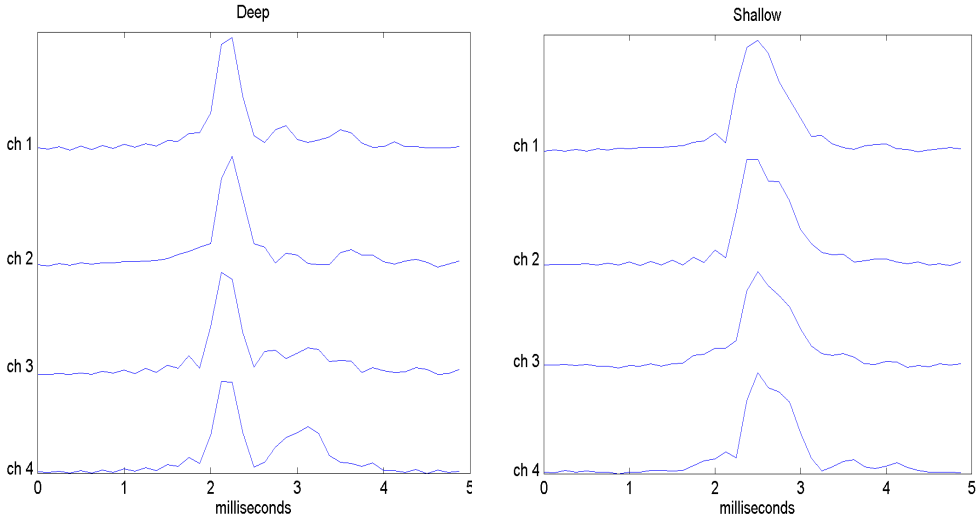


***Figure 3.4.5*** *Channel Impulse Response, in dB at 10 m depth, channel 1 at the top of the array (left). Channel Impulse Response, in dB, at 6 m depth, Ch. 1 at the top of the array (right).*

Given that it is possible to communicate acoustically with AUVs under ice in water as shallow at 6 m, their use near Prudhoe Bay for a variety of missions appears very viable. Large areas could be surveyed with only a modest number of transponders in place. The fast ice is very easy to operate on, so installing the transponders and modem gateways (which could communicate to operations personnel at Northstar via radio) is straightforward. In shallower water, more care would be needed - largely due to the depths of ridge keels in rubble areas. In these shallower areas, an ROV may be a viable alternative to an AUV because of the more limited area needed to survey. Based on these tests, it seems the limiting factor may not be acoustics, but navigation hazards due to ice rubble occluding large portions of the limited water column. Placement of the acoustic systems does need to be done with care relative to rubble fields that could also create ridging below the ice.

One area of interest is further offshore in the shear zone between the fast ice and the pack, where deep, potentially grounded ridges can occur. A potential future task of interest would be to characterize the ice underside in both these areas (by AUV/ROV) so that vehicle navigation, acoustic communications performance, and spread of oil in a potential future spill could be better understood.

# 4. Sensor suite development and laboratory experiments

This chapter describes development and testing of various sensors to determine their potential efficacy for detection of oil trapped beneath, and possibly encapsulated within, sea ice from an AUV platform. This is divided into three sections. Section 4.1 describes the instrumentation used, and the following sections describe the suite of three laboratory experiments performed. Results of acoustic tests are reported in Section 5, and reports of optical tests (digital imagery and laser fluorescence) are reported in Section 6.

## 4.1 Sensor suite

A series of three laboratory experiments were performed to test various sensors for detection of oil under ice. These included:

1. Oil spill experiments in an indoor ice tank at the US Army Cold Regions Research and Engineering Laboratory (CRREL) in Hanover, NH, in May 2013. Sensors included narrowband and broadband sonar, cameras, and a benchtop prototype laser fluoresensor (see Section 4.2)
2. Experiments in the Arctic Environmental Test Basin wave tank facility at the Hamburgische Schiffbau-Versuchsanstalt GmbH (Hamburg Ship Model Basin; HSVA), Germany, in December 2013. The use of the HSVA facility was supported by the EU Integrated Infrastructure Initiative HYDRALAB-IV, Contract no. 261520, and the EU ACCESS project within the Ocean of Tomorrow section of the European Commission 7th Framework Programme. (Section 4.3)
3. Sonar experiments of ice encapsulation in ice tanks at the Scottish Association for Marine Science (SAMS). The use of this facility was supported by the Oil Spill Recovery Institute at the Prince William Sound Science Center, Cordova, Alaska. (Section 4.4)

### 4.1.1 Sonar Systems

The principle sonar systems used for the experiments were a sensitive, high frequency narrowband sonar and laboratory broadband system.

The narrowband sonar was an Aquatech Aquascat 1000 echosounder (http://www.aquatecgroup.com) with transducers ranging from 300 kHz to 5 MHz, depending on the experiment. The Aquascat 1000 is a monostatic sonar system, with transducer half beamwidths ranging from 1-6 degrees, depending on frequency. Pulse width is controllable between 2.5 mm and 40 mm. Typically used in short range applications to measure small scatterers in the water column, this system is was chosen for its excellent range resolution and high-fidelity, permitting as much as 60 dB of signal to noise in these tests.

The laboratory broadband system is a bistatic system consisting of pairs of piston-like transducers providing frequencies between 120-1050 kHz, depending on the experiment. The transducers in each pair are closely spaced to approximate monostatic measurements. The pulse-echo system is controlled by a National Instruments data acquisition system (PXI-1000B) with an embedded computer controller (PXI-8175, Windows 2000) and a custom LabView script. Transmitted signals are generated by a 12-bit, 40 MHz Arbitrary Waveform Generator (PXI-5411) and amplified using an ENI 2100L amplifier with 50 dB gain. A Ritec SS-40 signal sampler (-40 dB) is used to record the transmit signal.

Received signals are filtered and preamplified with a RITEC BR-640A receiver. The transmit and receive signals are sampled at 4 MHz. Transmitted signals consist of linearly modulated chirps with transducer dependent half-beamwidths of 1.5-6 degrees. The system is fully programmable and any desired waveform can be transmitted. The ping rate, signal duration, and transmitted power, are also fully-programmable. Both spectral and temporal domain processing is possible with the data collected with this system. It has a range resolution of between 3 mm and 10 cm.

### 4.1.2 Laser fluorometer

Laser fluorescence was tested using several versions of a custom system developed within this project. The system has gone through several stages of development. For the CRREL tests, a 'benchtop' prototype was used so that initial testing of the feasibility of detecting oil under ice could be determined. To permit modification of the design, the system was built on an open breadboard (Fig. 4.1.1).

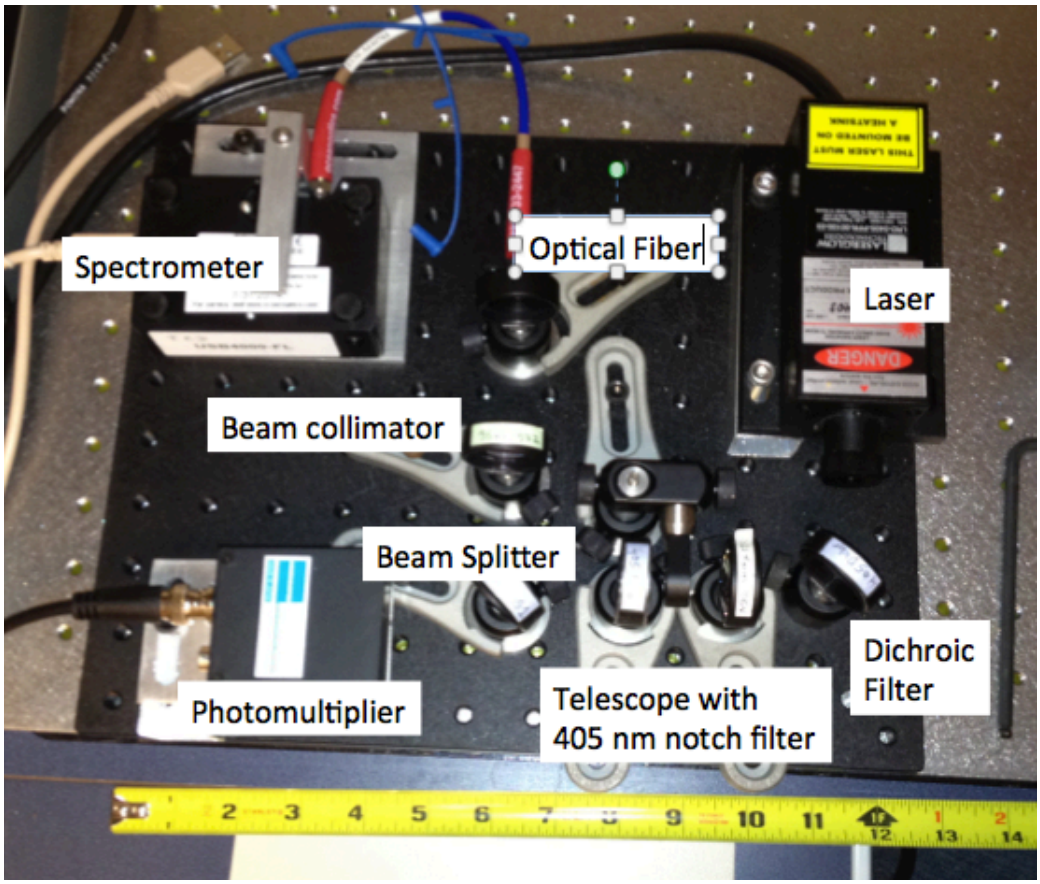


***Figure 4.1.1***. *Laser fluorometer "bread board" prototype. The 405 nm laser is reflected towards the target to the right by the dichroic filter. The returned signal passes through this filter and focused onto the photomultiplier by the telescope, with the 405 nm signal filtered out to remove any interference from the laser. This signal is fed into the lockin amplifier to detect only the signal at modulation frequency of the laser, reducing ambient noise. The signal is also passed to the USB4000 spectrometer so that the returned fluorescent spectrum can be detected.*

The basic design is based on phase-sensitive detection of a frequency modulated fluorescence signal, following techniques used in similar systems (e.g. Bello and Toomey, 2012). The system consists of a 50 mW 405 nm laser. This wavelength permits a broad spectral response (only wavelengths above the excitation wavelength will fluoresce) while avoiding the strong attenuation in water that deeper violet lasers would suffer from. Thus this is a practical wavelength for maximizing the fluorescent signal. The laser is reflected from a 405 nm dichroic mirror at 45 degrees so that the laser source is not aligned with the return beam path. The returned fluorescent signal is then focused onto a photomultiplier using a simple Galilean telescope, and then through a 405 nm notch filter to further block any noise from the excitation source. This beam is then split between a Hamamatsu 7827 photomultiplier and an Ocean Optics USB4000-FL spectrofluorometer.

The output from the photomultiplier (PMT) is fed into a Stanford Research Systems SR810 lock-in amplifier so that only those signals modulated at the same frequency as the laser are detected (Fig. 4.1.2). The SR810 has common mode rejection of up to 100 dB so that a signal can in principle be detected in noise up to 100,000 times greater. In practice, this is limited by the saturation level of the PMT.

The second generation of this system that could be fully immersed was used in the HSVA experiments. The optics were housed in an aluminum enclosure to eliminate stray light. The telescope was replaced with a 75 mm PCVX lens that focussed on the 8 mm PMT aperature. To reduce size, the laser was replaced with a Quantum 405 nm 100 mW laser diode, the SR810 was replaced with a FEMTO LBV-150 miniature lock-in amp, the PMT power supply was replaced with a DC/DC convertor board , the external DigiKey signal generator was replaced by a PIC-based signal generator. Due to a laser failure just before the tests, the original laser was installed for the HSVA experiments. This was housed in a watertight PVC housing approximately 10” in diameter and 18” long.

Since these tests, the design has been improved and made more compact with the smaller laser and a TERN microprocessor control board. The control board allows control of the lock-in and PMT gain via the operator terminal via RS232 (Fig. 4.1.3, 4.1.4)

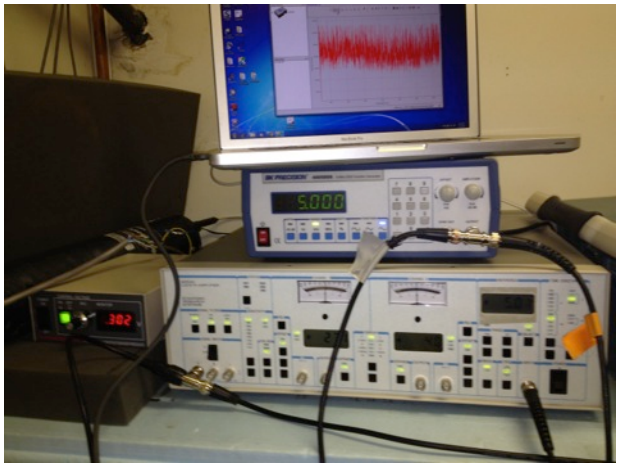

***Figure 4.1.2*** *Laser fluorometer bench set-up. This includes a lock-in amplifier to detect the signal (bottom), a signal generator to modulate the laser (middle), and the power supply for the PMT (left). The laptop on top displays the USB4000 spectral response. In this case, there is no oil deployed, and so the returned spectrum is very nearly white noise, as expected.*

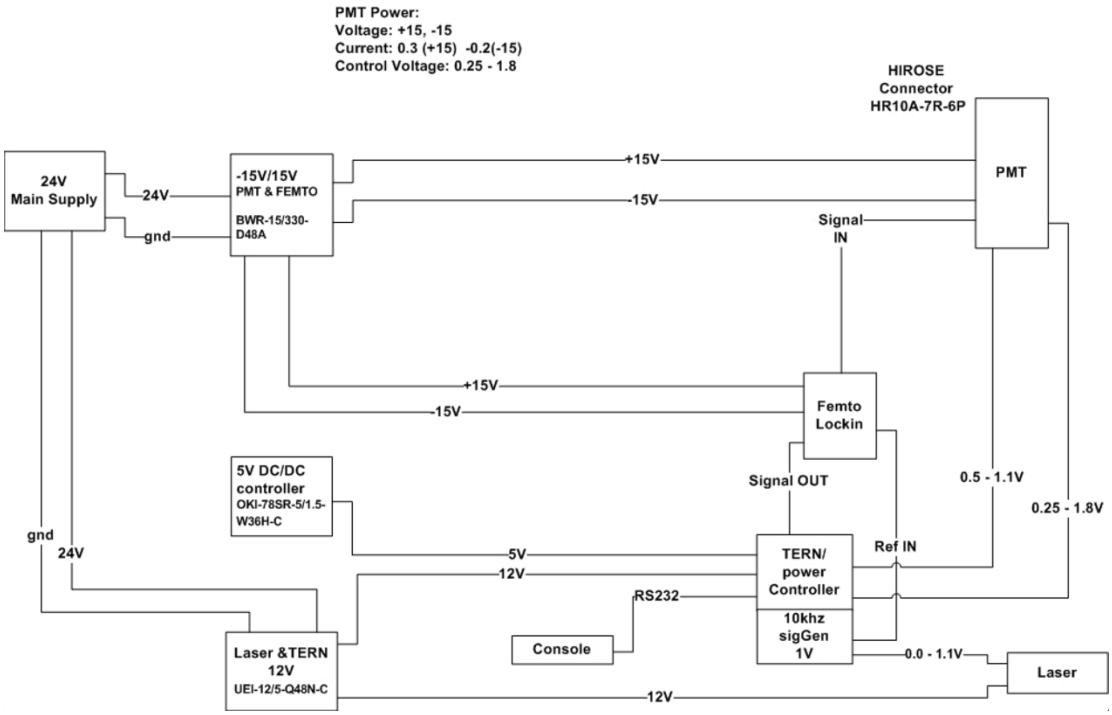


***Figure 4.1.3*** *Block diagram for the laser system. The Femto lock-in amplifier, signal generator, and PMT are controlled using the TERN microcontroller. Various DC/DC controllers provide appropriate power to the PMT, laser, and lock-in. The complete systems is controlled through a single RS232 interface.*

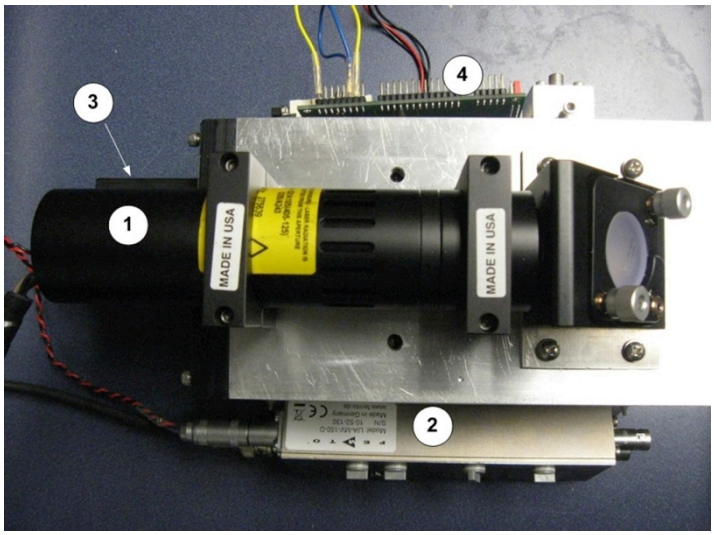


***Figure 4.1.4****. Laser fluorometer system. A 100 mW, 405 nm laser (1) is mounted on the aluminum optical housing. A mirror focuses the laser onto a dichroic in the housing, reflecting it out through the lens. The returned signal is focused on the PMT (3) through a 405 nm notch filter with a 75 mm lens within the housing. The lens is recessed within the housing so that only vertically incident light is received at the PMT, limiting ambient light. The power and control electronics (4) and lock-in amplifier (2) are mounted on the optical housing. The laser is approximately 6" long.*

### 4.2. CRREL experiments

Experimental tests of the sonar systems and laser fluorometer were performed the week of May 20-24, 2013 at CRREL in Hanover, NH. A cylindrical plastic container approximately 2m in height and 3m in diameter was placed in a large cold room facility at CRREL (Fig. 4.2.1). Artificial seawater (at an initial salinity of about 32 psu) was brought to the freezing temperature prior to the installation of the instrumentation, which had to be placed prior to freezing of sea ice. The tank was positioned next to the cold room wall so that instrument cables could be run into a warm room from where the instruments could be monitored and data recorded. The tank was insulated with fiberglass around the sides, and Styrofoam underneath. The latter allowed significant heat flow so that freezing of anchor ice occurred on the tank bottom and instruments. To cool the tank evenly, an impeller was placed in the tank. Although the tank was cleaned prior to the experiments, the impeller stirred up residual particulate, which potentially could impact the acoustic measurements due to scattering in the water column. Instruments were installed in the tank on May 16, and the cold room was then dropped to around -25 ºC to form the initial sea ice layer over the next several days.

***Figure 4.2.1*** *The test tank viewed from above, with illumination provided from below. Note the dark area in the center where the oil was deployed beneath the ice.*

As the laser system could not be placed in the bottom of the tank looking up (both to avoid the need to enclose the laser system and also provide access to it so that adjustments could be made), a system to mount the laser externally on top of the tank was constructed. This consisted of an insulated PVC tube about 2 feet in length that was frozen into the ice (Fig. 4.2.2). The base of the pipe was below the level of the oil to prevent oil from rising out onto the ice. Below the pipe, a mirror was suspended at an angle so that the laser beam would reflect and travel upwards to the center of the tank where it would excite the oil from below. The fluorescent signal is isotropic, so part of the signal will return along the same path. In this arrangement, the effective depth of the sensor beneath the oil was about 2 m. A heat tape was placed in the PVC pipe to prevent the water from freezing inside, thus providing a beam path through water.

The laser breadboard was mounted vertically above the PVC pipe (Fig. 4.2.2). To maintain the temperature of the laser system, a resistive heater was mounted on the back

***Figure 4.2.2*** *Set-up for the laser fluorescence installation. An insulated PVC tube with a mirror beneath was use to keep a clear optical path from above the ice (left). Laser system viewed from behind (below).*

of the breadboard and when in operation, an insulated box was placed over the whole apparatus to keep it warm during the tests, although this was removed for the actual measurements because the styrofoam fluoresced fairly strongly in stray laser light. During the experiments, the primary effect of the temperature appeared to be to lower the laser power somewhat, but this was easily controlled with the laser power supply to maintain near constant power throughout the experiments.

The sonar systems deployed included (Fig. 4.2.3):

1. A Marine Electronics 11001 multi-return altimeter that was used successfully in experiments at CRREL in 2012,
2. The Aquatec Aquascat 1000 profiling sonar with two transducers nominally at 1 MHz and one at 5 MHz,
3. The bi-static broadband laboratory system with Airmar transducers at 160 kHz and 500 kHz.

A Prosilica camera with wide dynamic range for use in low-light conditions was also deployed at the bottom of the tank at CRREL (Fig. 4.2.3). Unfortunately, the camera failed prior to the release of the oil. Therefore, imagery was taken with a GoPro Hero 3 camera lowered down the laser hole after the experiment.

The cooling of the cold room was slower than anticipated between May 17 and May 20, so that only a thin skim of ice was present on May 20. Testing was delayed until May 22 so that at least 15 cm of ice could be grown.

On Wednesday, May 22, once initial measurements with all sensors were made of the ice underside, oil was released through a second PVC pipe frozen into the ice. This release occurred fairly rapidly, and the oil spread across most of the width of the tank (see Fig. 4.2.1) to a thickness of about 5 cm (the ice was thicker at the tank edges, which restricted

the flow). As all sonars detected this thickness, and as there was a desire to encapsulate the oil as much as possible, it was decided not to spill additional oil so that the ice could continue to freeze significantly in the next few days. Measurements were taken on May 22-24 as encapsulation of about 1 cm occurred. The sonars were left on over the weekend to allow continued encapsulation. The sonars suggested a growth of about 4 cm of ice beneath the oil by this date. The surface temperature of the ice reduced to ~ -16 °C by Tuesday, May 28. This is consistent with ice growth predicted by the Stefan growth law of about 1 cm/day.

During the experiment, anchor ice formation (large, flat platelets of ice, about 1-2 cm in size) were forming on the tank bottom and instrument mount as the water at the tank bottom supercooled. This occurred as cold brine formed during ice growth descended to the tank bottom and heat was lost through the ice bottom. By May 28, these covered much of the instrument mount by the end of the experiment, and visible on the edges of the laser mirror. These would periodically dislodge and rise to the ice underside and the acoustic scattering from them as they rose was visible in the sonar data. These platelets could be seen on the ice underside. Because of the completely quiescent conditions in the tank, the supercooling at the base of the ice was greater than is found in natural sea ice (Petrich and Eicken, 2009). This would tend to enhance the lamellar ice structure at the base. These two factors probably led to an enhanced mushy layer in the ice basal layer (Wettlaufer et al., 1997).

***Figure 4.7*** *The sonar transducers mounted at the bottom of the test tank. From left to right: Marine electronics 1.1 MHz profiler, two 160 kHz Airmar transducers for the broadband system, two 500 kHz Airmar transducers for the broadband system, and four Aquascat transducers (there 1 MHz (two connected) and one 5 MHz). A Prosilica low-light camera is mounted in an underwater housing on the side of the instrument platform.*

At the end of the experiment, a temperature and salinity profile through the water was taken with a YSI salinometer. Both profiles were fairly uniform at 36 ppt and -1.9 °C until a slightly colder, brinier layer was found at the bottom, although this was below the level of the sonar transducers. For practical purposes, the sound speed could be considered constant at about 1450 m/s throughout the experiment.

### 4.3 HSVA experiments

Experiments at the Arctic Environmental Test Basin (AETB) wave tank facility of the Hamburgische Schiffbau-Versuchsanstalt GmbH (Hamburg Ship Model Basin; HSVA) in Germany were performed in December 2013. The use of the HSVA facility was supported by the EU Integrated Infrastructure Initiative HYDRALAB-IV, Contract no. 261520, the EU ACCESS project within the Ocean of Tomorrow section of the European Commission 7th Framework Programme. Experiments under the ACCESS programme were intended to examine the interaction of oil spills with ice during the early stage of growth – namely frazil/grease ice, pancake ice, and white nilas (see, e.g. Weeks, 2010). These experiments were augmented under the BSEE contract to test detection of the oil using the instrument suite described above. Additional support to augment the instrumentation was provided by Alaska Clean Seas.

These experiments provided a unique opportunity to examine the efficacy of undersea oil detection techniques in ice types typical of early ice growth and that have not been previously examined. A second quiescent tank experiment was run in a separate cold room to repeat the prior CRREL experiment.

#### 4.3.1 Young sea ice types

Here we provide a brief description of young sea ice types, as the mode of formation of each affects its structural and chemical properties; in particular, the crystal structure, microphysical pore structure, salinity, and mechanical behavior. These morphological properties will in turn impact acoustic scattering and radiative transfer (i.e. interaction of light with the ice), and thus the sensor signal characteristics. The structural variation will also impact the interaction of oil with the ice. For details of these ice types the reader is referred to the most authoritative texts such as Thomas and Dieckmann (2009) and Weeks (2010).

Initial freezing of ice in seawater occurs through the formation of tiny free-floating discs and spicules known as frazil ice. In calm conditions (as will occur in quiescent tanks) these crystals coalesce to form a thin ice skim. Once the surface of this skim cools below the freezing point, ice growth will begin to progress downward forming a thin ice layer known as nilas. The downward thickening of this ice due to vertical heat conduction through the ice is known as congelation growth. As growth continues, a morphological instability occurs, causing the freezing front to form a corrugated surface of ice lamellae, with the salt rejected from the growing crystal lattice forming briny layers between the lamellae. As cooling and ice growth continues, some brine (as well as some gas bubbles) between the lamellae becomes trapped in brine pockets and some drains into the seawater below, to be replaced by less dense brine within the solidifying basal sea ice layer. Thus, the basal layer of the ice is continuously changing during ice growth. The microstructure in the basal layers, particularly changes in pore structure, fluid, and trapped gas will affect the sound scattering properties of the ice.

In a more turbulent environment, such as in the presence of waves, the frazil crystals remain loosely suspended in the water column. The frazil crystals may be broken by collisions during agitation, which provides sites for nucleation of additional crystals. This, combined with continued heat loss to the atmosphere allows rapid ice production. In vigorous turbulence or large waves, the frazil crystals may be stirred to significant

depth beneath the surface. Frazil damps capillary waves, so that if it is relatively calm, the frazil may calm the surface sufficiently such that the crystals congeal to form white nilas, recognizable by its white surface appearance. While this is relatively level, as for congelation ice, the crystal and pore structure may be significantly different and hence the ice may have different properties affecting a particular sensor.

In a wave field, continued collisions of the frazil crystals will cause them to agglomerate into ice clumps, and eventually these clumps form small rounder pans known as pancake ice. The pancakes will damp the wave energy until it is calm enough for them to freeze together to form a consolidated sheet, and further thickening will occur through congelation growth. Prior to this, however, the space between the pancakes and the action of the waves will cause an oil spill in pancake ice to behave quite differently than it would under a continuous sheet. The oil will pool in the space between the pancakes and the pumping caused be repeated collisions will cause the oil to be pumped onto the surface.

These ice types not only have differing physical properties, but these differences will cause oil-ice interactions to differ among these ice types. These experiments were designed to examine the differences in these interactions and to determine the effects these differences in behavior would have on potential detection of oil with subsea sensors.

### 4.3.2 HSVA AETB ice tank set-up

The AETB is a 30m long, 6 m wide, and 1.5m deep basin in a climate controlled cold facility with a wave-maker so that frazil and pancake ice can be created. The AETB was sub-divided into three separate regions (Fig. 4.3.1) so that experiments in congelation, frazil and pancake ice could all be conducted.

Tank 1 was a quiescent tank in which nilas was to be grown. Due to heat exchange through the far wall of the facility ice did not grow during the experiments, so a nilas experiment was performed in tank 2 with white nilas created by turning of the waves. Frazil was generated by a wave-maker in tanks 2 and 3 (Fig. 4.3.1). By controlling the wave period and amplitude, frazil formation could be sustained in tank 2 while pancakes were eventually created in tank 3. Tanks 2 and 3 were separated by a plywood divider. At the bottom of each tank guide tracks allowed a sensor trolley to run along the bottom.

***Table 4.1*** *Comparison of properties of Alaska North Slope and the medium crude oil used in the experiments*

| | **Alaska North Slope** | **Medium Crude** |
|---|---|---|
| **Density** | 0.858-0.887 kg/m$^3$ | 0.856-0.890 kg/m$^3$ |
| **Viscosity at 30 °C** | 8.1 cSt | 11.5 cSt |
| **Pour point** | -18 °C | -9 °C |

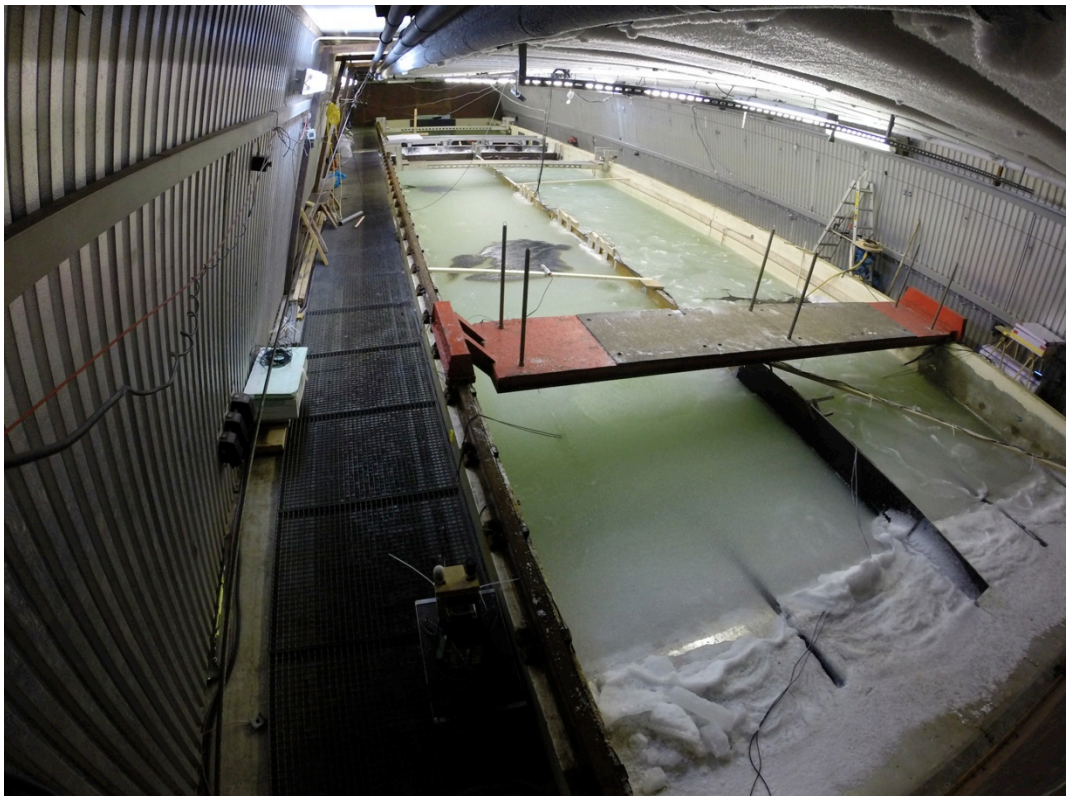

***Figure 4.3.1*** *The AETB facility at HSVA, Hamburg, Germany. Toward the back is the wave-maker. The basin was divided into three tanks. Beyond the wave-maker was the quiescent tank (tank 1). Tank 2 (at left) was used to produce frazil and white nilas. Tank 3(at right) was used to produce pancake ice. The instruments were deployed on a trolley that ran along rails on the bottom of the tank. The trolley was lowered from the movable bridge across the tanks and pulled back and forth toward the "beach" in the foreground where the wave energy was dissipated. Spilled oil can be seen in the center of tank 2.*

For the spill experiments, medium crude was used, as this had properties similar to that of Alaskan North Slope crude (44.3.1). These include a density of 0.856-0.890 kg/m3, viscosity of 11.5 cSt (at 30 °C), and a pour point of -9 °C. The oil was deployed at temperatures of about 5 °C, at the tank bottom. As heat was lost to the water as the oil rose, the oil cooled during release and melting of the ice by the oil was minimal. Because of the low temperature, the oil was very viscous when released.

### 4.3.3 Instrumentation in the AETB facility

**Camera systems**

The camera systems included a suite of fixed GoPro Hero cameras and a high-definition underwater video camera. GoPro cameras included. The GoPro cameras used were a combination of GoPro Hero 3+ Black (12 MP), and Silver (11 MP) editions with flat lens mounts (when underwater). These have an f-stop of f/2.8 and a native field of view of 170 degrees (effective focal length of ~12 mm for a 35 mm camera equivalent).

1. Three cameras were mounted overhead looking vertical downward to monitor ice and oil over the length of tank 2. These took images at one minute intervals. They

were generally in operation for the duration of the experiments. Two cameras were switched to tank 3 when the pancake experiment was performed.
2. Three cameras were mounted looking upward in tank 2. Images were captured at one minute intervals. Two of these cameras failed during the course of the experiment, but upward-looking imagery was obtained during most experiments.
3. During most experiments, GoPro cameras were mounted on the instrument trolley. Typically one looked vertically upward. A second one was mounted looking to the side of the tank to track the trolley location during some experiments.
4. One camera was placed in the corner of the facility to provide time-lapse monitoring the entire experiment.
5. A high-definition underwater video camera was used to monitor each oil spill from below. This was a Delta Vision HD underwater camera with 1080p resolution, focal length of 3.6 mm, and a light sensitivity of 1 lux.

**Sonar systems:**

1. Two sets of AQUAscat 1000 (http://www.aquatecgroup.com) narrowband sonar transducers were deployed at different positions on the tank bottom. Transducers operated at nominal frequencies of 300 kHz, 500 kHz, 1 MHz, 2 MHz, and 5 MHz. One set of transducers was place on the instrument trolley during the oils spill experiments.
2. Two sets of Panametrics transducers at frequencies of 350-565 kHz and 700-1050 kHz were deployed on the trolley. The broadband system was the same one that was used in the CRREL ice tank tests.
3. Three pairs of Panametrics transducers (200-300 kHz, 350-565 kHz, and 700-1050 kHz) were used with the broadband system

**Optical systems:**

1. Three TRIOS RAMSES hyperspectral radiometers were deployed to investigate the spectral attenuation and scattering of light through the oil spills. One irradiance and one radiance sensor were deployed on a mobile trolley, and one irradiance sensor was deployed above the ice to measure the incoming radiation field
2. The WHOI laser fluorometer was deployed on a separate mobile trolley and profiled the underside of the ice after the oil spills.

**Oil injection system**

The oil injection system used at HSVA can be seen in Fig. 4.3.2. For each spill 10 litres (for frazil and nilas) or 5 liters (for pancake) of crude oil (at 5°C) was poured into the funnel from pre-measured 10 litre cans. Care was taken that no air was introduced during this procedure. When the oil left the hose (diameter 5 cm) it separated into globules that rose up to the underside of the ice. The whole procedure took only a few minutes.

### 4.3.4 Experiments in AETB tanks

During the first week of the experiments, instrumentation was installed and tested, and ice growth was begun. At this time, a separate project to examine wave-ice interaction was conducted. Oil spill experiments were begun on 17 December, 2013.

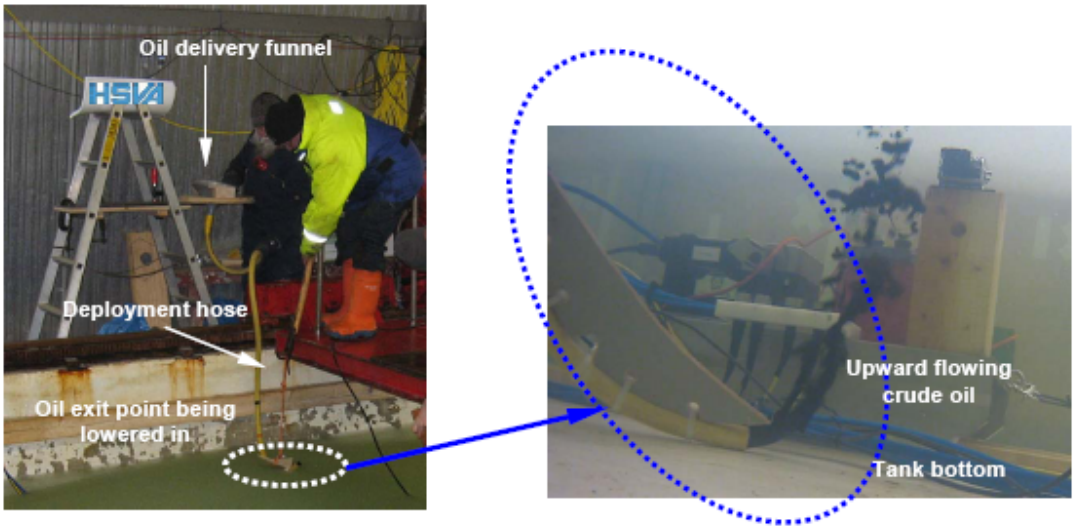


***Figure 4.3.2*** *Oil deployment procedure at the HSVA experiments. Oil was delivered below the ice using a funnel connected to a hose from above (left), which was held at the bottom of the basin so that oil could rise upward to the base of the ice (right).*

#### 4.3.4.1 Frazil ice spill

On 17 December 2013, an approximately 8 cm thick layer of frazil ice was produced (Fig. 4.3.3). The frazil was about 1 week old; it was prevented from consolidating by maintaining a 0.65 Hz wave propagating through the tank.

Ten liters of oil was spilled below the frazil layer with the wave-field present. The buoyant oil rose to the base of the oil layer. Once at the bottom of the frazil, spreading was fairly minimal, but the oil penetrated the frazil layer until it reached the surface where it spread laterally, displacing the frazil ice (Fig. 4.3.4). Two mechanisms contributed to the penetration of the oil through the frazil ice. First, the buoyancy of oil would tend to cause it to push through the porous, unconsolidated frazil layer. Although this ice is very porous, it is more likely that the oil would displace the frazil rather than percolate through due to the high surface tension and viscosity of the

***Figure 4.3.3*** *A lexan tube was used to measure the thickness of the frazil layer.*

oil spill. The repeated dilation and contraction of the frazil layer in the wave-field would also have aided the transport of the oil to the surface, as this would simultaneously spread the frazil and accelerate the oil movement towards the surface.

Over time, the oil spread at the surface. Fingers of oil spread from the edges of the originally circular spill into the frazil, and the shape deformed somewhat in the wavefield.

Once spreading had nearly ceased, the wave-maker was turned off and the frazil froze together to form a continuous sheet of white nilas. Once the frazil had frozen together to form a solid ice sheet three ice cores were taken at different locations in the spill and the nearby clean ice (Fig. 4.3.5). The cores were frozen at -20°C for 24 hours. These cores showed that the oil had almost entirely percolated to the surface layer, with clean ice below (Fig. 4.3.5), suggesting that while a spill in frazil ice may be seen from above, it may be more difficult to see it from below in a very thick frazil layer. For thicker frazil layers, however, it is not clear how well the oil would percolate through the thicker ice.

***Figure 4.3.4*** *Oil pushed its way through the frazil layer and spread over the surface.*


***Figure 4.3.5*** *The frazil spill as seen from above (left) after consolidation of the frazil ice, and the location of core sampling sites. The core samples showed the oil had entirely percolated to the upper ice layer (right).*

#### 4.3.4.2 Nilas ice spill

With the wave-maker turned off, the frazil layer was allowed to consolidate to form white nilas. The ice cooled overnight prior to the second oil release. Because of the short time to cool the ice and the thickness of the initial frazil layer, the ice would have had a high

brine content and be fairly porous, with possibly some unconsolidated frazil at the base. The frazil layer may have led to a slightly irregular ice underside.

A second ten litre oil release was performed under a clean area of this nilas. Because of the surface tension of the cold oil, it rose to the surface in small droplets and blobs, which accumulated into an irregular slick on the underside. The oil spread to a roughly circular patch about 2 meters across. However, the topography of the spill was irregular, with many small-scale undulations and with a pock-marked appearance (Fig. 4.3.6). Percolation of oil through brine drainage tubes could be seen at the surface. The oil spill could be seen through the ice at the surface, although little oil percolated all the way through, so most of the oil stayed underneath the ice. It is unclear what was the relative contribution to the oil spill bottom topography from the oil properties, the ice underside topography, or the percolation of oil through brine drainage features.

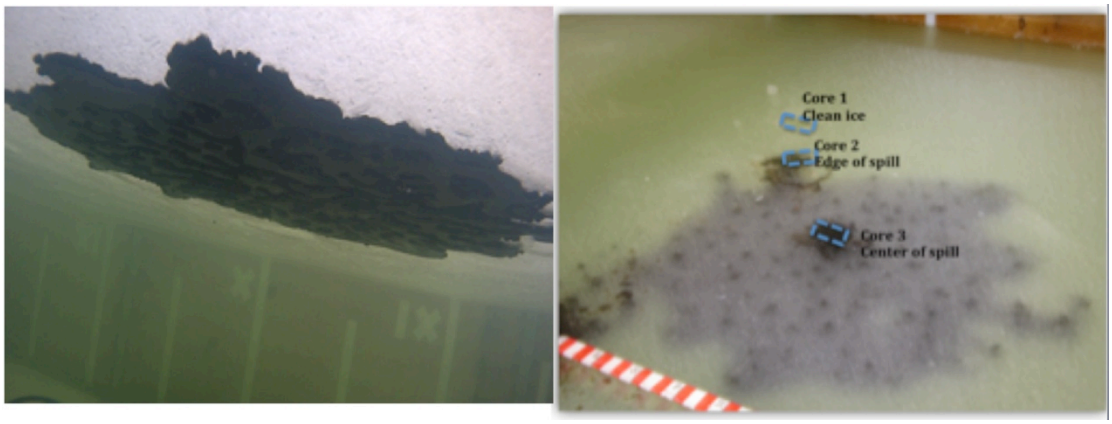


***Figure 4.3.6*** *The oil spill under nilas viewed from below showing an undulating topography (left). The spill could be seen from the surface due to the thin ice, although little oil percolated through. A pock-marked appearance resulted from oil percolating part way through brine drainage features. The location of cores taken after the experiment is indicated. Note the oil on the surface is due to spillage during deployment or taking of cores.*

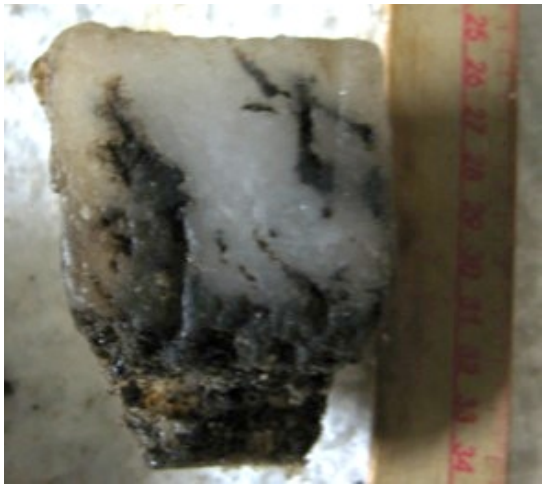

***Figure 4.3.7*** *A thick section of the ice core sampled in the center of the nilas spill as shown in Figure 4.3.6. Most of the oil is found under the ice, although percolation of oil through the brine channels is clearly seen. However, little oil percolated all the way to the surface. Other sections of the same core showed no oil above the bottom layer; i.e. the oil in the upper ice was confined to isolated channels.*

Three ice cores were taken (see Fig. 4.3.6) from the spill site, which were frozen at 28°C for later analysis. Results confirmed that the oil was contained at the bottom of the ice.

However further sectioning of these cores provided evidence of the upward percolation of the oil through the porous ice (see Figures 9 and 10).

#### 4.3.4.3 Pancake ice spill

On 18 December, 2013 five litres of crude oil were spill under pancake ice in tank 3 using the same technique as before. At the time of release, the pancakes were 20-50 cm in diameter and about 10 cm thick. When the oil droplets rose to the ice underside, they flowed along the bottom immediately and accumulated in the gaps between the pancakes rather than form a continuous slick. The cyclic motion of the pancakes induced by the wave field caused repeated dilation and contraction of the space between the pancakes, pumping the oil horizontally along the gaps between the pancakes, and pumping some oil onto their surface. Although the oil could be seen from below in the gaps between the pancakes, little oil was present on the underside of the pancakes. If the ice were to continue to freeze, most of the oil within the gaps would quickly encapsulate. It is unclear if this behavior would be the same for much larger oil volumes.

These results show that the nature of the ice cover and the presence of a wave field have a significant impact on the ice-oil interaction, but also on the appearance of the oil spill from underneath. This will have a significant impact on the mode of detection of the oil using undersea sensors.

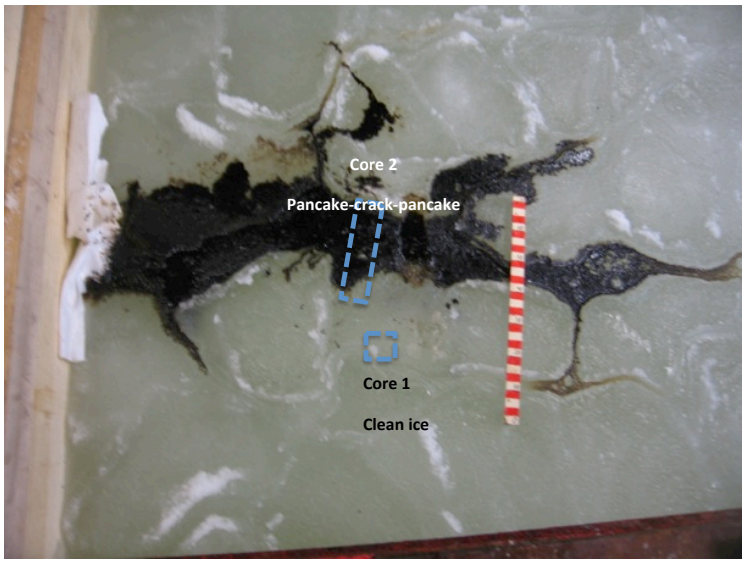


***Figure 4.3.8*** *Oil trapped beneath pancakes and pumped onto the surface due to cyclic wave motion. Little oil was seen after the spill on the bottom of the ice.*

### 4.3.5 HSVA small tank experiments: broadband sonar

Additional acoustic scattering experiments were carried out in a small tank at HSVA in a separate cold room. These were intended to supplement the broadband sonar measurements made at CRREL using the same broadband system, but with a wider variety of transducers and with better spatial scattering statistics.

The experiment was performed in a 1.4 m diameter, 2000L capacity plastic tank (Fig. 4.3.9). Prior to filling the tank seven pairs (bistatic) of broadband, piston-like transducers were mounted on the bottom of the tank. The pairs were closely spaced to approximate monostatic measurements. Three pairs of transducers (200-300 kHz,

350-565 kHz, and 700-1050 kHz) were used to obtain stationary measurements during ice growth and following the deployment of the oil at a single location. The other four sets of transducers (two 350-565 kHz, two 700-1050 kHz) were used for spatial sampling of the bottom of the water/ice and water/oil interfaces. The four transducers for spatial sampling were deployed on plastic mounts that could be pulled along threaded rods from the surface. The ropes to pull the carts were marked at 5 cm intervals so that sampling could be performed at the same locations throughout the experiment. The tank was filled to a depth of 116 cm (90 cm above the transducers). A GoPro Hero 3 camera with wired power and live feed was mounted looking up at the bottom of the tank, although this failed before the oil was spilled. Instead, another GoPro camera was lowered through the access tube through which the pull-cart ropes were run. Once the tank was filled, it was covered and left overnight to allow the surface disturbances to dampen. Each transducer pair was calibrated by taking scattering data from the undisturbed water surface. Following the calibration, the temperature of the room was decreased to -18°C and ice formation began.

Three types of sampling were performed in the tank: overnight sampling with the 700-1050 kHz stationary transducer pair, "time series" measurements using the three stationary transducer pairs, and spatial measurements using the "mobile" transducer pairs. During overnight hours, access to the facilities was not possible so the 700-1050 kHz stationary transducer was programmed to obtain measurements once per minute. At a minimum, data were obtained using all three stationary transducer pairs each morning and afternoon with the exception of the weekend when access to the facilities was limited. Spatial samples were obtained using the mobile transducer pairs each morning and afternoon (with the exception of the weekend).

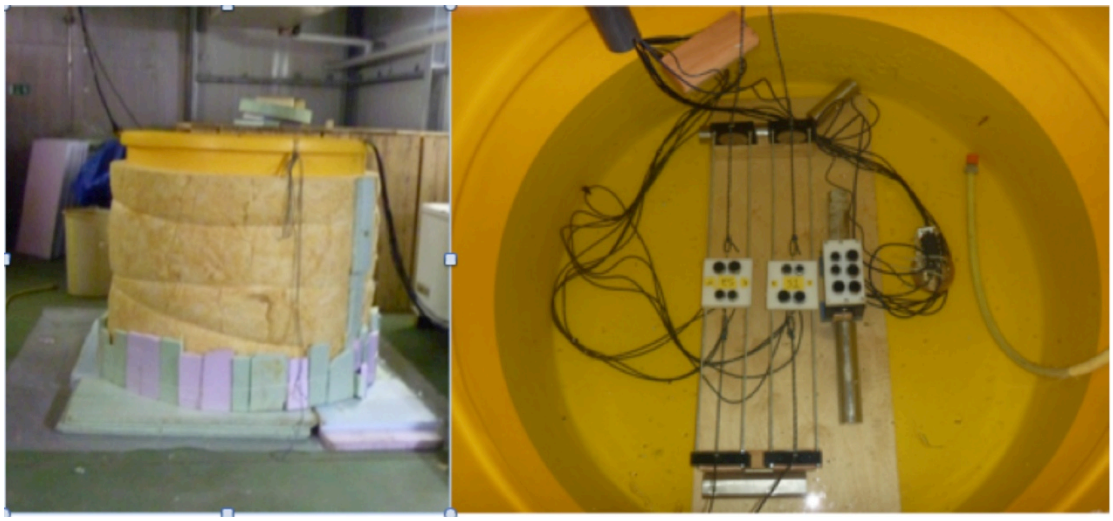

**Figure 4.3.9.** A 1.4 m diameter insulated tank was used to perform broadband measurements of oil under congelation ice at HSVA (left). The six 'time series' transducers were centered horizontally and located at the center of the tank. The four pairs of transducers for spatial measurements were deployed on two rail systems allowing the transducers to be pulled horizontally to span a range of approximately 90 cm (right). Various pipes through the ice were used for cables runs, to release hydrostatic pressure, and to move the carts.

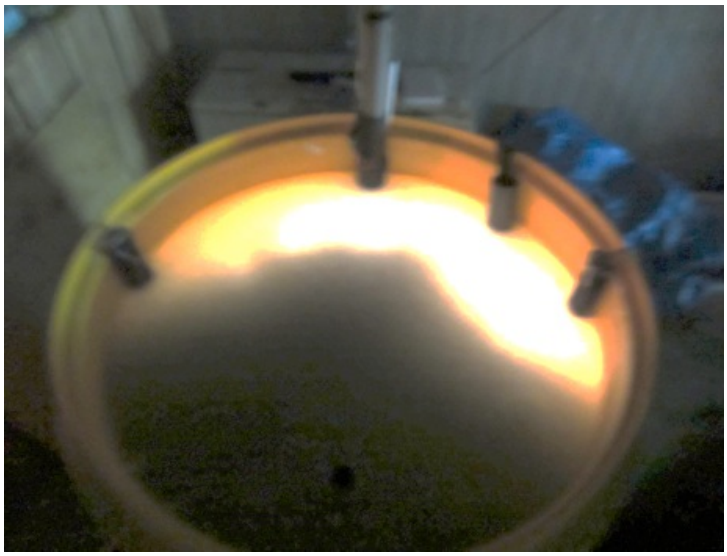

***Figure 4.3.10.*** *Lighting from below the surface shows the distribution of the oil beneath the ice. The stationary measurements were obtained in the areas beneath the oil (closest to the camera) while the spatial measurements cross from an area with little or no oil (center-right), under thicker oil (center), and again to an area with little or no oil (center-left).*

Ice growth began on late in the evening on December 12. The ice continued to grow undisturbed until the afternoon of December 16. At that point, 50 L of crude oil were introduced to the tank using a pipe that had been drilled through the oil surface on December 14. It was expected that the 50 L of oil would spread evenly below the surface of the ice producing a homogenous 3 cm layer of ice; however, this did not occur (Fig. 4.3.10). While the oil was being introduced, the ice surface lifted by roughly 2.5 cm (inferred from the sonar data). Following the spill, the experiment continued until December 20. Changes in the backscattered acoustic signal suggest that ice formation below the oil began late on December 18. By December 20 more than 2 cm of ice had formed beneath the oil.

### 4.4 SAMS acoustic experiments

Based on the results of the two prior ice tank experiments, additional sonar oil-under-ice detection experiments were performed in two ice tanks in a cold room at the Scottish Association for Marine Science (SAMS). For these experiments, an Aquatech Aquascat 1000 system was used again, but with lower transducer frequencies to attempt to better detect encapsulated oil.

#### 4.4.1 Experimental set-up

Sea ice was grown in two identical water butts (top diameter: 740mm, bottom diameter: 720mm, height: 1140mm, water volume: ~320 litres). The outside of the butts were insulated using household fibreglass insulation. They were then housed in a wooden structure (Fig. 4.4.1). This thick insulation ensured that heat was only lost through the open water surface, and not through the sides of the tank, to ensure only downward ice growth.

At the bottom of the tank a concrete plinth was installed on which the instrument trolley and associated rails were placed. Located on the trolley were 4 transducers at 300 and 500 kHz and 1.0 and 5.0 MHz (Fig. 4.4.2). A heater pad was placed at the bottom of the tank to increase the water temperature during the melting phase of the experiments.


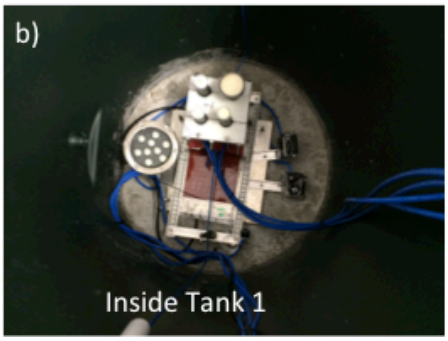


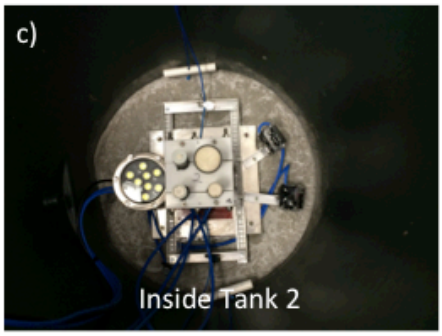


**Figure 4.4.1 a)** Photograph showing the two water butts. Tank 1 (left) is fully enclosed in its wooden housing. Tank 2 (right) shows the insulation around the tank before wooden housing is installed. Blue cables in the photograph lead to the transducers that are mounted on the trolley. **(b)** and **(C)** Photograph of bottom of tank showing the lighting system (large round circle on the left) and trolley with the four transducers (centre), heater pad (red rectangle).

Both tanks were identical, except two ice mass balance sensor chains (IMB) were installed in Tank 2 to provide ice temperature and thickness data during the growth and melt phases (Jackson et al., 2013).

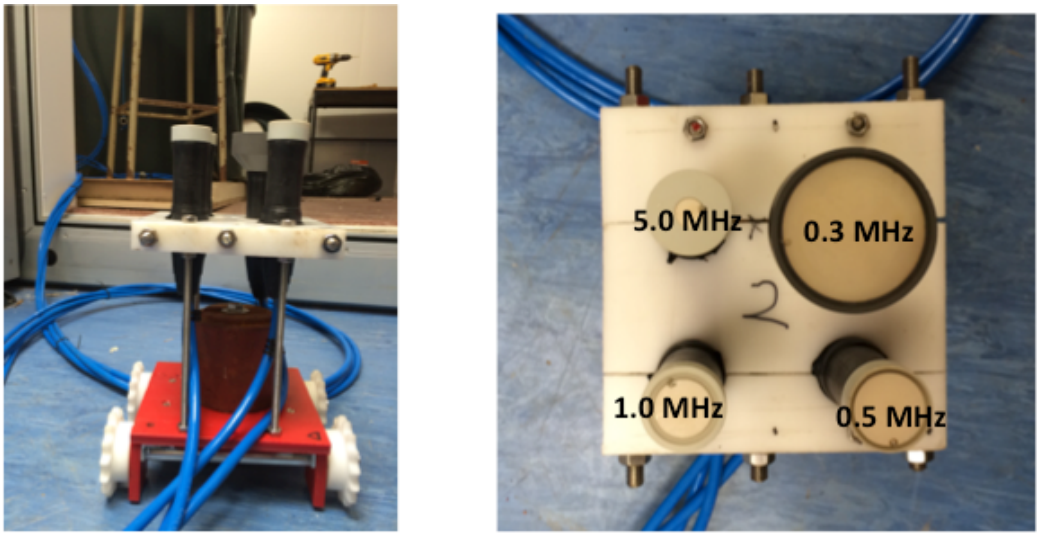


**Figure 4.4.2** Side view of the trolley and its cog-wheels (left). The cogs ensured that the location of the trolley was known at all times. Four acoustic transducers were mounted on the trolley (top view, at right)

### 4.4.2 Sea ice growth

Seawater was pumped into the tanks and allowed to cool and settle so that any particulate would fall out of the path of the sonars. At this stage the water and air temperature was about 15°C. The air and water temperature profile (from the IMB chain) for the duration of the experiment can be seen in Fig. 4.4.3.

On April 25, 2014, the cold room was cooled to down to around -3°C. We kept this temperature over the weekend, as we wanted the water to cool but remain ice-free.

**Ice growth phase**

On April 28 the water was indeed ice-free so we turned the air temperature down to about -20°C until ice began to form. When the ice was about 5 cm thick insulation boards were placed over the upper surface of the growing ice to produce hollows on the underside of dimensions of about 0.5 m in diameter due to the retarded growth rate under the insulation (Fig. 4.4.4). The trolleys were parked directly below the hollows.

On April 30 oil was injected into the hollow below the ice in Tank 1 and Tank 2. At this stage the ice thickness away from the hollow was about 0.12 m and about 0.07 m in the hollow itself. The evolution of the ice thickness (in Tank 2 as seen by the IMB) to the side of the hollow, is seen in Fig. 4.4.5. Over the next week the temperature continued below freezing. During this ice growth stage the temperature was cycled. This was performed in order better understand the acoustic signature of growing sea ice with different growth rates, although this is not investigated in this report.

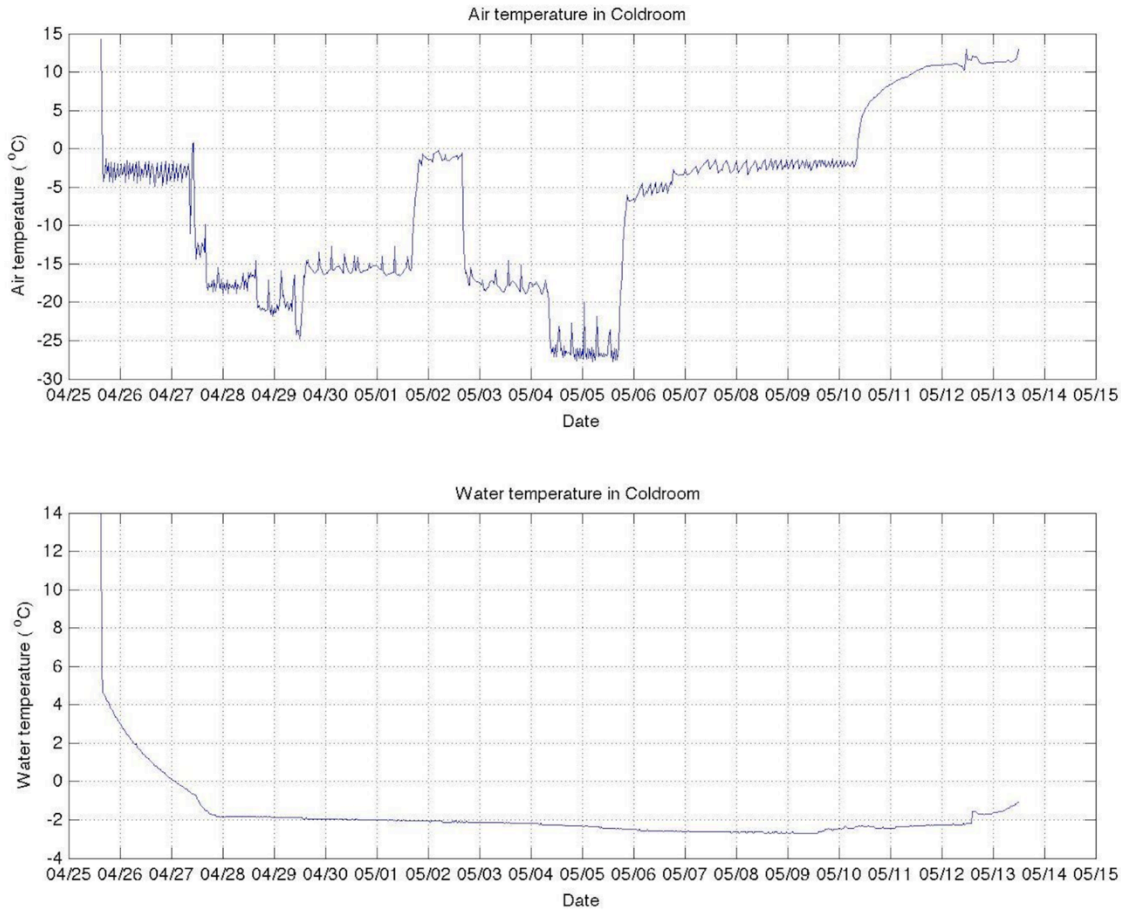


***Figure 4.4.3*** *Air (top panel) and water (bottom panel) temperature during the experiments as measured by the IMB. The water cooled to the freezing point on April 25th. The air temperature was cycled between -3 °C and -25 °C to potentially examine the acoustic signature of the basal ice layer for different growth rates.*

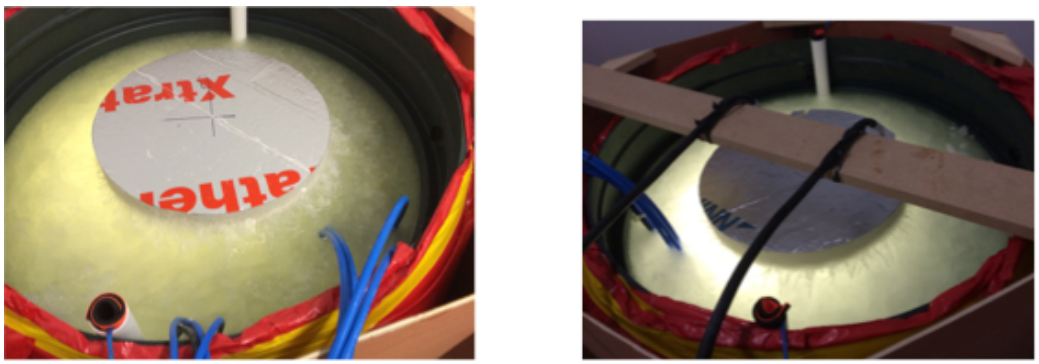

***Figure 4.4.4****. Location of the insulation in Tank 1 (left) and Tank 2 (right) used to create a hollow in the ice thickness to contain the spilled oil. Illumination from below was provided by lighting installed in the tanks.*

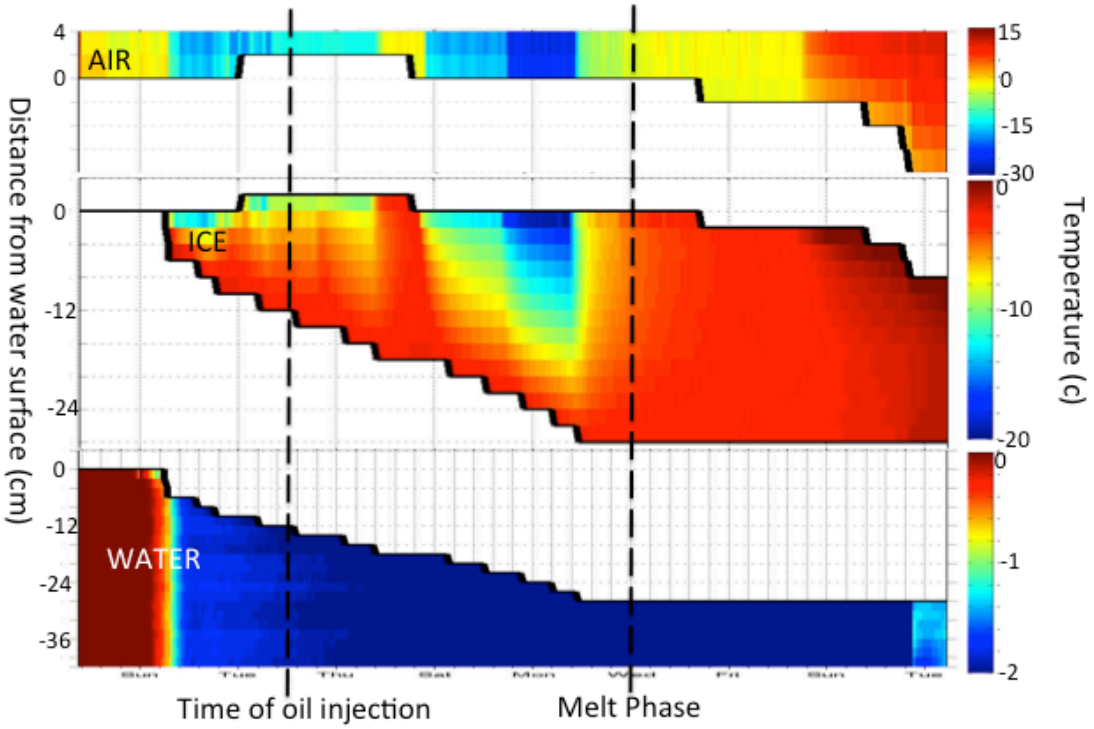


***Figure 4.4.5.*** *Temperature profiles through the air (top), ice (middle), water (bottom). Ice growth is seen by the step staircase at the bottom of the ice temperature profile (which is due to the discrete sensor placement and is not a physical effect).*

**Ice melt phase**

On May 7 the melt stage began – one week after the oil injection. During this time, about 15 cm of ice (as indicated by the IMB results) grew beneath the oil layer. The air temperature was increased to -2 ℃. The heaters on the bottom of the tank were turned on for 8 hours to simulate solar heating of the ocean. The heater was again turned on May 8, for 9 hours. The following day the heaters were turned on constantly, and on May 10 the cold-room was turned off. This resulted in the air temperature increasing significantly and the water temperature only rising very slightly (Fig. 4.4.3).

With the above zero air temperature the surface melt of the ice began in earnest. This can be seen in Fig. 4.4.5 (ice profile) where the surface of the ice moves from 0 to -10 cm. As the ice was locked to the side of the tank, the melting ice produced a lens of water above the ice surface. Interestingly, the oil began to be released before the ice melt reached the encapsulated oil layer. This release occurred as small droplets rose though the brine pore space in the ice before being released into the water column, and then rose to the water surface (Fig. 4.4.6).

Once the melting ice surface reached the encapsulated oil pocket all the oil was released. The region that contained the oil seemed to melt preferentially, and the hollow that once contained the oil was left remarkably clean (Fig. 4.4.6).

***Figure 4.4.6*** *The melt phase of the ice* ***a)*** *At this stage the oil hollow is still below the ice surface, but droplets of oil can be seen rising up through the ice internal pore space and into the water.* ***b)*** *The Ice surface once the water and oil has been removed. Very little evidence of the oil can be seen. However this may be due to the melting out of oil contaminated ice. The hollow extends beyond the open area seen in the photo.*

## 5. Acoustic experiment results

This section describes the results of sonar experiments for each of the three experiments. Although similar measurements were made in each test, the results are grouped here by experiment because the conditions in each varied (see Section 4, above). These sections describe the general characteristics of the acoustic scattering from the oil and ice underside, its variability during the experiments, and changes in the signal as the oil became encapsulated. A key result is the ability to detect oil thickness through the characteristic multiple returns from the oil/water and ice/oil interfaces. This will permit the determination of the thickness of the oil layer, and hence, when mapped over the extent of the spill, the oil volume. Discussion of the determination of thickness and volume is summarized in Section 5.4.

### 5.1 CRREL acoustic results

#### 5.1.1 Broadband acoustic results

The laboratory broadband system used in the experiments is described above in Section 4.1.1. For these experiments, pairs of Airmar transducers at 160 kHz and 500 kHz center frequency were used and alternated during the experiment. The sampling regime was varied throughout the experiment, but for the results presented here, a pulse consisting of a 250 μs linearly modulated chirp was used with a 1s sample interval during attended tests, and 1 min interval when run overnight or other long periods. Most tests were run with the 500 kHz transducers with a 200 kHz bandwidth, as these provided the better vertical spatial resolution. The 160 kHz transducers were run with 80 kHz bandwidth. The lower frequency transducers were used as the lower frequency may provide better penetration into the basal ice layers. For these experiments, the transducers were not calibrated, in part because a possible grounding issue caused a somewhat variable signal level. Nevertheless, the signal had good temporal consistency so that variation in the scattering signal provided robust results in terms of the ability to detect oil.

The principal reason for use of broadband techniques is the improved range resolution provided by pulse-compression techniques (e.g. Turin, 1960). Rather than a range resolution given by

$$R = \frac{1}{2} c_w T$$

where $c_w$ is the sound speed in seawater (~1443 m/s here) and $T$ is the pulse width, for a chirp pulse the range resolution, R, is given by

$$R = \frac{c_w}{2B}$$

where B is the signal bandwidth. So rather than a range resolution of 18 cm, which would could not resolve the layering, the resolution is 0.9 cm for the 120-200 kHz transducers, and 0.4 cm for the 400-600 kHz transducers. At these frequencies, one could of course transmit a shorter narrowband pulse (with a minimum of one wavelength, or about 3 mm for the 500 kHz transducers, though in practice this would need to be much greater to acquire reliable scattering statistics for quantitative determination of reflection

coefficients), but at the expense of much less energy input. On the other hand the matched filter must be chosen to minimize effects of side lobes. For the transducers used at the approximately 1.3 m range to the ice, the sonar footprints are estimated to be of order 10-20 cm. This scale is well above that of individual ice skeletal layer lamellae but only somewhat larger than that of individual (e.g. Weeks, 2010) crystals and similar in scale to that of individual brine channels for thin ice (Wakatsuchi and Kawamura, 1987) so that scattering could vary depending on the crystal alignment or ice structure.

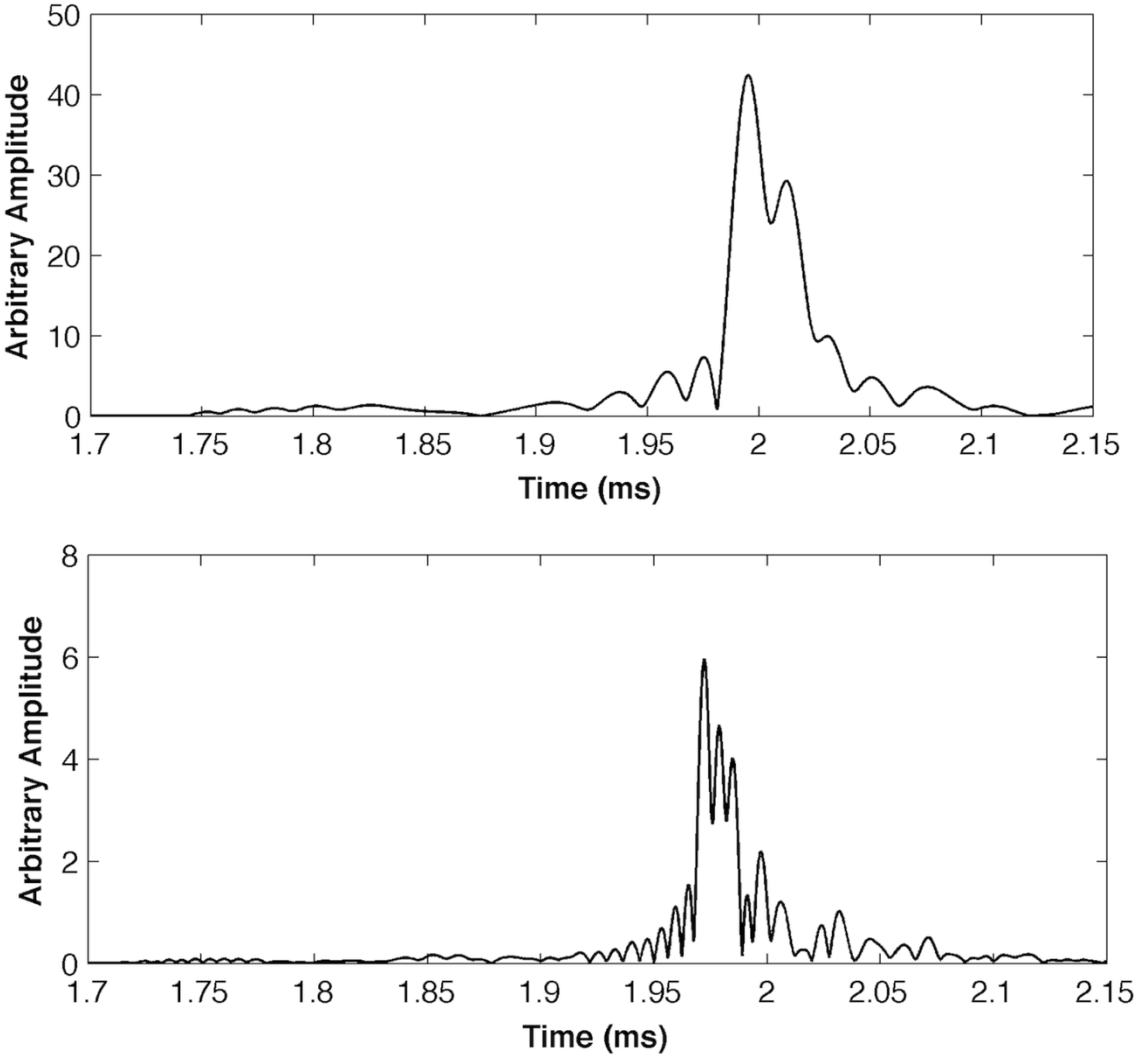


***Figure 5.1.1*** *Backscattered pulse compressed output for 160 kHz (top) and 500 kHz (bottom) signals from the basal ice layer prior to oil release. The ice bottom is located at 1.96-1.98 ms (the two traces were taken two hours apart), corresponding to a range of 1.41 – 1.43 m. The ripples ahead of the main peak are due to side lobes and/or effects of the matched filter processing. More structure after the ice/water interface is visible after the main peak.*

Backscattered signals of the base of the 15 cm ice layer on May 21 before the release of oil are shown in Fig. 5.1.1 for both 160 kHz and 500 kHz signals. These traces, taken two hours apart, show a strong peak at the ice/water interface, corresponding to a range of

~1.41 -1.43 m (the differences are due to a combination of variation in ice thickness and some ice growth. Some rippling in the signal is visible due to limitations of the matched filter processing and transducer side lobes. In both signals, structure within the basal ice layer is apparent, extending at least an apparent 10 cm beyond the ice/water interface (this distance is actually less, as the sounds speed in the ice basal layer is significantly more than in the seawater – up to about twice the speed for pure ice, but likely somewhere in between and variable in this porous layer). This structure was not constant, but changed on time scales of minutes to hours. The causes of this variability is not clear, but may be due to brine exchange and phase change processes in this basal layer. The multiple peaks visible in the 500 kHz signal may be due to reverberation within this basal layer, possibly representing the first scattering horizon in the ice and a second above where there is a significant sound speed change, perhaps where there is some kind of transition in the connectivity of the brine network. If so, this technique may be useful for performing non-destructive investigations of the basal ice structure. Understanding these scattering properties may be important for understanding potential contrasts between clean sea ice and sea ice with thin layers of oil beneath.

As the ice continued to grow overnight, the main peak in the 500 kHz signal split (Fig. 5.1.2). This is possibly the signal of a platelet layer (see Section 4.2) formed as anchor ice crystals rose to the surface. The upward movement of these were occasionally seen during the experiment when the sonar was recording at a high repetition rate. If this is the case, the thickness of this layer appears to be ~7-10 mm, depending on an appropriate sound speed through the ice-water 'mush'.

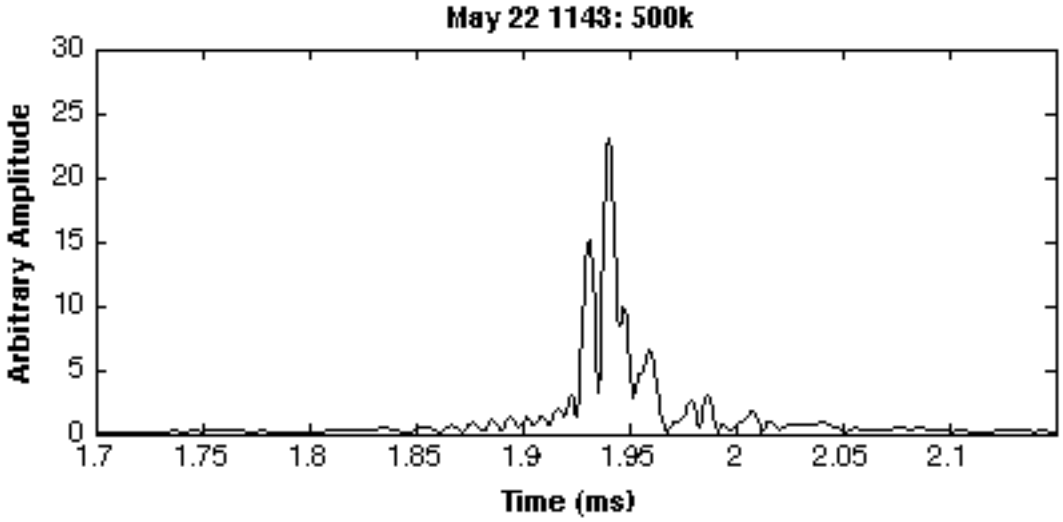


***Figure 5.1.2*** *The echogram at 500 kHz on 11:43 AM on May 22, 22 hours after the results in Fig. 5.1.1. The ice has grown by 3 cm overnight, but more structure has appeared as the main peak has split in two. Comparison with Fig. 5.1.1 shows that there is coherence in the smaller peaks after ~ 2 ms (although they are time-shifted due to the change in sound speed), suggesting that this represents physical structure in the ice.*

After the release of oil at 16:00 on May 22, the returned signals changed dramatically. The oil/water interface and oil/ice interfaces are shown clearly in the

160 kHz signal, as was shown for the 1.1 MHz narrowband sonar demonstrated in Wilkinson et al., in press. After 1 hour, a ~5 cm layer of oil was visible. (Fig. 5.1.3)

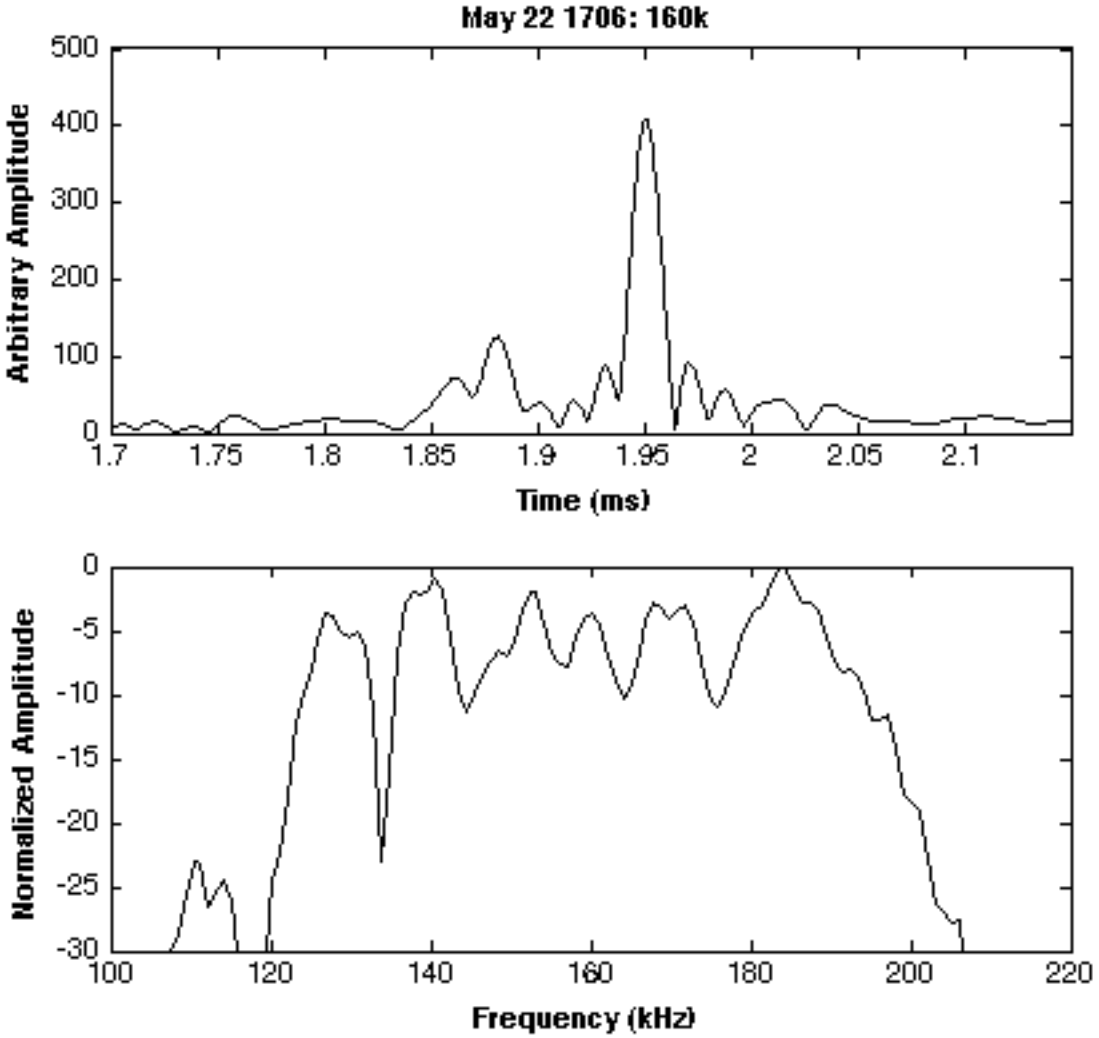


***Figure 5.1.3*** *The echogram at 160 kHz 1 hour after the oil spill on May 22 (upper panel). The dual peaks of the oil/water and oil/ice interfaces are clearly visible. The frequency response provided by the broadband data provides an alternate means of characterizing the water/oil/ice system (lower panel). The spacing of the peaks and nulls is a function of the spacing of scattering layers in the spatial domain.*

In contrast, the 500 kHz signal shows a surprising result, the reasons for which remain unclear. As soon at the oil was deployed, the visible structure in the ice vanished, as if the oil destroyed the basal structure. No oil peak was apparent even for several hours after (Fig. 5.1.4). This phenomena was not seen in any other test, and the proximity of the transducers in the tank suggests they should have overlapping footprints, so it is difficult to draw any conclusions from this test, except that it does appear that the oil layer may alter the basal ice layer (possibly due to mechanical alteration, penetration into the ice, or melting), as this effect is also apparent to some degree in the 160 kHz signal (compare Fig. 5.1.1 and 5.1.3).

Another advantage of the broadband sonar is information in the frequency spectrum can be exploited to also characterize the ice structure. Following Lavery and Ross (2007) the frequency dependence of the scattered pressure can be expressed as the normalized frequency dependent Pressure, *P(ω)* as follows:

$$P(\omega) = \frac{P_{scat}(\omega)}{P_{inc}(\omega)} = G(\omega)\frac{V_R(\omega)}{Vcal_R(\omega)}\frac{r_{scat}}{r_{cal}}$$

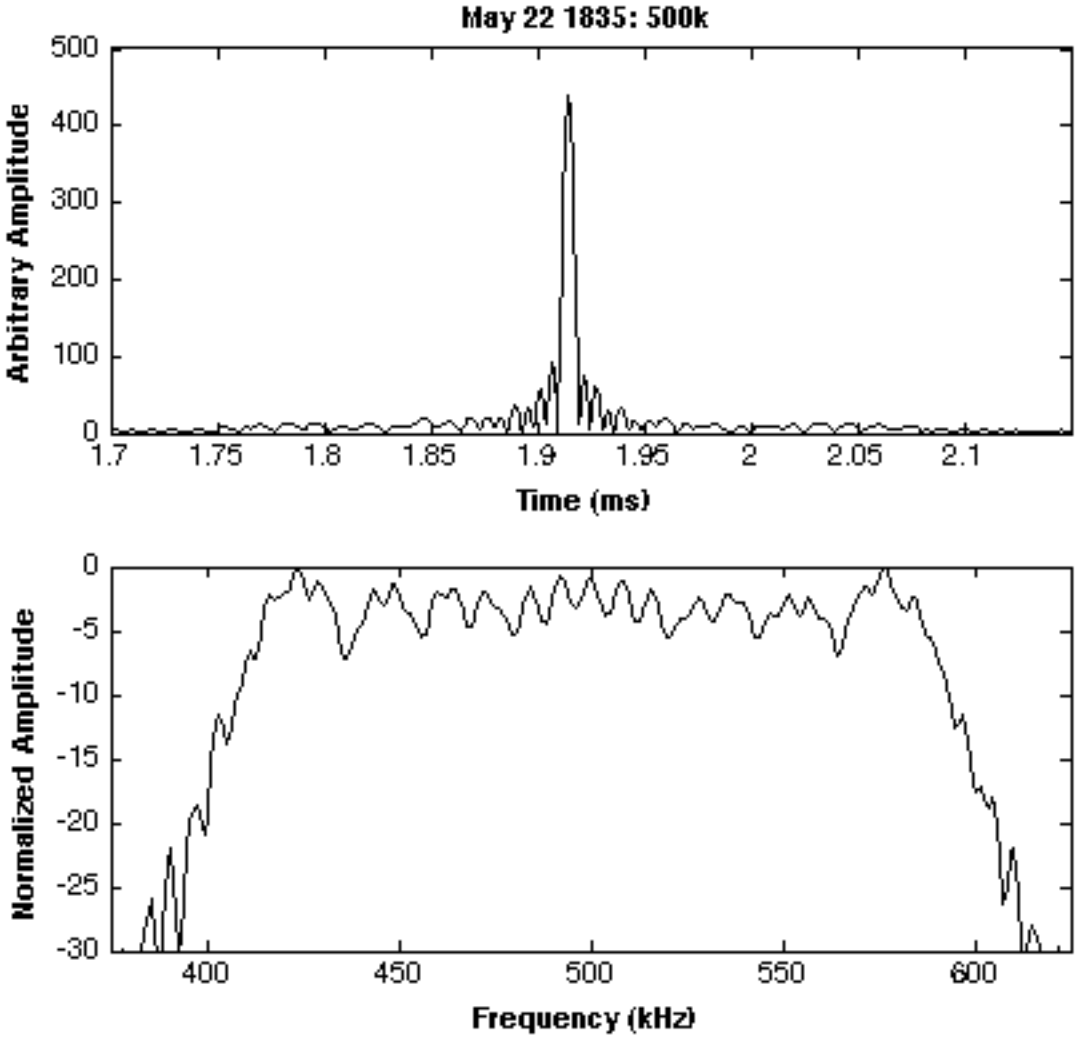


***Figure 5.1.4*** *The echogram at 500 kHz 2 hours after the oil spill on May 22 (upper panel). In contrast to Fig. 5.1.2, the oil peak is not apparent. In contrast, the ice/water interface is a sharp peak – the only peak visible. It appears that the oil has altered the basal ice structure upon spreading – possibly spreading quite thin in the region insonified by the 500 kHz sonar, although this is not clear. The frequency spectra shows no significant structure.*

where $P_{scat}$ and $P_{inc}$ are the scattered and incident pressure, respectively, $V_R$ and $Vcal_R$ are the Fourier transforms of the returned signal voltage and the calibrated signal returned voltage, $r_{scat}$ and $r_{cal}$ are the range and the calibrated range, respectively. $G(\omega)$ is the ratio

of the absolute value of the Fourier transforms of the transmit calibration voltage time series to that of the transmit voltage time series. Since the transducers were not calibrated, only an approximate spectrum could be obtained from the Fourier transform of the received voltage time series. While not quantitatively correct, the signals were consistent enough such that this provides qualitative frequency spectra of the returned signal. These are shown in Fig. 5.1.3 and 5.1.4.

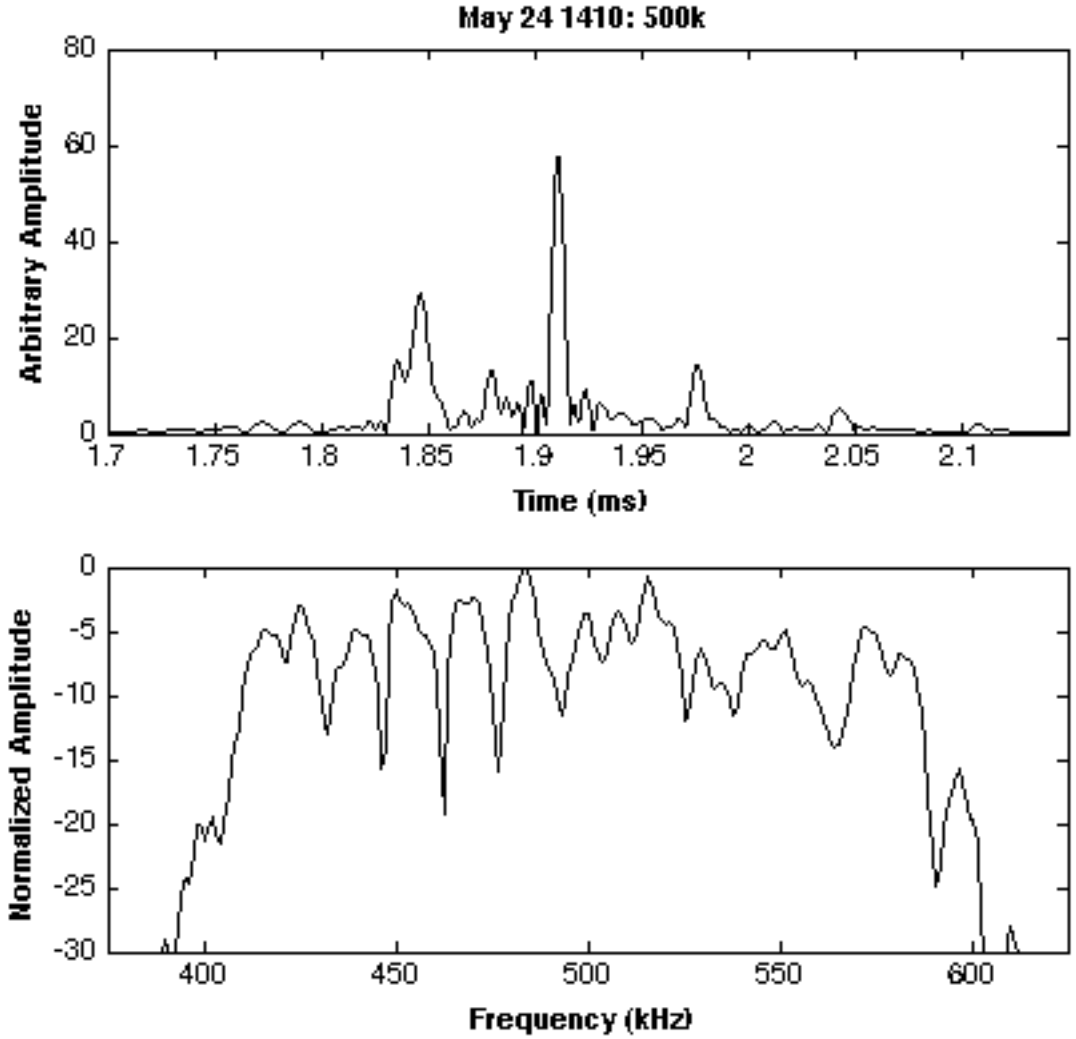


***Figure 5.1.5*** *By the 24th, two days after the oil was spilled, encapsulation had begun. The oil peak (visible late on the 22nd) had begun to split as a thin ice layer formed beneath the oil (top panel). Reverberation in the oil layer was apparent by regular sequence of peaks beyond the original ice/oil peak. A series of nulls in the frequency spectra (bottom panel) appeared due to this reverberation.*

The spectra show a series of peaks and nulls. The nulls represent frequencies for which destructive interference of signals at that frequency cancel out. This will happen when reverberation between two interfaces caused superposition of two returned signals. This occurs, for example if a layer is a precise number of wavelengths in thickness. Because this would occur at any integral number of wavelengths, these nulls repeat at a frequency

spacing that is related to the thickness of the layer. This regular pattern of nulls is clearly seen in Fig. 5.1.3, where there are two distinct interfaces, but absent in Fig. 5.1.4 where the oil/water interface appears absent.

The oil layer became clear in the 500 kHz signal overnight. By the 24th, encapsulation had begun (Fig. 5.1.5). At this point a thin ice layer had begun to form beneath the oil layer, which was about 4.7 cm thick at this point. The frequency spectra now showed a clear signal of destructive interference due to reverberation in the oil layer.

Over the next four days, encapsulation progressed until about 5 cm of ice had grown (as determined by the change in sonar range) (Fig. 5.1.6). For the bottom traces, the peaks at 1.85 ms are the bottom of the oil layer (1.34 m from the transducer with a sounds speed of 1443 m/s). The peak at 1.91 ms is the original oil/ice interface. The peak at 1.97 ms is due to reverberation in the oil layer. Note that the original oil/water interface appears to move downward as it encapsulated (e.g. note the peak in the 4th trace from the top at ~1.82 ms on the morning of May 28). This is because the sound speed in the ice layer is as much as twice that in the water or oil, so these peaks are received earlier than they would be without the ice layer beneath (for 5 cm of ice, this would be received about 0.3 ms earlier than without ice).

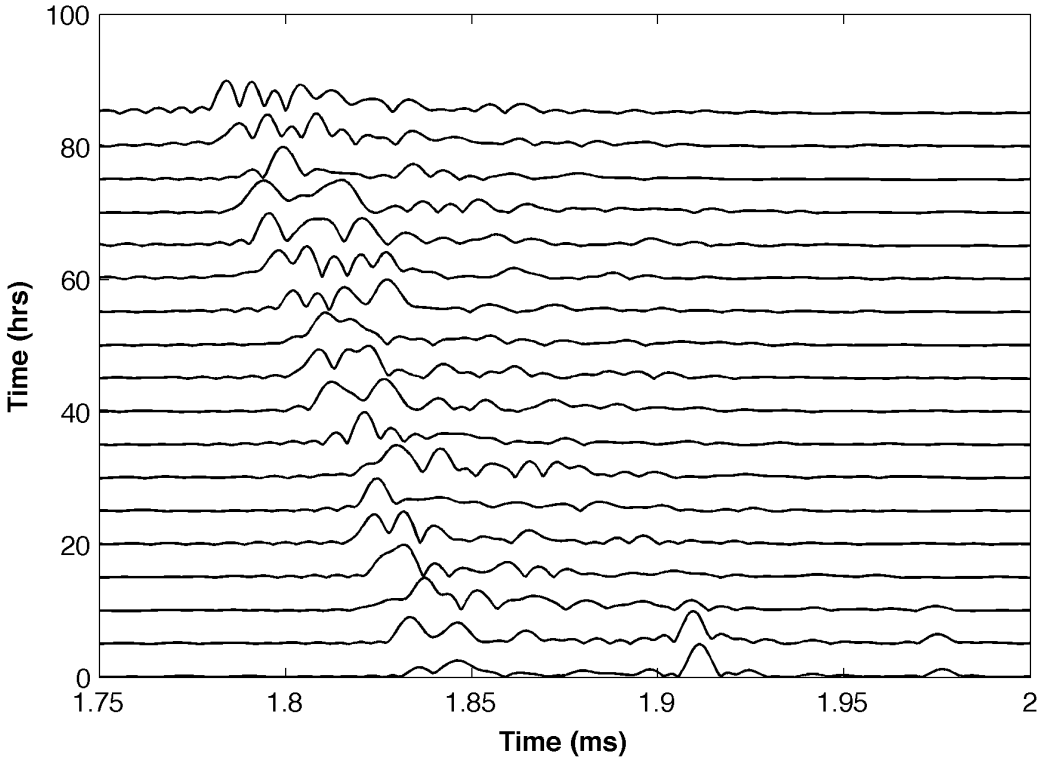


***Figure 5.1.6*** *Traces of the received echogram from the 400-600 kHz transducer over time (vertical axis) during encapsulation of the oil. The trace on the bottom is the echogram on May 24, after about 1 cm of ice had grown, to the afternoon of the 28th, after about 4.5 cm of ice had grown. The x-axis is in acoustic travel time, rather than range, because of variations in the speed of sound.*

Even after 5 cm of ice growth, some evidence of the original ice interface is visible, although in a real scenario, it might be difficult to clearly identify this.

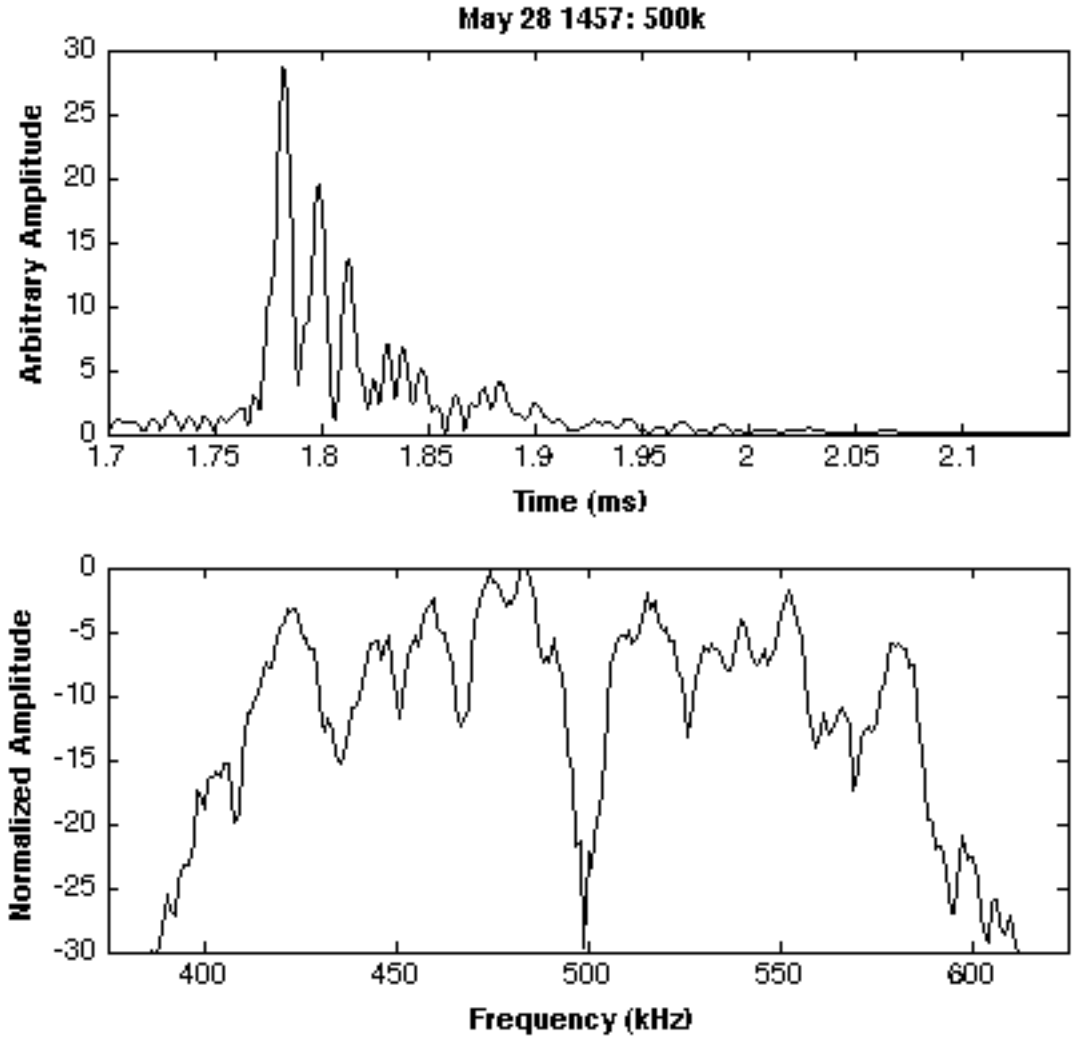


***Figure 5.1.7*** *Time domain (upper) and frequency domain (lower) response of the 400-600 kHz signal at the end of the experiment, once 5 cm of ice had formed beneath the oil*

Fig. 5.1.7 and 5.1.8 show the scattered signal on May 28th after 5 cm of ice had formed beneath the oil for 400-600 kHz and 120-200 kHz, respectively. Reverberation within the encapsulating ice layer now appears to occur in the 400-600 kHz, with possibly some reverberation apparent in the oil layer beyond, though the signal is weak. This appears to be layering within the encapsulating ice layer itself, rather than across the entire layer. In the 120-200 kHz data, this secondary reverberation is clearer, demonstrating the ability of lower frequencies to penetrate deeper into the ice. The ice reverberation is not apparent, possibly because of the reduced range resolution. On the other hand, the frequency spectra for the 400-600 kHz signal are more informative. Two sets of nulls are apparent (Fig. 5.1.7, lower panel). The more frequent nulls represent reverberation in the oil layer, while the single null at 500 kHz is likely due to the reverberation in a layer within the encapsulating ice (more closely spaced layers in time will have larger spacing between

nulls in the frequency domain). In this case, the spacing corresponds to a layer of 1-1.5 cm, so this cannot be reverberation across the entire encapsulating layer. This demonstrates the potential utility of broadband sonar, as both the time domain and frequency spectra provide tell-tale information of layering in the ice-oil-water system.

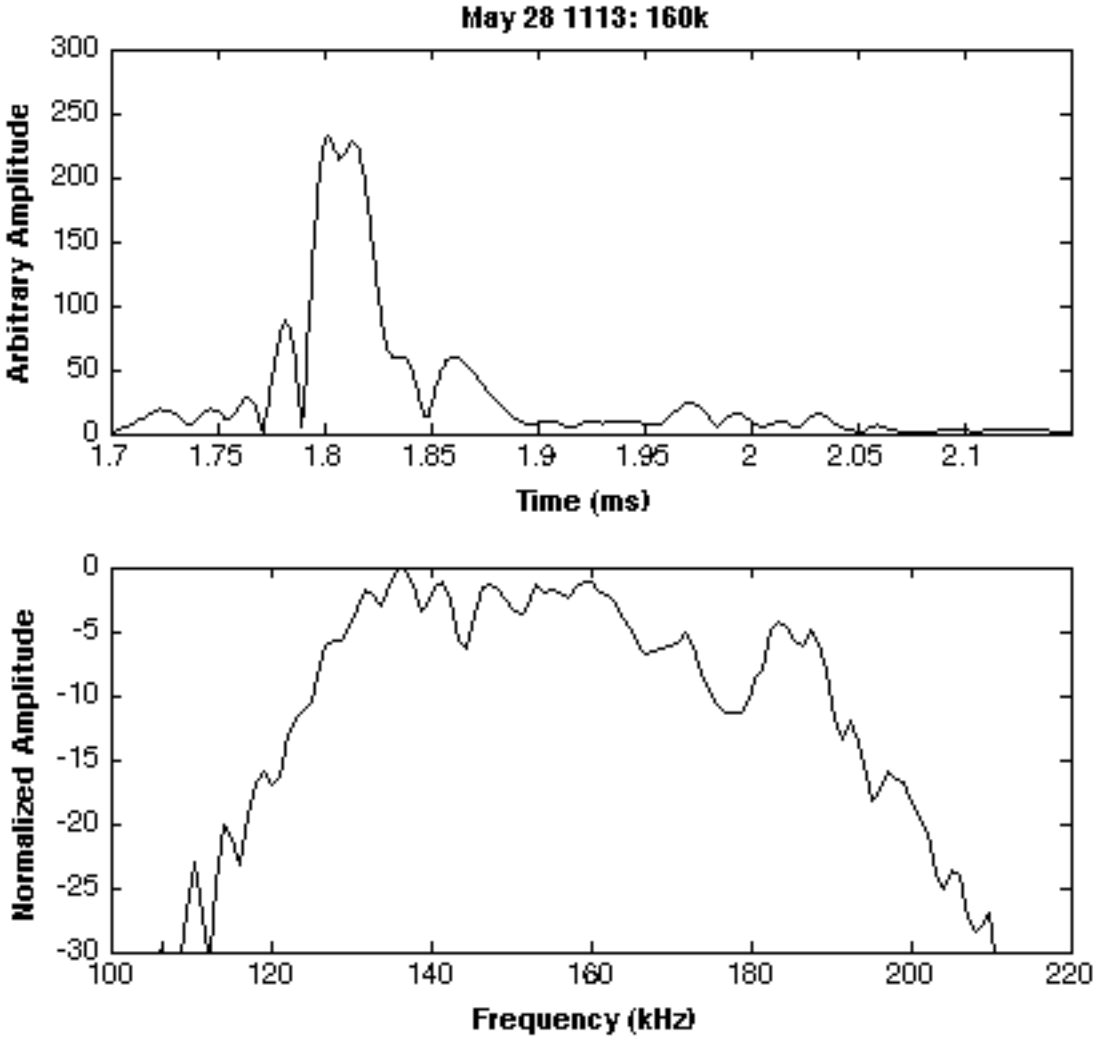


***Figure 5.1.8*** *Time domain (upper) and frequency domain (lower) response of the 120-200 kHz signal at the end of the experiment, once 5 cm of ice had formed beneath the oil.*

### 5.1.1 Narrowband acoustic results

The narrowband results are similar to the broadband, in that the layering within the oil and ice system was clearly visible, although the higher frequency of the Aquascat transducers meant that this layering was less visible as encapsulation took place. The temporal variability in the basal ice layer was clearly seen prior to oil release (as for the broadband sonar) (Fig. 5.1.9). The sampling was set to 8Hz with a 2.5 mm pulse width, although this was occasionally varied, but no significant improvement in resolving the layering was seen with longer pulse widths. The rising ice platelets can be seen as

diagonal lines beneath the ice and oil. Once the oil was released, the structure in the sea ice basal layer disappeared, and reverberation in the oil layer was clearly seen.

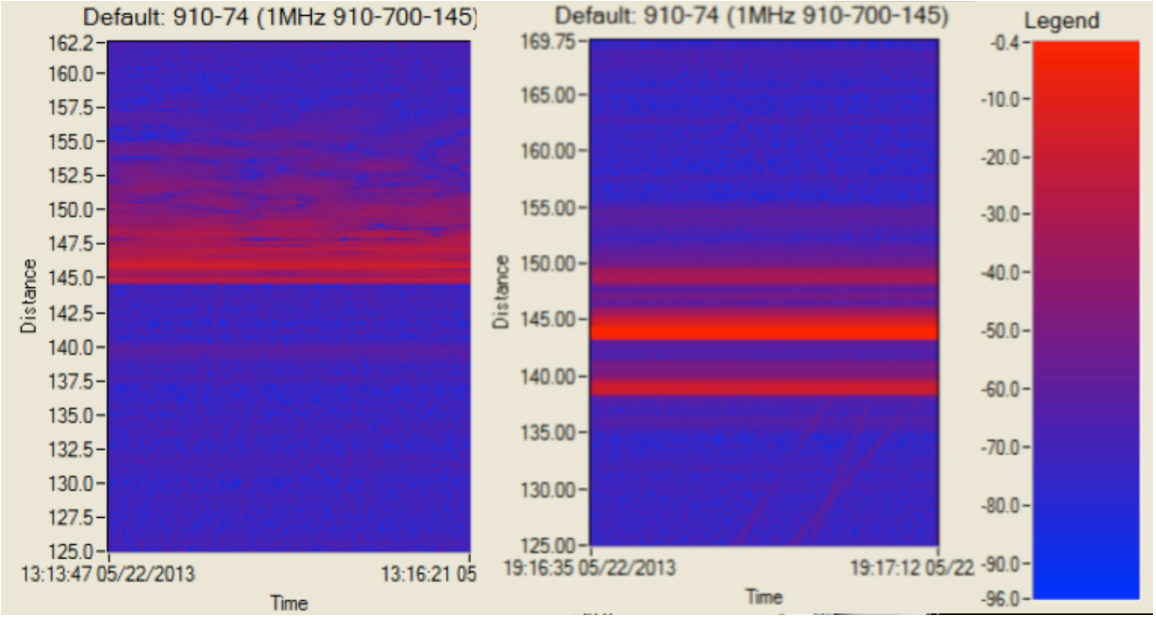


***Figure 5.1.9*** *Amplitude of the 1 MHz Aquascat signal prior to oil release (left) and after oil release (right). Note the range scales are different. The temporal variability in the ice before oil release is apparent in the region several cm above the ice/water interface. The oil and ice layers are very clearly seen after release, as well as reverberation in the oil layer, with peaks visible down to -60 dB. Note the upward diagonal traces that rise over time – these are due to scattering from rising ice crystals.*

As the oil encapsulation proceeded over the next several days, the presence of the oil layer became progressively less clear (Fig. 5.1.10). Initially, the reverberation in the oil layer became more apparent, with at least six multiple reflections visible one day after the release. This was also seen in the broadband data to some degree. What appears to happen is as ice begins to nucleate on the bottom of the oil, but before any detectable change in thickness, the oil/water interface becomes a stronger reflector so that multiple internal reflections can occur, but there is little attenuation due to the presence of ice or excess initial scattering from this layer – i.e. the layer is probably discontinuous. As 1 cm or more of ice forms, less energy penetrates into the oil layer and the reverberation is less visible. This layering is still visible to some degree up to an encapsulation thickness of about 2 cm, but then is difficult to discern once 3-5 cm of ice has formed.

These tests were also performed with a 5 MHz transducer. This provided clear identification of the oil and ice interfaces initially, but penetration beyond about 1 cm of ice was not visible.

These results clearly illustrate that a sonar with a high dynamic range (60 dB or more is desirable) is useful for detecting layering, including some encapsulation due to the reverberation. Detection of layering is strongly frequency dependent; using lower frequency transducers may be worthwhile, even at the expense of reduced range resolution.

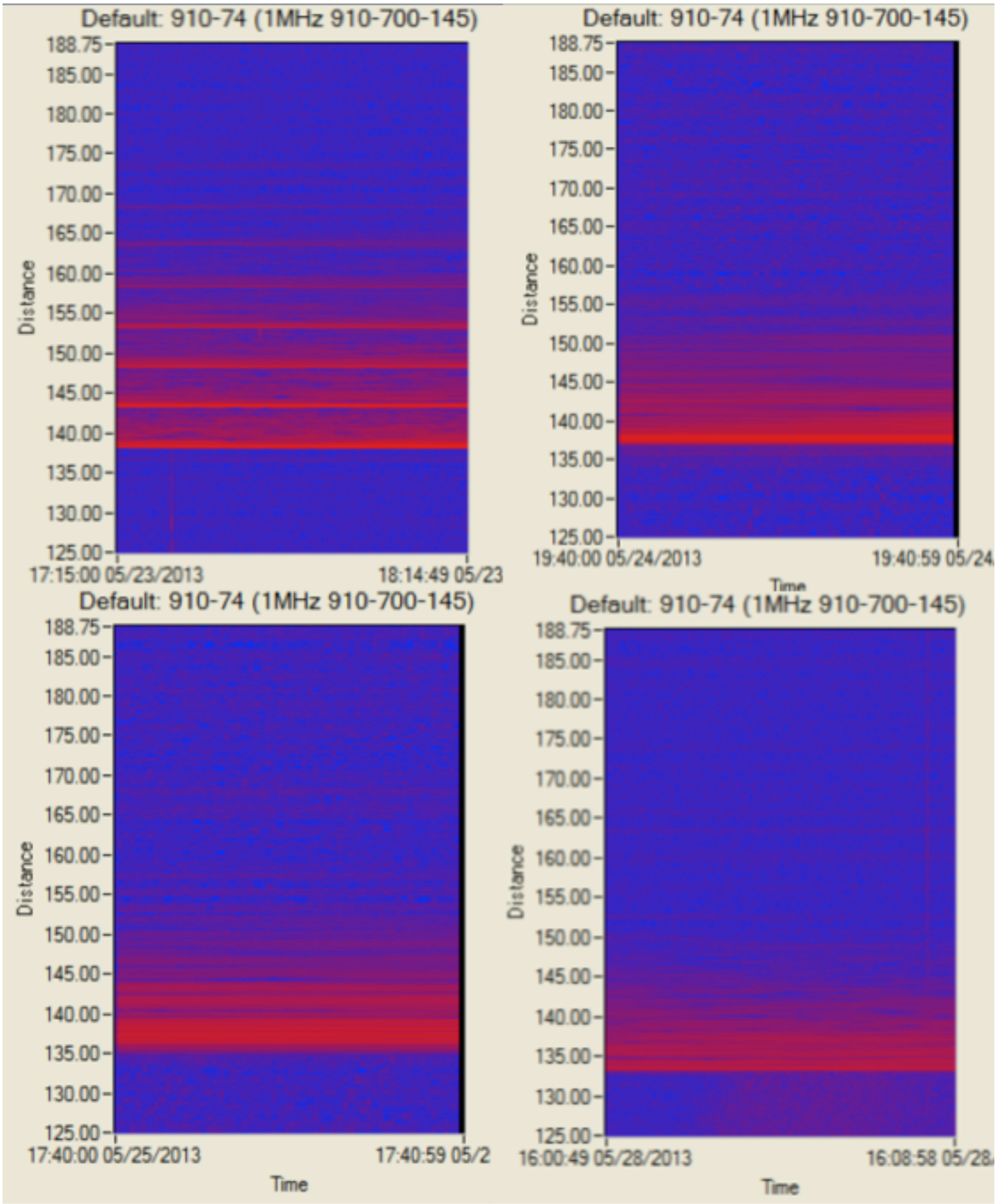


***Figure 5.1.10*** *Narrowband scattering at 1 MHz during ice encapsulation on May 23rd (top left), May 24th (top right), May 25th (bottom left), and May 28th (bottom right). Reverberation improved as encapsulation initiated, but the oil layer became more difficult to see very quickly (after only 2 cm encapsulation). By the 28th, the oil layer was no longer clearly apparent, with ~ 5cm of ice beneath the oil layer.*

## 5.2 HSVA acoustic results

Here we describe the results from the two separate experiments – the quiescent tank in which detailed broadband measurements were made, and the wave tanks in which acoustic measurements under frazil, nilas and pancake ice were made.

Unlike the CRREL experiments described above, the acoustic scattering was observed in the tank from before ice had formed. This enabled calibration of the transducers using the still water surface as a smooth pressure release surface. For the broadband system, the transducers were characterized in each tank as shown in table 5.1

***Table 5.1***. *Broadband transducer parameters for the HSVA experiments*

| **Transducer parameter** | **Quiescent Tank** | | | **Frazil tank** | |
|---|---|---|---|---|---|
| **Frequency range (kHz)** | 200-300 | 350-565 | 700-1050 | 350-565 | 700-1050 |
| **Wavelength (cm)** | 5.6 | 2.9 | 1.4 | 2.9 | 1.4 |
| **Beamwidth (3 dB)** | 13.4 | 8.8 | 3.4 | 6.6 | 4.4 |
| **Footprint radius (cm)** | 11.3 | 7.5 | 3.8 | 5.3 | 3.8 |
| **Range resolution** | 0.7 | 0.3 | 0.2 | 0.3 | 0.2 |

### 5.2.1 Broadband quiescent tank

The growth of the ice as seen by the broadband transducers in the quiescent tank (see Section 4.3.4) is shown in Fig. 5.2.1. By December 16$^{th}$ prior to the introduction, the ice had grown to a thickness of 12 cm. With the calibrated transducers, the maximum of the envelope of the compressed pulse envelope provides an approximation of the reflection coefficient. With the exception of the measurements with thin ice cover when reflections from the ice/air interface may have contributed to the scattered return, the observed reflection coefficients prior to introducing the oil were less than 0.1. Once the oil was introduced, the reflection coefficient increased, roughly doubling, due to contributions from the water/oil and the oil/ice interfaces. The acoustically inferred thickness of the oil by the 200-300 kHz sonar pair was approximately 3 cm. Once oil encapsulation occurred, the reflection coefficient decreased again.

The compressed pulse output envelopes of received scattered signals are shown in Fig. 5.2.2 prior to introduction of the oil and in Fig. 5.2.3 roughly one hour after the introduction of the oil. Prior to the introduction of oil the envelope contains a strong single peak from the water/ice interface in the 200-300 kHz data. After the oil has been introduced the envelope of the scattered signal includes two peaks associated with the water/oil and oil/ice interfaces. These same patterns are also visible in the 350-565 kHz and 700-1050 kHz data; however, identification of the individual peaks associated with the interfaces is more difficult because there are other identifiable peaks that are not identified with the 200-300 kHz transducers due to a lower temporal resolution.

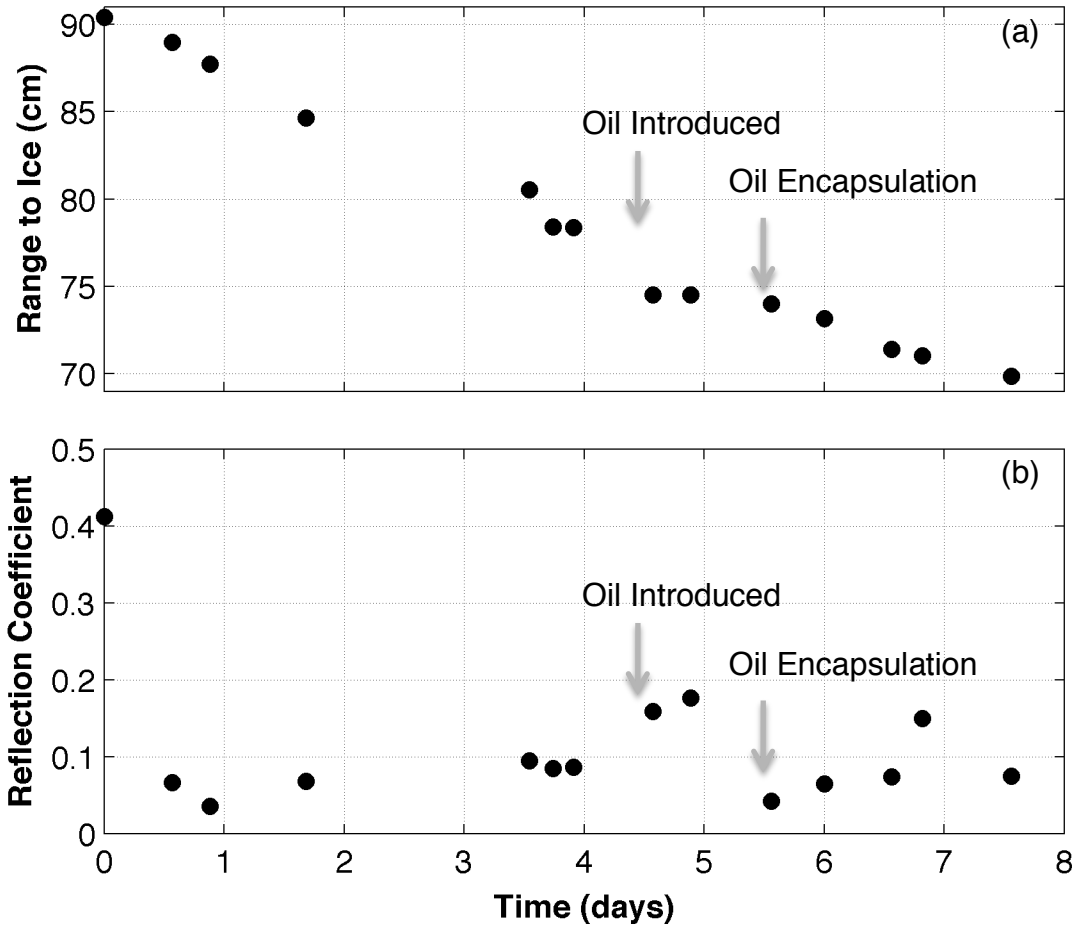


***Figure 5.2.1*** *(a) Time series of range to the bottom of the ice inferred acoustically using the 200-300 kHz stationary transducer pair. (b) The reflection coefficients obtained by integrating the received scattered spectrum. The large reflection coefficient in the first sample is attributed to contributions from the air/ice interface when the ice is thin. After the oil is introduced the reflection coefficient increases because the method for calculating the reflection coefficient includes energy contributions from the water/oil and oil/ice interfaces. Once oil encapsulation occurs the reflection coefficient drops again.*

As for the CRREL experiments, the frequency spectra show a clear pattern of nulls as specific frequency intervals. The spacing of these nulls is consistent with a ~4 cm thick oil layer.

Following encapsulation, the pulse-compressed output did not show the clear indication of the oil layer beyond the ice as was shown in the CRREL data. There was more noise in these data, probably due to other operations at HSVA, so that the small signal levels in the reverberation layer did not rise above the noise floor. In a real-world scenario, it will be important that the effects of vehicles noise or other acoustics on board an AUV is kept to a minimum.

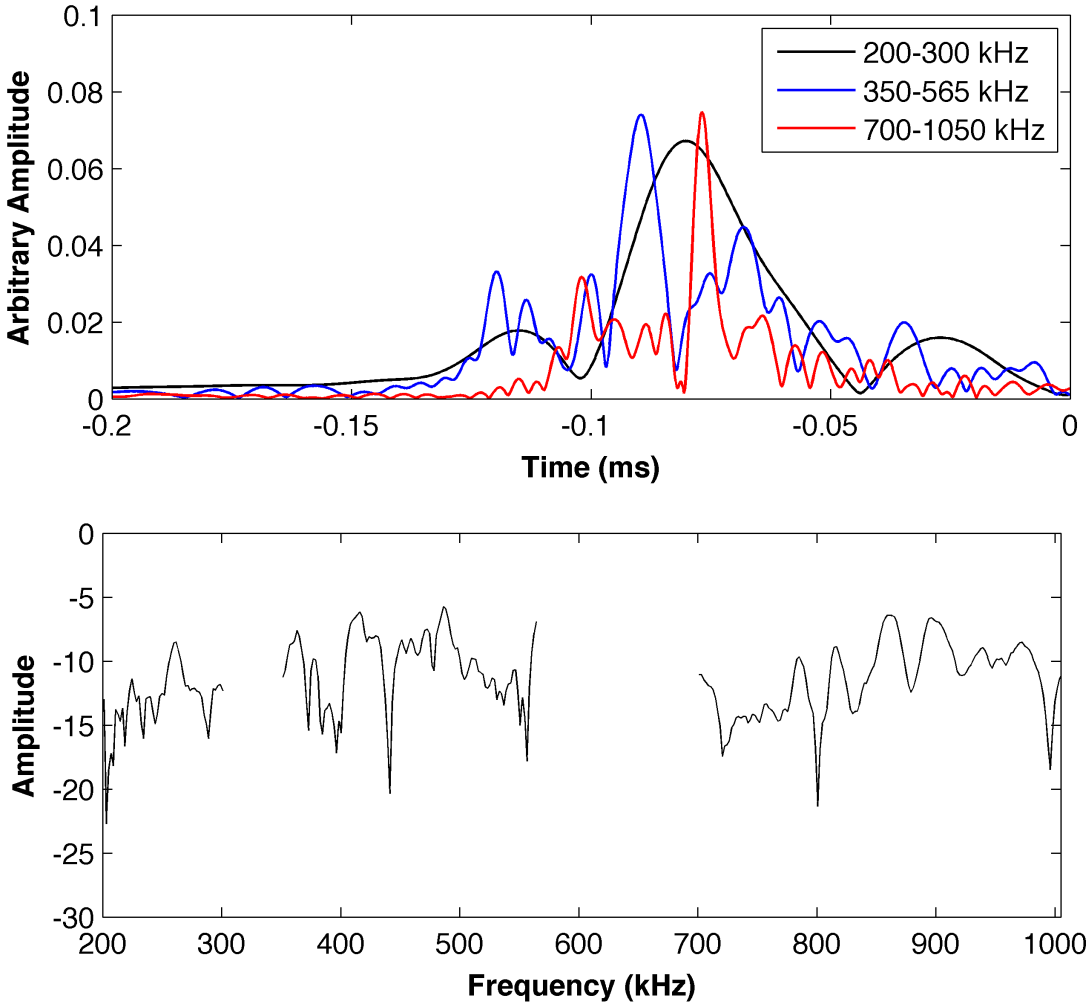


***Figure 5.2.2*** *Time series of the pulse compressed output for three frequency ranges prior to deploying of the oil. (top), and the corresponding frequency spectra (bottom). As with the CRREL experiments, a complex basal ice structure was observed.*

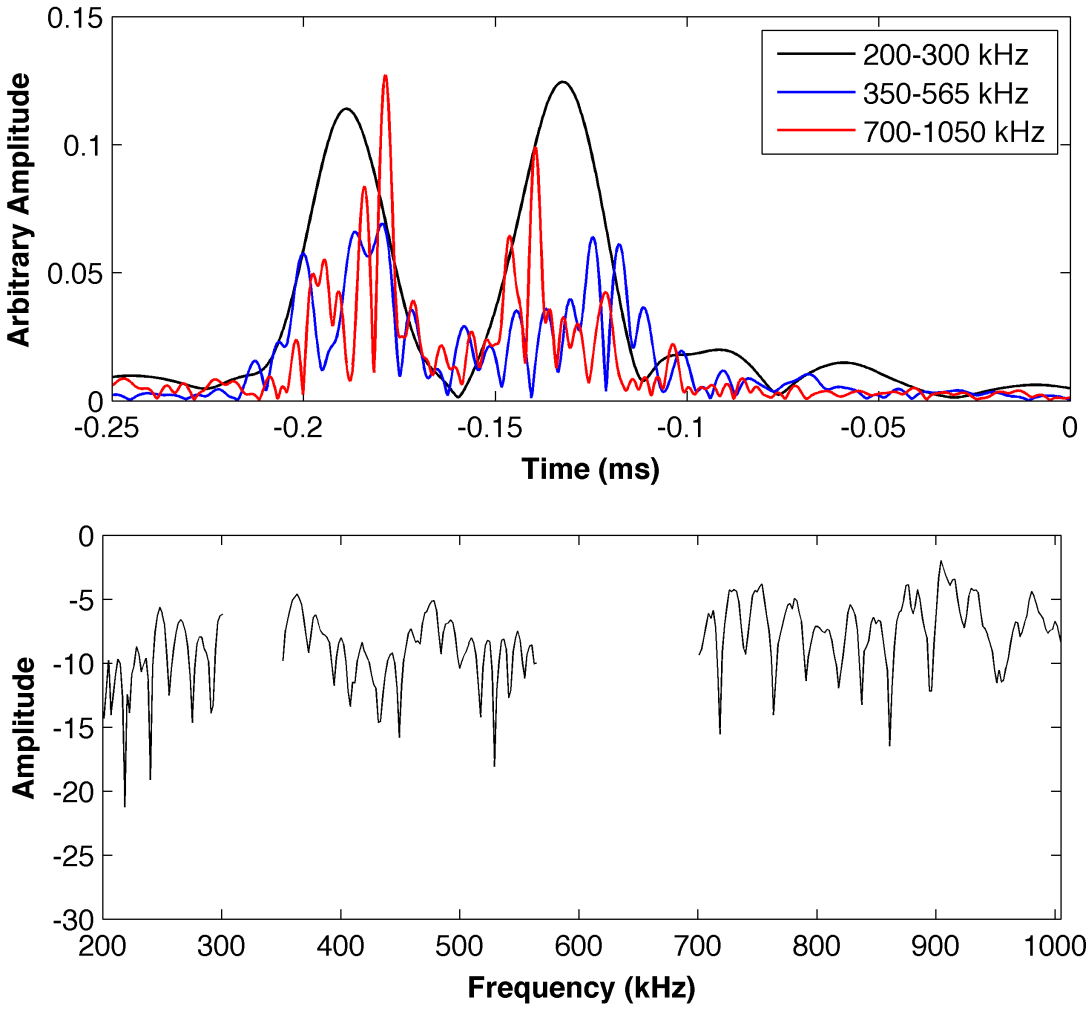


***Figure 5.2.3*** *Time series of the pulse compressed output for three frequency ranges after deploying of the oil (top), and the corresponding frequency spectra (bottom). Less change in the basal ice structure was observed than in the CRREL experiments, perhaps due to the lack of a platelet layer. The acoustically inferred ice thickness was ~ 4 cm. Some reverberation is seen within the layer (most notably at 200-300 kHz), and the repeating pattern of nulls is apparent in the frequency response.*

### 5.2.2 HSVA wave-tank acoustic results

The acoustic scattering from the broadband sonar for the frequency range 700-1050 kHz (chosen to maximize the range resolution) from underneath the frazil ice during wave-motion is shown in Fig. 5.2.4. The oscillating frazil/water interface due to the wave motion is clearly visible. Volume scattering due to the thickness of the frazil is also evident in the scattering from above this interface. As the oil is released, droplets in the water column are visible in scattering from below this interface. Also seen is the buoying up of the surface as the oil pushes up and spreads at the top of the frazil, as describe in section 4.3 above. After the oil spill is complete, the

interface returns to its previous position. While the spill is obvious in the sonar data when taking place, it is difficult to detect its signature after it has spread.

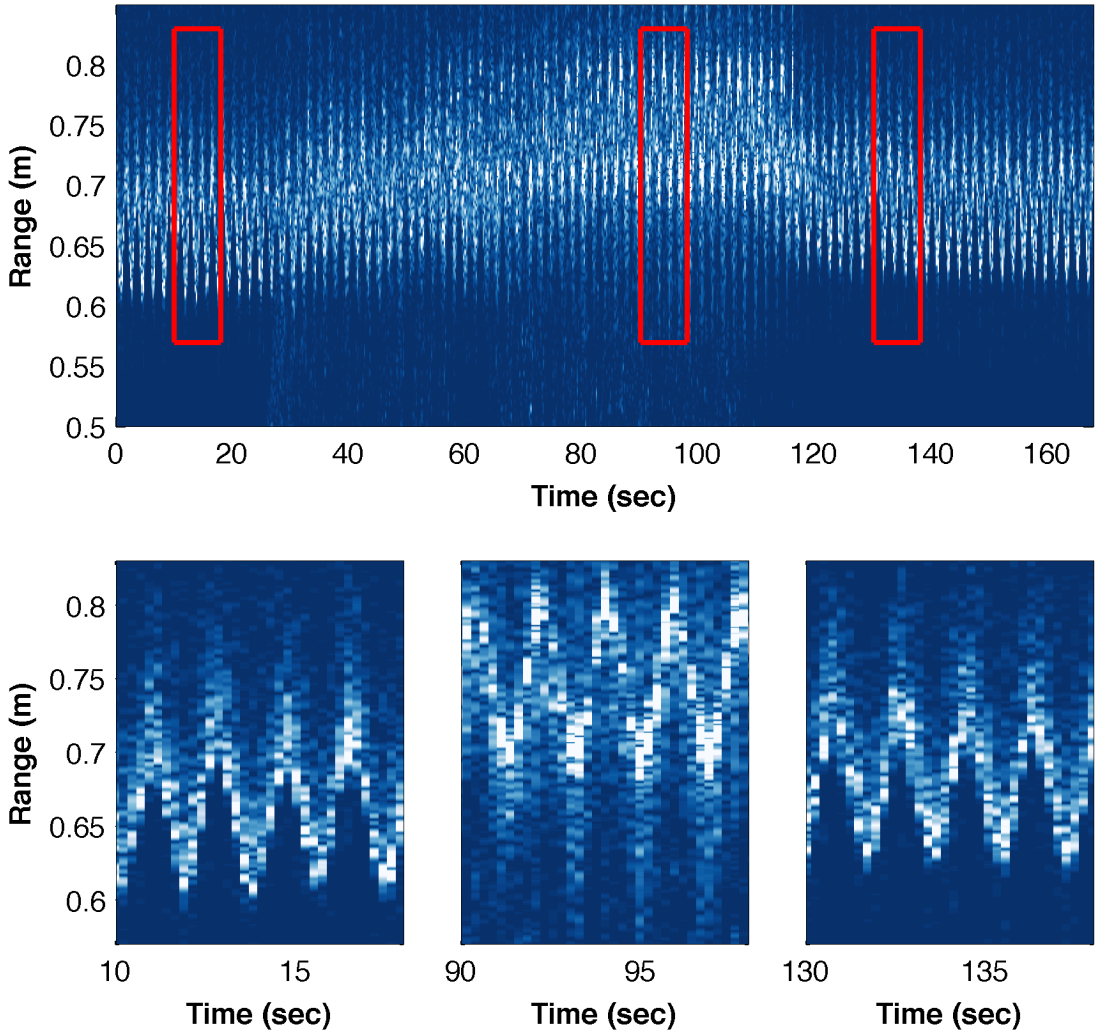


***Figure 5.2.4*** *The scattering from the broadband sonar (750-1050 kHz) versus time (top panel). Three sections (red boxes) are blown up in the lower plots. The oscillation is due to the propagating waves with an amplitude of about 15 cm. The oil release occurs around 30 seconds, causing a temporary upward displacement of the interface as the oil buoys up through the frazil (see description in Section 4.3). Also visible is scattering beneath the water/frazil interface (lower middle panel), due to oil droplets rising to the ice bottom.*

The spill beneath the nilas is more clear. There is a strong reflection from the base of the nilas, as in previous experiments, but significant structure through its thickness (Fig. 5.2.5), possibly with the ice/air interface visible above 0.7 m range. The waviness with time is due to propagation of an ice-coupled wave traversing through the barrier from the adjacent pancake tank. The wave-maker noise significantly

impacted the signal to noise ratio during the experiments; the results may improve in the natural environment, although there will be different noise sources present. The most apparent difference between the scattering before and after oil release is the presence of an interface below the ice bottom – i.e. the water/oil interface. The ice/oil interface and structure beyond it remained visible.

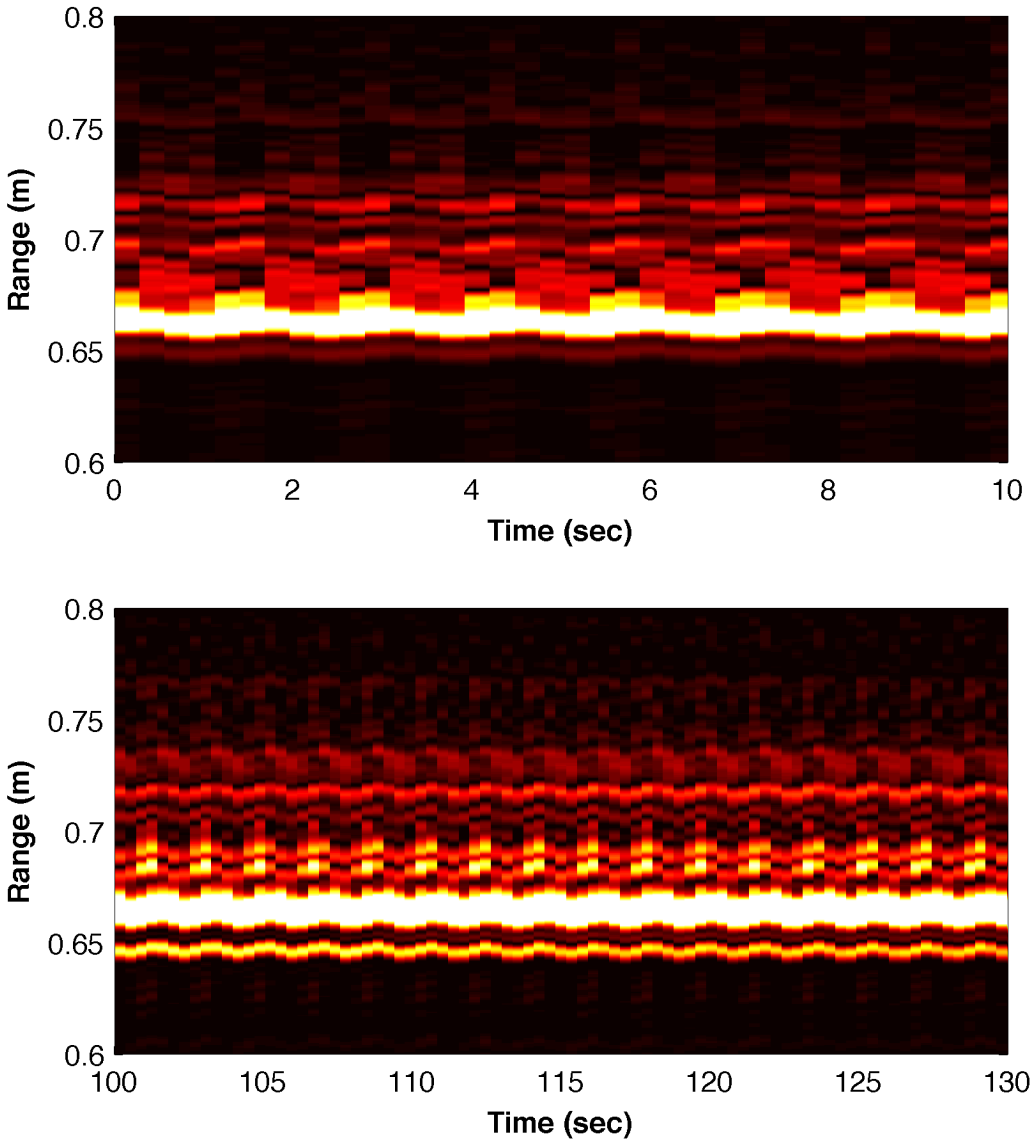


***Figure 5.2.5*** *Scattering intensity from the 700-1050 kHz broadband transducers under the white nilas prior to oil release (top) and after (bottom). The principle change observed is the appearance of the oil/water interface (range = 0.65 m) below the strong reflection at the base of the ice (range = 0.66 m).*

The oil spill beneath the nilas was clearly evident as the instrument trolley was moved from under clean ice, under the spill, and to clean ice again (Fig. 5.2.6). The signal quality was impacted by jerkiness in the motion of the cart, but the reduced range to the oil is clearly seen, along with the double oil/water and oil/ice interfaces.

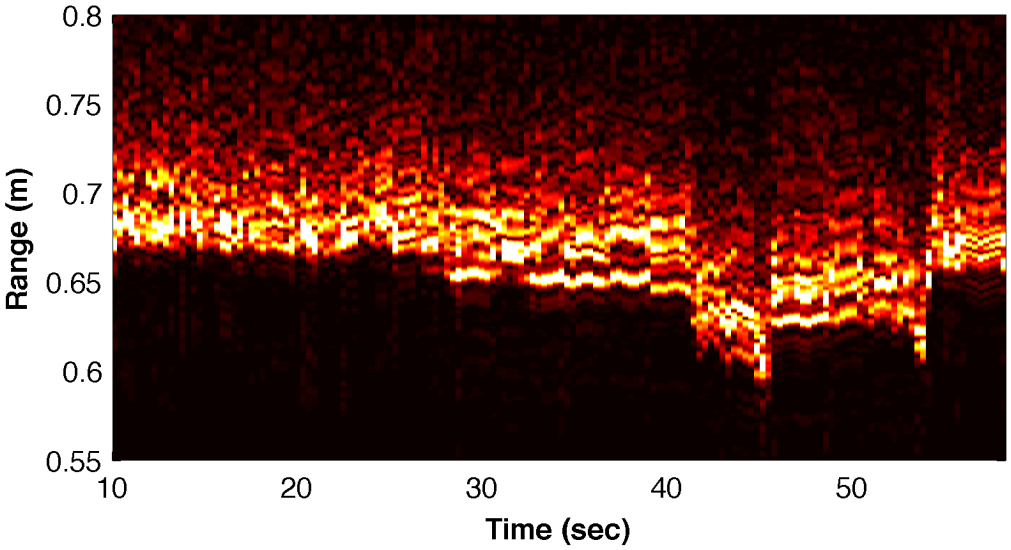


***Figure 5.2.6*** *Broadband scattering from under the nilas as the sensor trolley was pulled under the spill (edges seen at about 28 s and 55s). The abrupt displacements at 41-46 s and 52-53 s are due to abrupt motion of the cart.*

### 5.3 SAMS acoustic results

Results for the SAMS tests are similar to the CRREL tests before for the narrowband sonar, although greater penetration into the ice was achieved with the lower frequency transducers at 500 and 300 kHz. The results depended strongly on frequency (as expected) and pulse length (which controlled range resolution and transmitted energy). Results for tank 1 for a pulse length of 2.5 mm (the shortest possible pulse for the system) are shown in Fig. 5.3.1. The scattering before oil was deployed, after oil was deployed, and after encapsulation within about 15 cm of ice is shown.

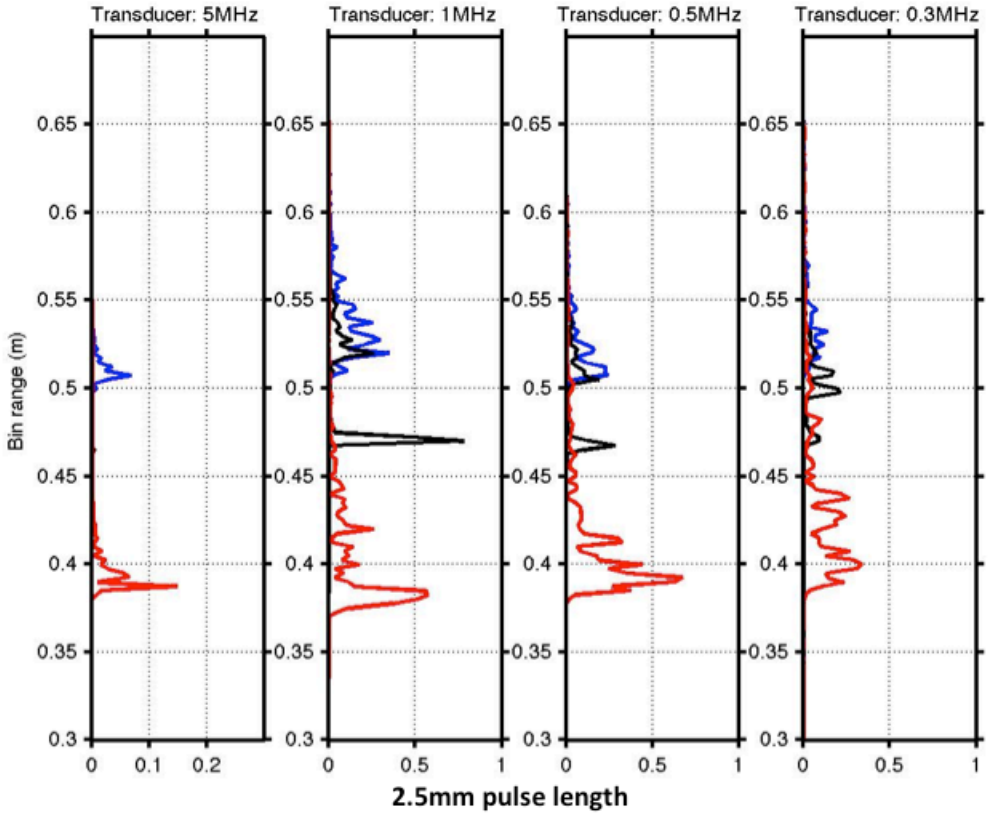


***Figure 5.3.1*** *echograms for the Aquascat transducers in the SAMS Tank 1 tests at frequencies of 5, 1, 0.5, and 0.3 MHz, from left to right for a pulse length of 2.5 mm. Range is on the vertical access, with the original water/air interface at about 0.6m before ice growth began, The blue trace shows the scattering after about 7 cm of growth. The Black trace is immediately after oil is deployed, and the red trace is the response after encapsulation within ~15 cm of ice after 9 days. Range uses a nominal sound speed of 1500 m/s. The difference is not significant for water or oil, but is for ice (sound speed unknown), so the ranges are not true ranges.*

At 5 MHz, there was almost no penetration beyond the first interface seen. Once oil is deployed, very little signal is received from the oil/water interface, while it is clearly seen at the other frequencies. Structure in the ice is evident at the lower frequencies, as seen previously. At 1 MHz, both the oil/water and oil/ice interfaces are clearly seen after the

oil is deployed. Once encapsulated, only the complex structure of the basal ice appears to be visible.

At lower frequencies, there is some evidence for the encapsulated oil as there are low amplitude peaks in the scattered signal. This is more clear for longer pulse widths due to the associated increase in transmitted energy (Fig. 5.3.2, and 5.3.3). For 300 kHz at 10 mm pulse width, two strong peaks are apparent in the encapsulated ice, with the second likely associated with the bottom layer of the encapsulated oil. Reverberation is more evident. For a 40 mm pulse, the range resolution starts to become too low to resolve features in the encapsulating ice layer, but the reverberation in the oil layer (as evidenced by the 5cm interval between peaks) becomes quite clear at the lower frequencies (Fig. 5.3.3).

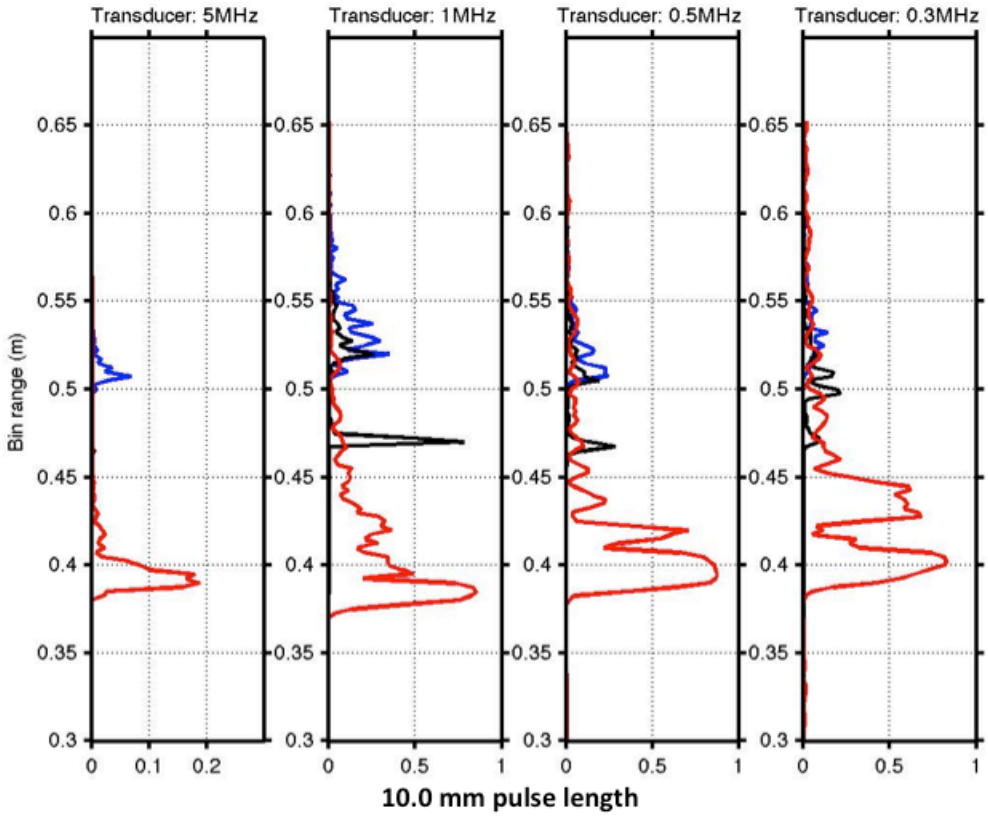


***Figure 5.3.2*** *as Fig. 5.3.1, except for a 10 mm pulse width.*

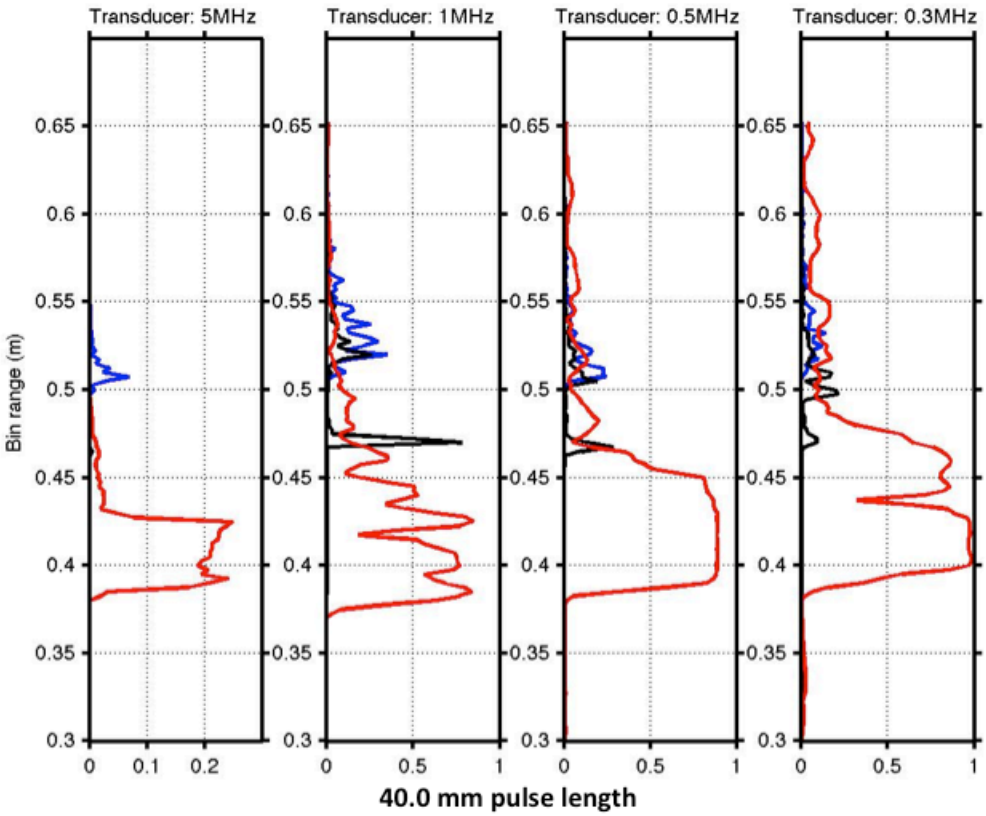


***Figure 5.3.3*** *as Fig. 5.3.2, except for a 40 mm pulse width.*

In contrast to the broadband results for the CRREL tests, there did not seem to be a dramatic change in the ice structure once the oil was released, at least at a 2.5 mm pulse length (Fig. 5.3.4). Rich structure is seen in the ice both prior to and after the oil release, and in the ice in the encapsulating layer. This may in part be an artifact of the very short pulse length; for longer pulse lengths, these small-scale features are less apparent (Figs 5.3.2 and 5.3.3), at the expense of range resolution.

These results highlight the need for care in interpretation of results from an individual sonar signal, as the apparent layering in the oil and ice is a strong function of the transmitted signal pulse length, frequency, and any structure in the ice basal layer. The narrowband data also show layering due to the oil layer with results generally comparable to the broadband data. However, for clear discrimination of interfaces, more energy (and hence a longer pulse width) may be necessary, at the expense of range resolution. Because of the combined properties of better range resolution, signal energy level, and frequency information, a broadband sonar, potentially at multiple frequencies may be the most efficacious acoustic instrument for detecting oil under ice. As yet, however, a small-scale broadband system suitable for use on a small AUV is not yet available.

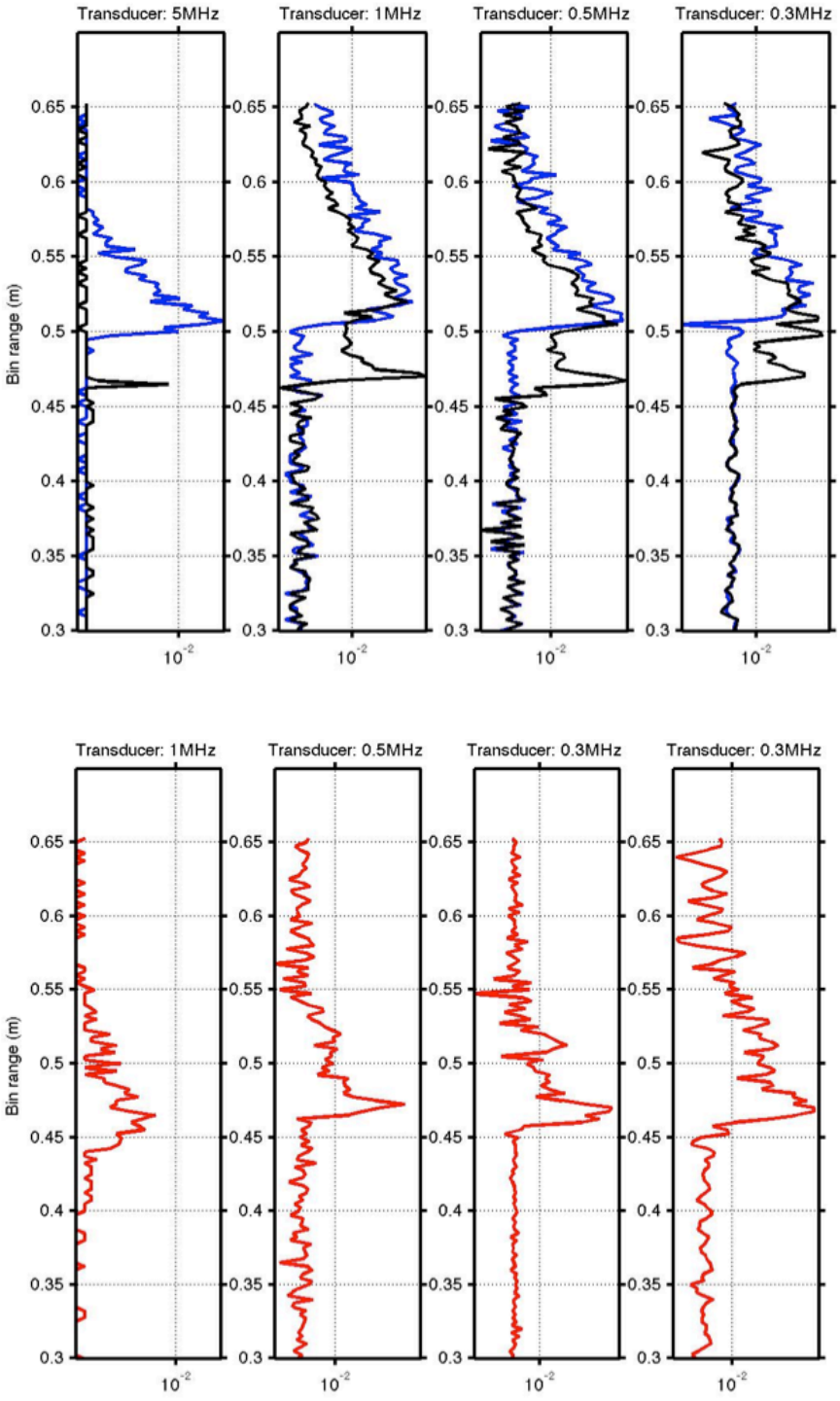


***Figure 5.3.4*** *The scattering from the oil/ice system in tank 1 with a 2.5 mm pulse width before the oil release (blue), after (black), and after two days once encapsulation had begun (red). The horizontal access is displayed on a logarithmic scale so that features are more clearly seen. Although there is rich structure in the ice, both before oil release and after, and in the encapsulated oil, it is difficult to determine the physical reason for it.*

### 5.4 Quantification of oil volume

For each of the three tank experiments described above, each sonar system demonstrated that oil thicknesses of a few centimeters could be clearly determined through detection of reflections from both the ice/oil interface and the oil/water interface. This capacity is unique for underwater sensors and permits the quantification of the oil volume by mapping the distribution of this thickness during a spatial under-ice survey by an AUV. A conceptual example is illustrated in Fig. 5.4.1. During the HSVA quiescent tank experiments described in Section 5.2.1 the transducers were pulled at a near constant rate across the tank bottom to sample the spatial variability of the acoustic scattering from the ice and oil. The transducers traversed across the center of the tank in a line running roughly from top to bottom of the photo in Fig. 6.1.3, so that the sensors traversed from under clean ice, to under a discontinuous oil patch. This is analogous to an AUV traversing beneath a patchy oil spill under sea ice.

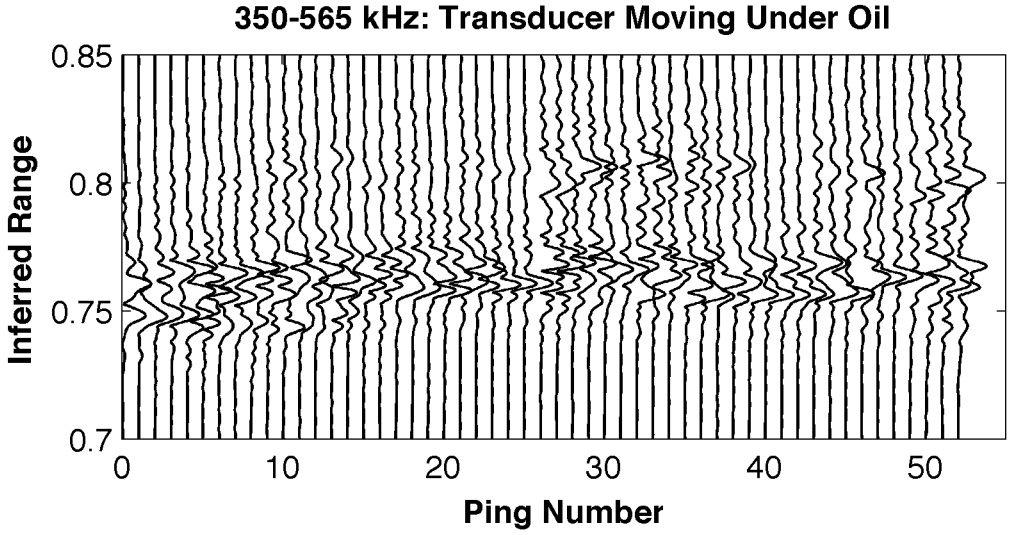


***Figure 5.4.1*** *Echogram from the broadband transducers traversing under thin ice during the HSVA experiments (see Figs 4.3.9 and 6.1.3). The sonar transducers were mounted on a shuttle and pulled slowly under a patch of oil at a roughly constant rate. Multiple reflections from the ice and oil layer underside are clearly visible as the transducers travel under oil patches between pings 26 and 37, and again between pings 46-52. The oil thickness is about 4 cm. By observing the spatial variability in the inferred oil thickness as host vehicle traversed beneath the ice and oil, the oil volume can be estimated.*

The suite of experiments demonstrate that quite thin layers of oil can be detected under level sea ice – as low as 3 cm thick for the HSVA quiescent tank experiments with broadband sonar. For a somewhat thicker oil layer (~ 5 cm) the discrimination between the two interfaces was very clear in the CRREL results. This was particularly true shortly after the deployment of the oil, where reverberation in the oil layer provided a very clear indication of the oil thickness. This property may provide a useful means of identifying the oil thickness where the scattering profile is more complex. This is apparent in Figures 5.1.9 and 5.1.10 where there is some complexity in the shape of the return from the ice

alone, but in the presence of an oil layer, the regular spacing of the peaks provides easy identification of the oil thickness. Where the scattering signal is more complex (e.g. for higher frequency broadband data in Fig. 5.2.3), the frequency domain information provided by broadband sonar may provide a complementary means of identifying the layer thickness based on predicted locations of nulls in the frequency spectra (Fig. 5.2.3).

What remains to be determined is how well the thickness can be resolved under the more complex ice conditions typical of the Arctic – i.e. highly variable ice thickness and at greater range. Greater range translates to a larger sonar footprint, and hence the acoustic scattering has a greater chance of occurring from a rougher surface, which will tend to broaden the peak of the reflected signal. This will make discrimination of two peaks more difficult for thinner layers. This is balanced to some degree by the fact that oil trapped beneath complex ice morphology will more often pool to greater thicknesses.

Quantification of oil volume is also possible for encapsulated oil, as demonstrated in the CRREL and HSVA experiments. In this case discrimination of thin layers (in these experiments, a few centimeters) is complicated by overlapping of peaks in the returned profile, such that clear determination of thickness becomes more difficult at modest. The SAMS test results suggest that careful choice of frequency and pulse width can improve the depth of encapsulation beyond which oil layer thickness becomes difficult. This may be alleviated for thicker oil layers, but it remains to be determined in tests with a more variable ice cover if this mitigates the expected increase in complexity of the scattering.

While a number of factors will increase the ambiguity in the detection of the oil thickness, complementary sensors (such as digital imagery) may be particularly useful for removing any ambiguity in identifying the presence of oil, and hence aiding in determining which profiles should contain thickness information. Further measurement of sonar scattering from ice and oil under more varied ice conditions are needed so that appropriate techniques for determining oil volume under a range of conditions using a fusion of sonar and complementary data (e.g. digital imagery) can be developed.

## 6. Optical measurement results (Laser fluorescence and digital imagery)

### 6.1 Underwater cameras

The effectiveness of digital imagery for detecting oil under ice was demonstrated with GoPro Hero3 cameras and an HD video camera deployed under the ice in the various experiments. Imagery taken from above when the ice was illuminated from below in the CRREL tests demonstrate that for level ice, the contrast between oil encapsulated by 15-20 cm or more of ice and surrounding clean ice is clearly visible (Fig. 6.1.1). For the AUV case, the light would be from above and be seen from below. In the presence of variable light levels due to snow cover or variations in ice thickness, positive detection of encapsulated oil may be more difficult. In ambient daylight, the oil could not be seen from above (through approximately 20 cm of ice).

***Figure 6.1.1*** *Photographs of the ice tank with the ice and encapsulated oil from above, illuminated from below in the dark (left), and in daylight from above with no underwater illumination (right).*

When viewed from below (Fig. 6.1.2, 6.1.3) after encapsulation for both the CRREL and the HSVA ice tanks, the oil patch could be seen, but differences in the light scattering in the basal ice layer caused dramatically different results. The distinction between oil and ice is a function of the depth of encapsulation, the lighting conditions, and presumably the structure of the basal ice layer. For the CRREL experiments, the oil patch encapsulated within the oil could be seen, and the edge of the oil was apparent, but the image contrast was not distinct. This was due to significant scattering of the light in the basal ice layer (in this case, it was ambient light that penetrated through the clear ice and through the fluorosensor access hole). This scattering is due to bubbles and the complex substructure of the sea ice (Fig. 6.1.2). For the HSVA tests, the thickness of the encapsulating ice layer was less, and the oil was illuminated from below, providing a distinct contrast between the oil and clean ice (Fig. 6.1.3).

Under other young ice types (Fig. 6.1.4 and 6.1.5), photographs in ambient light also provided reasonable contrast between the oil and ice, although in this case the ice was thin and discontinuous, so there was more ambient light than would be expected under continuous thick ice with a snow cover.

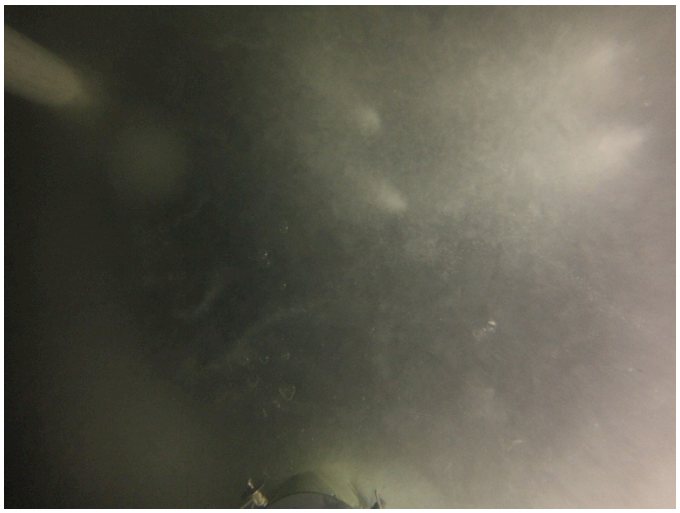

***Figure 6.1.2*** *The ice underside of the tank at CRREL viewed from below with 5 cm of oil encapsulated within 5 cm of ice. The edge of the oil can be seen at the left, although there is significant scattering of light from within the ice layer beneath the oil, obscuring much of the image.*

***Figure 6.1.3*** *The oil spill in the broadband sonar tank at HSVA viewed from below. Lighting is provided from beneath the ice (at right of image) Oil percolated from the deployment hose (at left) to the right of the tank, creating an irregular boundary and variable thickness of oil. The oil is encapsulated within about 1-2 cm of ice, with scattering in the ice layer very minimal.*

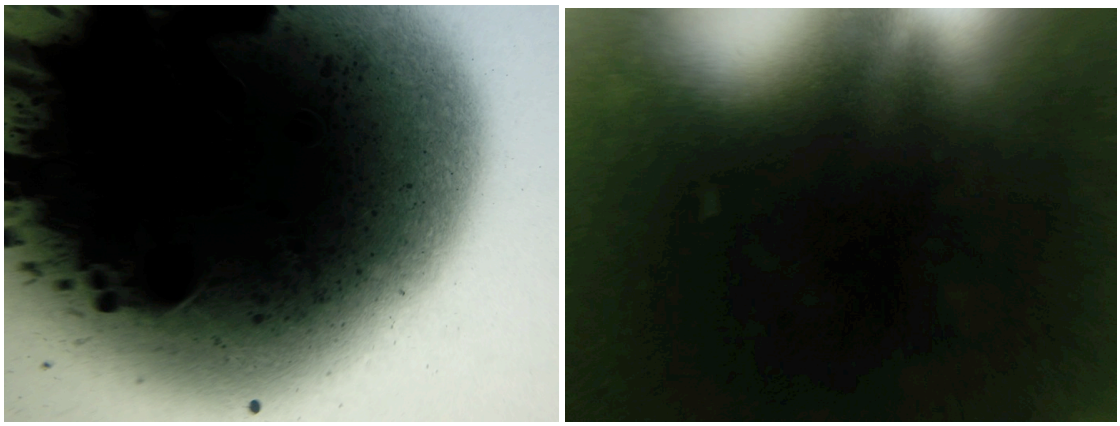

***Figure 6.1.4*** *Upward looking photos of the spill under nilas (left) and frazil (right) at HSVA. Oil can be identified by its contrast with the clean ice around it, but for the oil encapsulated within the frazil, the more greyish color suggests that under ice of variable thickness discrimination of the encapsulated oil from thick ice or ice with a thick snow cover may be more difficult. These photos were taken in ambient light*

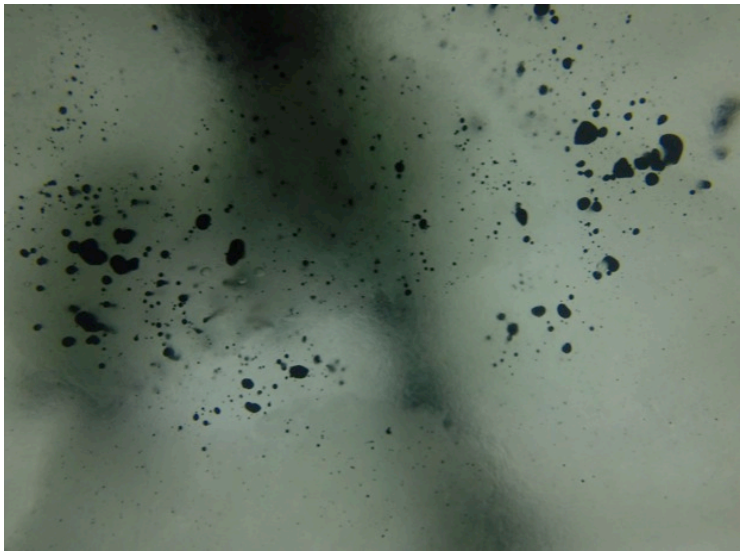

***Figure 6.1.5*** *Upward looking photos of the spill pancake ice at HSVA immediately after the spill. This is the only location where significant droplets remained under the pancakes. Most of the oil was forced between the pancakes, where the color contrast may be difficult to distinguish from variability in the ice thickness or overlying snow cover. Photo taken in ambient light.*

Based on these results, upward looking underwater photography provides a clear contrast between oil and ice patches, although because of the lack of spectral detail in the images (i.e. mostly grayscale), oil is best identified when it can be contrasted to clean ice conditions.

The greatest challenge for detection of oil with cameras will be deeply encapsulated oil or oil under a thick ice cover of irregular thickness and variable light levels. Those images lit from below provided the clearest contrast, so a strobe should be mounted on the AUV, but light scattering in the layer of basal, encapsulating oil may make discrimination of clean versus oily areas more difficult. A strobe would also be essential during the prolonged periods of darkness in the winter. While this will increase AUV power consumption, these results show that even when there is some transmitted light from above (e.g. Fig. 6.1.3), lighting from below may be more effective in delineating the edges of the spill. This would be expected under thick ice with a deep snow cover. Another potential challenge is that for real-time identification of oil, only a small volume of imagery can be transmitted acoustically, so that automated processing of the images onboard the AUV may be necessary. Work remains to determine if oil under realistic conditions can be automatically detected from digital imagery – possibly be taking advantage of spectral variations in the detected light levels rather than just grayscale contrast.

### 6.2 Laser fluorescence

At CRREL, the laser fluorometer was mounted externally to the ice tank with a mirror in the tank to aim the laser through an access hole at the base of the ice, and receive the fluorescence signature along the same path, as described in Section 4.2. The output is provided in terms of the voltage output of the lock-in amplifier, so it is in arbitrary units as the level depends on the gain and settings of the lock-in. Gains on the photomultiplier (PMT) and laser were set to prevent saturation of the PMT. The background level was

recorded at 27.0 (arbitrary units) on the lock-in. When set up to test with a direct view of oil, this rose initially to 70.0, providing a signal to noise ratio of about 2.5.

When the laser was set up over the tank, the background level was 25.6, similar to out of the tank. This level is likely due to laser light leakage into the PMT because the telescope was not enclosed. This limits the sensitivity of the device. After oil was deployed, the signal level rose to 53, for a signal to noise of ~ 2. The following day, the level had dropped to 43.2, perhaps as scattering due to ice crystals on the oil bottom reduced the signal level. The following day, the oil was not detectable, thus to detect encapsulated oil a significantly more sensitive device is needed.

To ensure that the device was indeed seeing oil, and not some other light source, received light spectra were taken with an Ocean Optics USB4000FL spectrometer. The spectra received at the laser fluorometer device (after an equivalent range of 2m) showed a very weak, but broad peak characteristic of oil after 1 cm of encapsulation (Fig. 6.2.1). The spectrum was integrated over 1 minute to reduce the noise level. The weak signal is in part due to the small aperture of the USB4000FL. Prior to the oil being deployed, no spectral response was seen, as expected, so that there is confidence that the spectrum is due to oil.

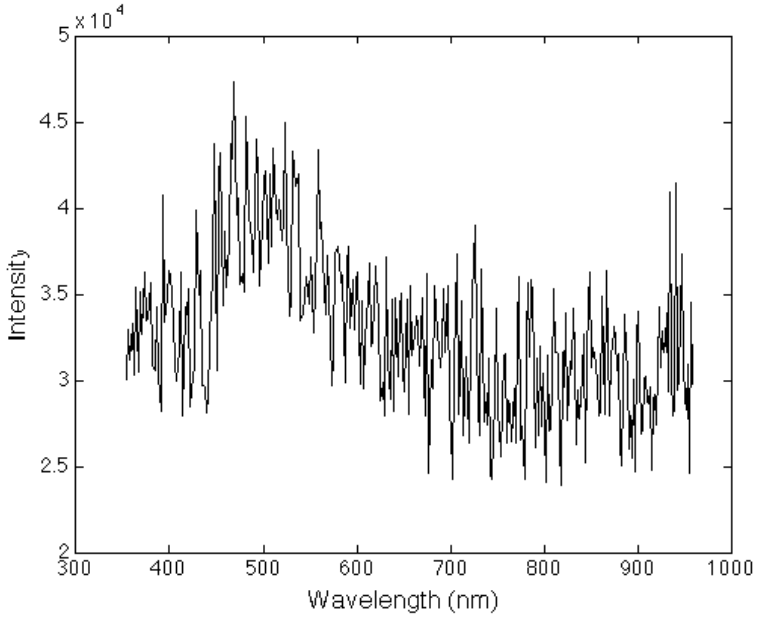


***Figure 6.2.1*** *Fluorescent spectrum observed from the oil after ~1 cm of encapsulation. The spectrum was integrated over 1 min to reduce noise. A broad spectral response with a peak at ~520 nm was seen, typical of crude oil.*

With the improved laser fluorometer which could be deployed underwater, oil detection tests were carried out at HSVA under the frazil and white nilas slicks. Unfortunately, the housing window reflected significant amounts of the laser light back into the detector, so that there was a large background signal. This limited the photomultiplier gain that could be used, and effectively, the sensitivity of the instrument. Nevertheless, the signal level under the oil rose significantly above the background level observed under the ice (Fig. 6.2.2). This is encouraging, as it shows that the signal level is significant and with

improved noise control in the sensor, the sensitivity of the system is likely to be high. Moreover, the fluorescence signal was detected under the frazil spill, where the oil had percolated to the surface. As the frazil thickness was about 8cm, this suggests that detection of oil encapsulated within ice of at least 8cm, but likely significantly more, is possible. The laser spot is shown underneath the frazil spill in Fig. 6.2.3, corresponding to the first peak in the left hand panel in Fig. 6.2.2

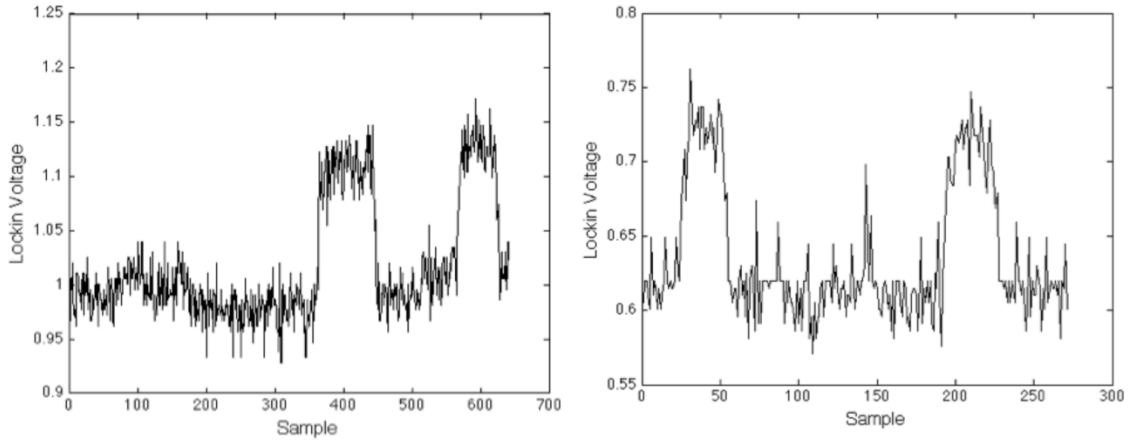


***Figure 6.2.2*** *Output of the laser fluorometer lock-in amplifier as the instrument was pulled under the frazil spill (left), and the nilas spill (right). The trolley was pulled under each slick twice, as shown by the two peaks. Note that the background level varies between the two slicks, so absolute values cannot be relied upon to discriminate oil from clean ice.*

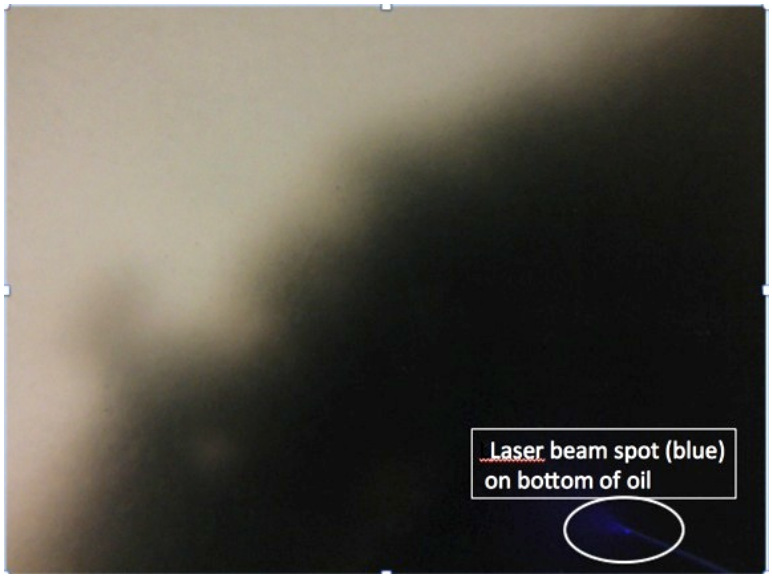


***Figure 6.2.3*** *Upward-looking camera view of the edge of the oil in the frazil ice (where the oil had percolated through the frazil to the surface) during the laser fluorescence experiment. A faint blue reflection of the laser is seen in the bottom right. This demonstrates the need for a sensitive detector, as the source level is much stronger than the fluorescence signal.*

These results demonstrate the utility of laser fluorescence to detect oil under sea ice, and encapsulated oil. With improved reductions in the noise level in the laser fluorometer in the latest prototype, it is expected that oil encapsulated to greater depths may be detectable. There are several caveats - first, in normal encapsulation of oil, the ice may have more air inclusions if it is more consolidated, increasing the light scattering. Second,

because of variations in the background level under natural sea ice, good signal to noise is essential.

There are several other factors which will control the effectiveness of this technique that warrant further investigation. First, these experiments were performed at close range (1-2 m). At ranges required for safe operation of an AUV (~10-20 m), the fluorescent signal level will be greatly reduced, while the noise (ambient light) will not. The relative strength of the fluorescence relative to realistic ambient light need to be determined at realistic ranges and for different water column turbidities. As ambient light levels will vary greatly in many cases under Arctic sea ice, the possible effect of these variations on potential false positives needs to be determined.

Experiments to determine the detection limits of this technique at greater encapsulation depths will be performed at upcoming experiments at CRREL funded by the Oil and Gas Producers Joint Industry Programme. Future tests to determine the fluorescence and ambient light signal characteristics and sensor performance at longer ranges under realistic ice conditions are also needed. Once these tests are performed, evaluation of the optimal choice of laser power and any required noise reduction can be determined.

## 7. Synthesis and Recommendations

This project investigated two aspects of the integrated problem of detection and mapping of oil spills in ice-covered waters – 1) the use of Autonomous Underwater Vehicles (AUVs) as platforms for detection of oil from beneath the ice, and 2) the efficacy of potential sensors for remote detection of the oil trapped beneath, or encapsulated with the ice.

Several potential sensors were evaluated in the three sets of laboratory experiments. As expected, underwater cameras provided the clearest and easily interpretable results, with oil clearly visible from beneath in all experiments covering all ice types. This is perhaps the greatest advantage of viewing the oil from below, in that a widely used, easy to interpret data source is minimally affected by the presence of the ice. In many instances, it may be that cameras are the only sensor needed to effectively map the oil. Even when the oil becomes encapsulated, the limited optical scattering in the basal ice layer compared to surface ice layers (or especially, snow) has a fairly modest impact on discrimination of oil from clean ice areas.

There are several potential complications that argue for not relying on imagery alone. First, a highly variable ice and snow thickness will lead to variations in lighting level that may mimic the dark oil regions. Second, as the distinction between oil and ice relies on the relative grayscale contrast, definitive identification may require a light field calibrated for ice thickness variations because of the strong variation in light level with both presence of oil and ice thickness. This can be mitigated fairly easily using a strobe, which based on the results of this study, produces better contrast than in ambient light, even when light levels from above are good. Lastly, the high bandwidth required to relay real-time imagery may be prohibitive in some (or most) circumstances. While we have developed techniques for acoustic transmission of imagery, a lower bandwidth sensor stream may be preferred (with imagery requested to confirm identification of oil).

A potentially reliable secondary data source is laser-induced fluorescence. Within this project, we have developed a compact prototype laser fluorosensor that was able to detect oil under ice, and even when slightly encapsulated. Recent improvements to the prototype are expected to improve this capability (and will be tested in upcoming experiments). Some potential limitations that were not explored within this project include the possible confounding effects of turbid water or ice algae giving a false positive. Further investigation of these effects and means for discriminating between different fluorophors (such as fluorescence polarization techniques) is warranted. As with cameras (and sonars, described below), these tests were performed at close range under level ice, and detection of oil is expected to be more difficult under variable ice conditions and greater ranges. Assessment of the effect of variable ambient light levels and sensor sensitivity requirements at realistic ranges needs to be performed.

One of the more intriguing sensing modalities is the use of high frequency sonar to detect oil layers at the base of the ice, as this can provide a measure of the oil thickness, such that the oil volume can be determined during a mapping mission. Thin layers of oil (< 5 cm) were readily detected with both narrowband and broadband sonars through detection of both the oil/water and oil/ice interfaces. For frequencies with better penetration into the ice, the oil layer can be identified by a characteristic reverberation in the oil layer.

Broadband sonars offer a distinct advantage over traditional narrowband sonars, in that a lower frequency can be used (to improve penetration into the ice) while maintaining excellent range resolution (to detect thin oil layers). In addition, the frequency response provided by broadband sonars can be used to provide additional information of the layering in the oil-ice-seawater system. Nevertheless, the high-frequency narrowband sonars tested were also able to detect thin oil layers, and for these experiments, performed equally well for detection of encapsulated oil. Encapsulated oil was detected up to a depth of as much as 15 cm in the series of experiments.

Despite these successes, these experiments were idealized in that relatively small areas of level ice were tested. In a real-life scenario, the spatial variation in sea ice thickness and physical properties will complicate oil detection in ways that have yet to be quantified. An intriguing result was that it appeared that the internal structure of the basal layer of the ice significantly impacted the scattering behavior, and this scattering behavior (and notably, the reflection coefficient) differed from that of crude oil. Further characterization of the scattering behavior from the basal layer of ice, under varied ice conditions (particularly at different roughness scales) should be performed so that the scattering behavior of ice and oil under ice is better understood.

Nevertheless, the broadband sonar results are particularly promising, and in addition to further experiments in more realistic conditions, development of broadband systems specifically for deployment on AUVs is warranted.

A clear outcome of these experiments is that any individual sensor performance is very much tied to the ice conditions in which the oil spill occurred. This is especially clear for the experiments with frazil and pancake ice. Because of the differing signal response characteristics for each of the sensors tested here, it seems that the most effective system will involve a suite of some or all of these sensor systems. Forthcoming work should focus on effective means of fusion of these data streams, in a range of realistic conditions so that definitive identification of oil can be achieved in the broadest range of scenarios. Given restrictions on a controlled oil release under natural sea ice, developing a clear understanding of the expected signal characteristics for each of the sensor modalities tested under this project should proceed along several avenues. Improved characterization of the under ice environment with a broad sensor suite in a variety of realistic ice conditions in the field is needed so that the expected signal behavior can be better characterized and modeled to guide future sensor and sensor suite design. The effects of range and water conditions can best be determined through these field tests and/or well designed laboratory experiments. Laboratory experiments that better simulate conditions of particular interest where the signal characteristics or sensor performance may deviate from what can be determined from either the level ice experiments performed within this project or inferred from field trials should also be carried out.

While this project has clearly demonstrated the promise of digital imagery, sonar, and laser fluorescence for oil detection under sea ice, until a more comprehensive characterization of the anticipated signal behavior under more realistic conditions can be evaluated, the optimal design of an appropriate sensor or sensor suite remains to be determined.

The AUV missions performed under this project have clearly demonstrated the viability of future rapid routine deployment of AUVs under sea ice. These missions have shown that AUV navigation is possible under temporally and spatially variable ice conditions, and that rapid deployment and recovery from non-stationary vessel is possible. Acoustic communication testing also shows that communication with a vehicle under fast ice in shallow water is possible over several kilometers. This makes the use of AUVs for rapid, large-scale surveys under ice conditions like those found at Prudhoe Bay possible.

To further develop AUV capability so that operational mission could be routinely performed to conduct large-scale under ice surveys in the conditions commonly encountered on the Beaufort/Chukchi outer continental shelf, there are several key areas of development needed:

1. Long-range capability. AUVs that can transit 100 km or more under ice exist. However, to be effective tools for the oil and gas industry to perform routine inspection under ice to detect potential spills, a precise navigation framework is required.
2. Precise mapping under multiple, independent floes. This will require improved techniques to accurately combine DVL (Doppler), inertial, and acoustic navigation and positioning along with local methods of navigation. We have provided a proof-of-concept that AUV missions with precise navigation in these conditions are possible, but further work to provide a map of the sea ice (and oil) in a consistent reference frame is needed.
3. Operation in shallow water under ice has been demonstrated to be viable. However, to safely perform large area surveys in such an environment will require improved capabilities for obstacle avoidance (i.e. grounded ice keels), and autonomous navigation to avoid these obstacles
4. We have demonstrated that adaptive missions can be remotely commanded by the AUV operator over acoustic communication. To improve on the ability to map oil under ice, improvements in automated detection and mapping of the extent of the spill should be developed.

The capabilities of AUVs for operation under the Arctic sea ice have only begun to mature in the last decade. Given the potential of these platforms to operate under all ice types and all conditions, and with a variety of sensor packages, there is significant potential for their use as an integral part of an Arctic oil spill response strategy. Investment in further AUV system development in the coming decade will ensure that routine, operational capability for under-ice AUV operation is achieved.

## 8. References


Bellingham, J. G., C. A. Goudey, T. R. Consi, J. W. Bales, D. K. Atwood, J. J. Leonard, J. J., and C. A. Chyrssostomidis (1994), Second generation survey AUV, In *1994 IEEE Conference on Autonomous Underwater Vehicles*, Cambridge, MA.

Bello, J. and P. Toomey (2012), Development of a fluorescence polarization submersible instrument for the detection of submerged heavy oil spills, *Proc. SPIE* 8372, Ocean Sensing and Monitoring IV, 83720B (June 1, 2012), doi:10.1117/12.919509

Bishop, G. C., (1989), A bi-static, high-frequency, under-ice, acoustic scattering model. II Applications. *J. Acoust. Soc. Am.* 85, 1912.

Brown, C. and M. Fingas (2003), Review of the development of laser fluorosensors for oil spill application, *Marine Pollution Bulletin*, 47, 477–484.

Chu, D., and T. K. Stanton (1998), Application of pulse compression techniques to broadband acoustic scattering by live individual zooplankton. *J. Acoust. Soc. Am.* 104**,** 39-55.

Dickins D. F., Vaudrey and Associates, and SL Ross (2000), *Oil Spills in Ice Discussion Paper - A Review of Spill Response, Ice Conditions, Oil Behaviour, and Monitoring*.

Dickins, D. F., and I. Buist (1999), Oil spill countermeasures for ice covered waters, *J. of Pure and App Chem.,* Vol. 71, No. 1, pp. 173-191.

Dickins, D.F. (2011), Behavior of oil spills in ice and implications for Arctic spill response, *Proc. Arctic Technology Conference*, Houston TX, Feb 7-9, pp. 15

Freitag, L., P. Koski, A. Morozov, S. Singh, J. Partan (2012), Acoustic communications and navigation under Arctic ice, *Oceans, 2012*, vol. 1, pp.8, doi: 10.1109/OCEANS.2012.6405005

Hagen, P. E., O. Midtgaard, and O. Hasvold (2007), Making AUVs truly autonomous. In *OCEANS 2007*, pp. 1-4, IEEE.

Hansen, K. A, M. Fitzpatrick, P. R. Herring, and M. VanHaverbeke (2009), Heavy Oil Detection (Prototypes) – Final Report, Report CG-D-08-09, U.S. Coast Guard Research and Development Center, pp 74.

Jackson, K., J. Wilkinson, T. Maksym, D. Meldrum, J. Beckers, C. Haas, and D. MacKenzie (2013), A Novel and Low Cost Sea Ice Mass Balance Buoy, *J. Atmos. Oceanic Technol.***,** 30, 2676–2688*,* doi:10.1175/JTECH-D-13-00058.1

Jenkins, A., P. Dutrieux, S. S. Jacobs, S. D. McPhail, J. R. Perrett, A. T. Webb, and D. White (2010), Observations beneath Pine Island Glacier in West Antarctica and implications for its retreat. *Nature Geoscience* 3:468–472, http://dx.doi.org/10.1038/ngeo890.

Jha, N. M., J. Levy, and Y. Gao (2008), Advances in Remote Sensing for Oil Spill Disaster Management: State-of-the-Art Sensors Technology for Oil Spill Surveillance, *Sensors*, 8, 236-255.

Kunz, C., C. Murphy, H. Singh, C. Willis, R. Sohn, S. Singh, T. Sato, C. Roman, K. Nakamura, M. Jakuba, R. Eustice, R. Camilli, J. Bailey (2009), Toward Extraplanetary Under-Ice Exploration: Robotic Steps in the Arctic, *Journal of Field Robotics*, vol. 26(4), pp 411-429

Lavery, A. C. and T. Ross (2007), Acoustic scattering from double-diffusive microstructure, *J. Acoust. Soc. Am.*, 122**,** 1449-1462.

Murphy, C. and H. Singh (2010), Wavelet compression with set partitioning for low bandwidth telemetry from AUV, in *Proceedings of the Fifth ACM International Workshop on Underwater Networks*.

National Research Council (2014), *Responding to Oil Spills in the U.S. Arctic Marine Environment*. Washington, DC, The National Academies Press.

NORCOR Engineering and Research Ltd. (1975), The interaction of crude oil with arctic sea ice. *Beaufort Sea Technical Report*, No. 27, Beaufort Sea Project, Department of the Environment, Victoria, BC, pp. 201.

Panetta, P.D., L.G. Bland, K. Winfield, D. McElhine, G.G. Cartwright, and C.T. Friedrichs (2013), Assessment of dispersent effectiveness using using ultrasound to measure oil droplet particle size distributions, Final Report, BSEE contract number E12PC00011.

Perkins, S. (2006), Intrepid explorer: An oceangoing rover gathers unprecedented data. *Science News Online, 170(5):72*. Retrieved December 27, 2007 from http://www.sciencenews.org/articles/20060729/bob9.asp.

Plueddemann, A.J., A.L. Kukulya, R. Stokey, and L. Freitag (2012), Autonomous underwater vehicle operations beneath coastal sea ice, *IEEE Trans. Mechatronics*, 17(1), doi:10.1109/TMECH.2011.2174798.

Petrich, C. and H. Eicken (2009), Growth, structure and properties of sea ice, in *Sea Ice*, Thomas, D. N. and G. S. Dieckmann (eds.), Wiley-Blackwell, pp. 23-77.

Sasano, M., H. Yamanouchi, A. Matsumoto, N. Kiriya, K. Hitomi, and K. Tamura (2012), Development of boat-based fluorescence imaging lidar for coral monitoring, *Proc, 12th Int. Coral Reef Symp.*, Cairns, Aus, 9-13 July 2012.

Singh, H., A. Can, R. Eustice, S. Lerner, N. McPhee, O. Pizarro, C. Roman (2004). Seabed AUV offers new platform for high-resolution imaging. *Eos Transactions, American Geophysical Union*, 85(31), 289, 294–5.

S.L. Ross, D. F. Dickens, Envision Planning (2010), *Beaufort Sea Oil Spills State of Knowledge Review and Identification of Key Issues*, Environmental Research Studies Funds Report No. 177.

Sohn, R. A., et al. (2008), Explosive volcanism on the ultraslow-spreading Gakkel ridge, Arctic Ocean, *Nature*, *4*53, 1236-1238, doi:10.1038/nature07075.

Stanton, T. K., K. C. Jezek, and A. J. Gow (1986), Acoustical Reflection and Scattering from the Underside of Laboratory Grown Sea Ice: Measurements and Predictions, *J. Acoust. Soc. Am.*, 80, 1486-1494.

Thorleifson, J., T. Davies, M. Black, D. Hopkin, and R. Verrall (1997), The Theseus autonomous underwater vehicle: A Canadian success story. In *Proceedings IEEE/MTS Oceans Conference and Exhibition*, 1001–1008.

Thomas, D. N. and G. S. Dieckmann (Eds.) (2009), *Sea ice*, John Wiley & Sons.

Turin, G.L. (1960), An introduction to matched filters. IRE Trans. Inf. Theory, 6(3): 311–329

USARC (2004), Advancing oil spill response in ice covered water, Dickins and Associates, pp28.

Wadhams, P., J. P., Wilkinson, and A. Kaletzky (2003), Sidescan sonar imagery of the winter marginal ice zone obtained from an AUV, *Journal of Atmospheric and Oceanic Technology*, 21(9):1462–1470.

Wakatsuchi, M., and T. Kawamura (1987), Formation processes of brine drainage channels in sea ice, J. Geophys. Res., 92(C7), 7195–7197, doi:10.1029/JC092iC07p07195.

Weber, T. C., A. De Robertis, S. F. Greenaway, S. Smith, L. Mayer, and G. Rice (2012), Estimating oil concentration and flow rate with calibrated vessel-mounted acoustic echo sounders. PNAS 109(50): 20240–20245, doi: 10.1073/pnas.1108771108

Weeks, W.F. (2010), *On Sea ice,* University of Alaska Press

Wettlaufer, J. S., M. G. Worster, and H. E. Huppert (1997), The phase evolution of young sea ice, *Geophys. Res. Lett.*, 24, 1251–1254.

Williams, K. L., G. R. Garrison, and P. D. Mourad (1992), Experimental examination of growing and newly submerged sea ice including acoustic probing of the skeletal layer. J. *Acoustic. Soc. of Am.*, 92: 2075-2092.

Williams, G. D., et al. (2013), Beyond Point Measurements: Sea Ice Floe, Characterized in 3-D, *Eos Trans. AGU*, *94*(7), 69.

Williams, G., T. Maksym, J. Wilkinson, H. Singh, C. Kunz, P. Kimball, Mapping ice thickness and extreme deformation of Antarctic sea ice from an Autonomous Underwater Vehicle, submitted *to Nature Geoscience*.

Wilkinson, J. P., P. Wadhams, and N. E. Hughes (2007), Modelling the spread of oil under fast sea ice using three-dimensional multibeam sonar data, *Geophys. Res. Lett.*, 34, L22506, doi:10.1029/2007GL031754.

Wilkinson, J., T. Maksym, H. Singh, T. Boyd, C. Roman, Detection and quantification of oil under sea ice: the view from below, in press, *Cold Regions Science and Technology*

Xanaki, A., P. Gerstoft, and K. Mosegaard (2013), Modeling and detecting of oil in sea water. J. Acoust. Soc. Am. 134: 2790.